Basics
of CT and CBCT

Marc Kachelrieß

German Cancer Research Center (DKFZ)
Heidelberg, Germany
www.dkfz.de/ct

Clinical CT

Clinical CT detector inside

e.g. Definition Flash dual source spiral cone-beam CT scanner, Siemens Healthcare, Forchheim, Germany.

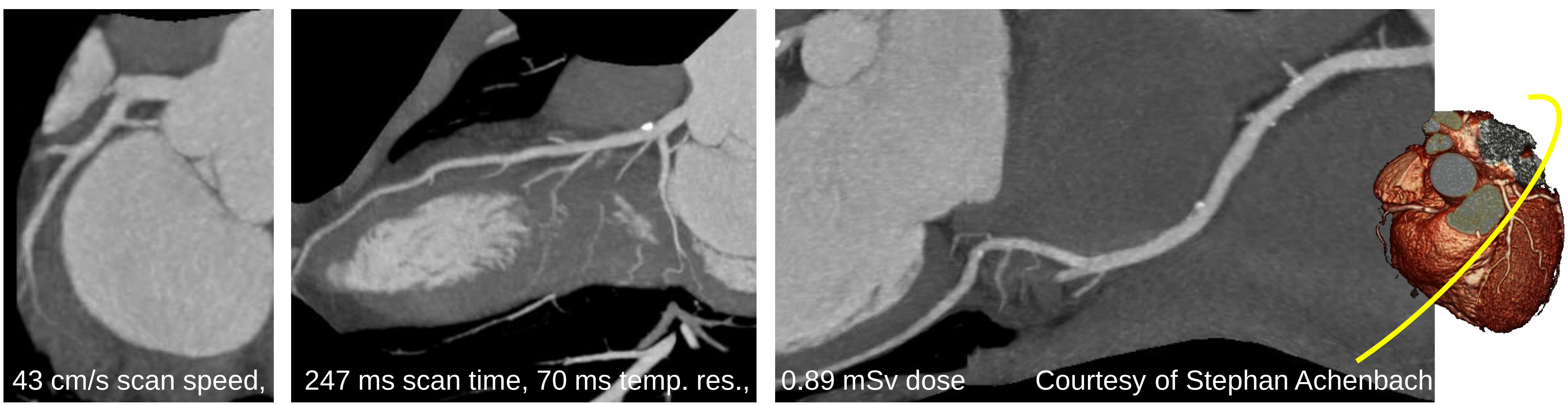

Fixed C-Arm CT

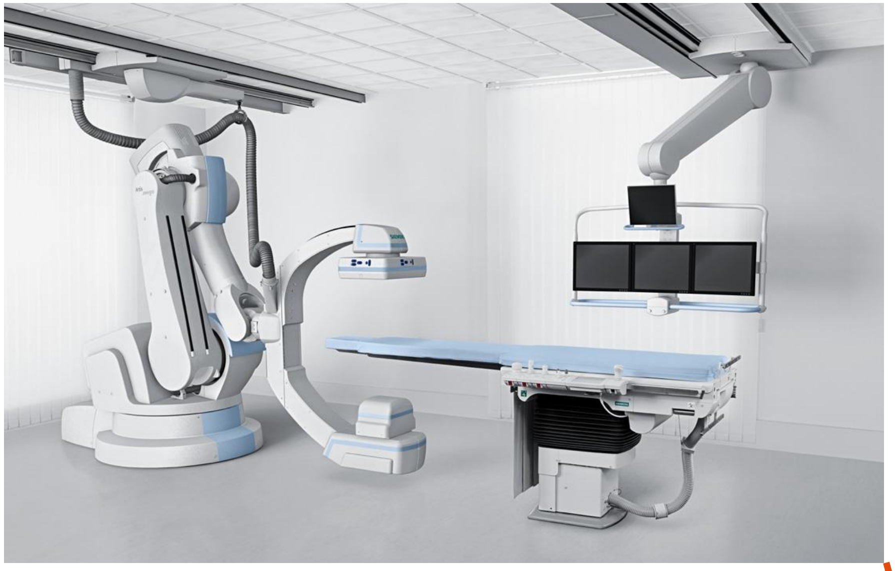

Flat detector inside

e.g. floor-mounted Artis Zeego or ceiling-mounted Artis Zee, Siemens Healthcare, Forchheim, Germany

C-Arm with Image Intensifier

Ziehm Vision R

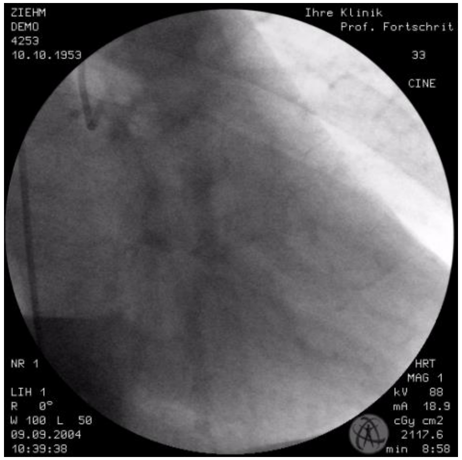

C-Arm with Flat Detector

Ziehm Vision RFD 3D

Mobile C-Arm CT

e.g. Vision RFD 3D, Ziehm Imaging GmbH, Nürnberg, Germany

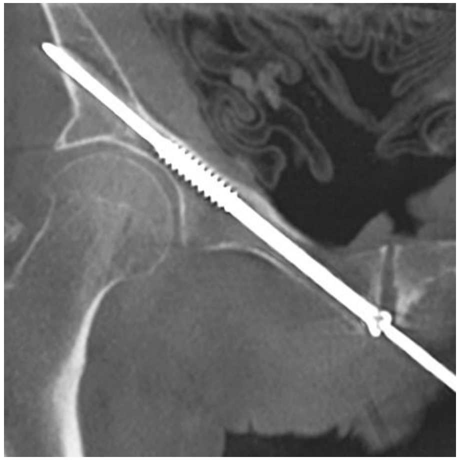

Image courtesy by Ziehm Imaging

Dental Volume Tomography (DVT)

e.g. Orthophos XG 3D, Sirona Dental Systems GmbH, Bensheim, Germany

Image courtesy by Sirona Dental

CBCT Guidance for Radiation Therapy

Flat detector inside

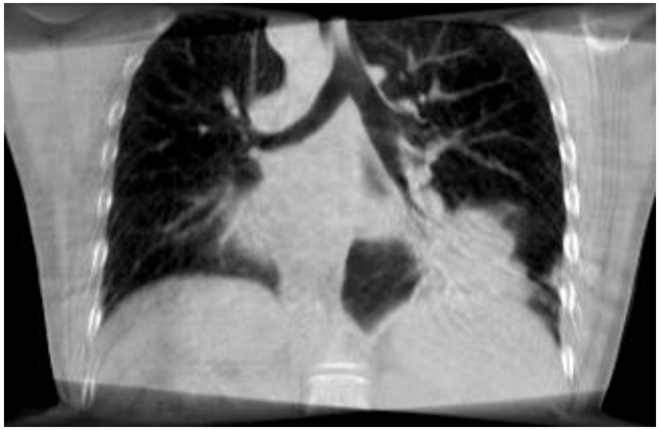

e.g. TrueBeam, Varian Medical Systems, Palo Alto, CA, USA

Micro CT for Preclinical Research

e.g. TomoScope, CT Imaging, Erlangen, Germany

Industrial CT

Flat detector inside

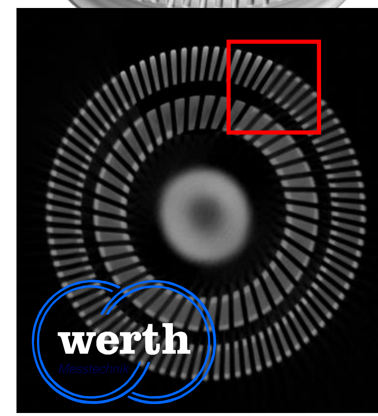

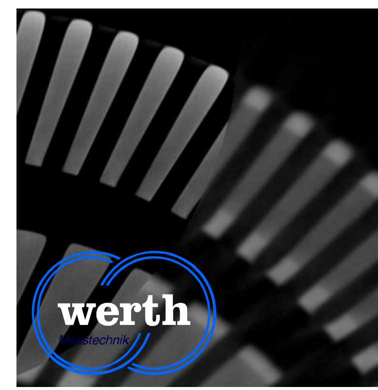

e.g. TomoScope HV 500, Werth Messtechnik, Gießen, Germany

Detector Technology

Clinical CT Detector

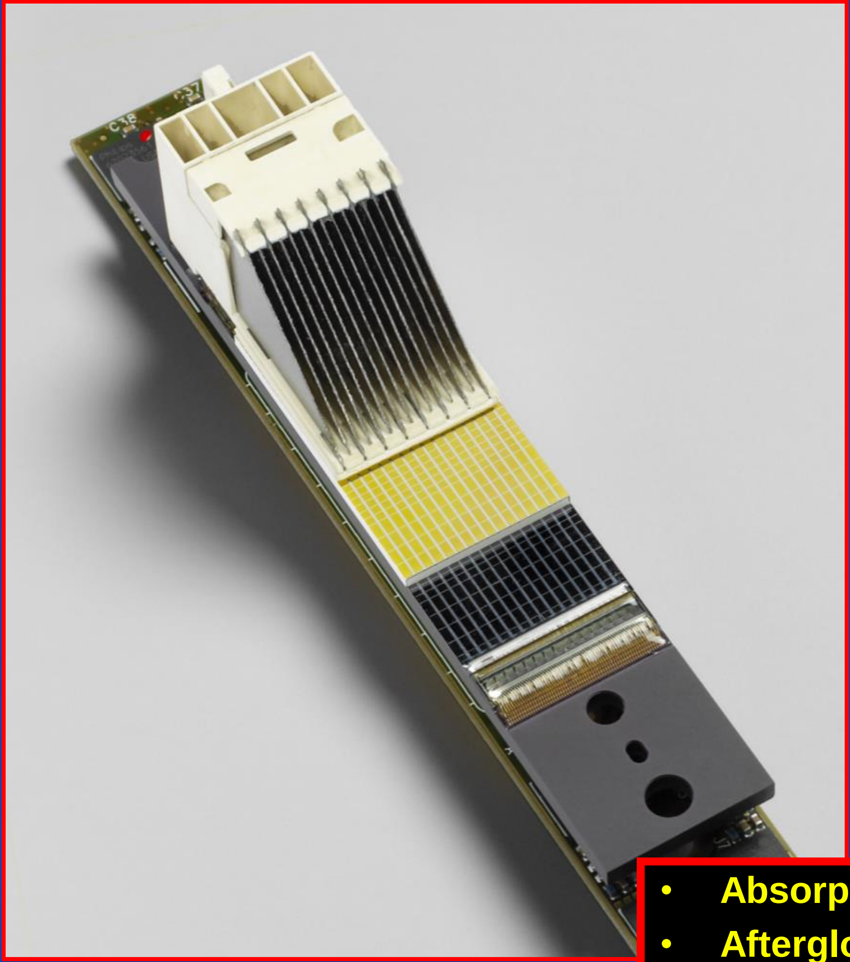

Flat Detector

- Absorption efficiency
- Afterglow
- Dynamic range
- Cross-talk
- Framerate
- Scatter grid

Siemens 2·2·96=384-slice
dual source cone-beam spiral CT(2013)

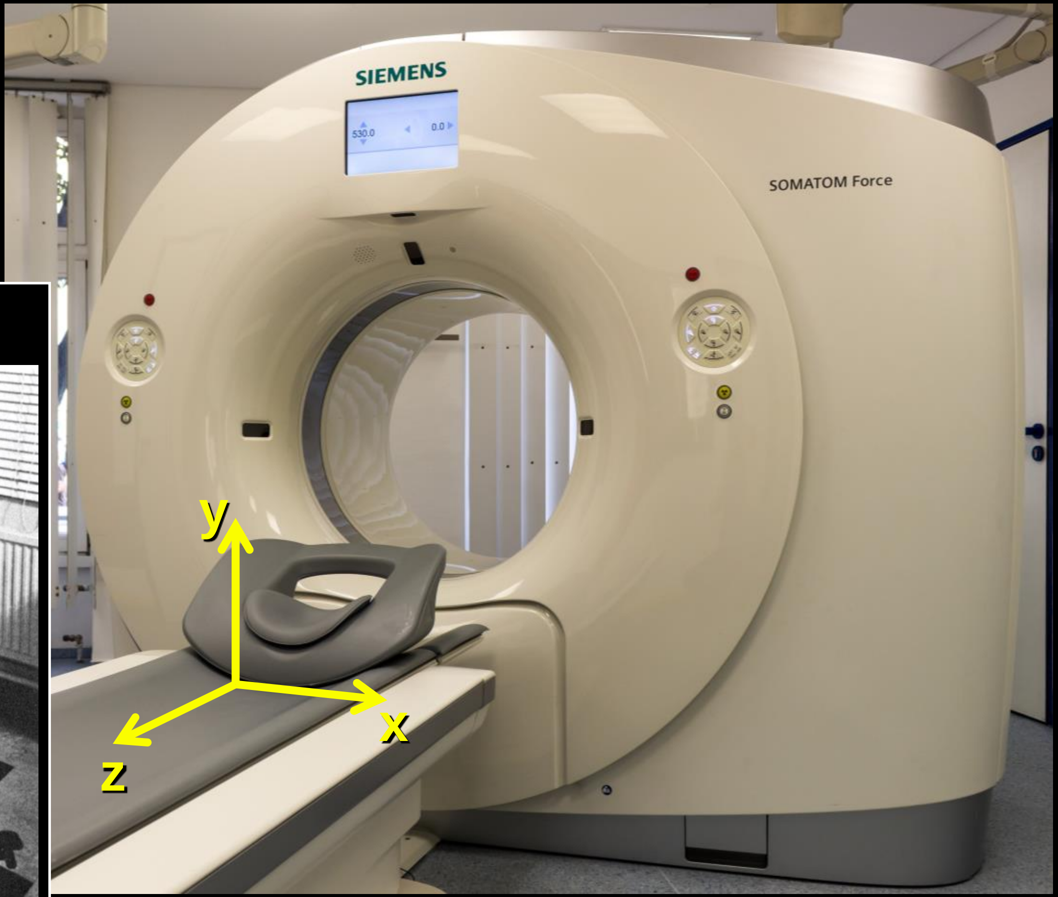

525 views (1050 readings) per rotation in 0.25 s

2·96×(920+640) two-byte channels per view

1,200 MB/s data transfer rate

up to 4 GB rawdata, 2 GB volume size typical

EMI parallel beam scanner (1972)

180 views per rotation in 300 s

2×160 positions per view

384 B/s data transfer rate

113 kB data size

Siemens 2·2·96=384-slice
dual source cone-beam spiral CT(2013)

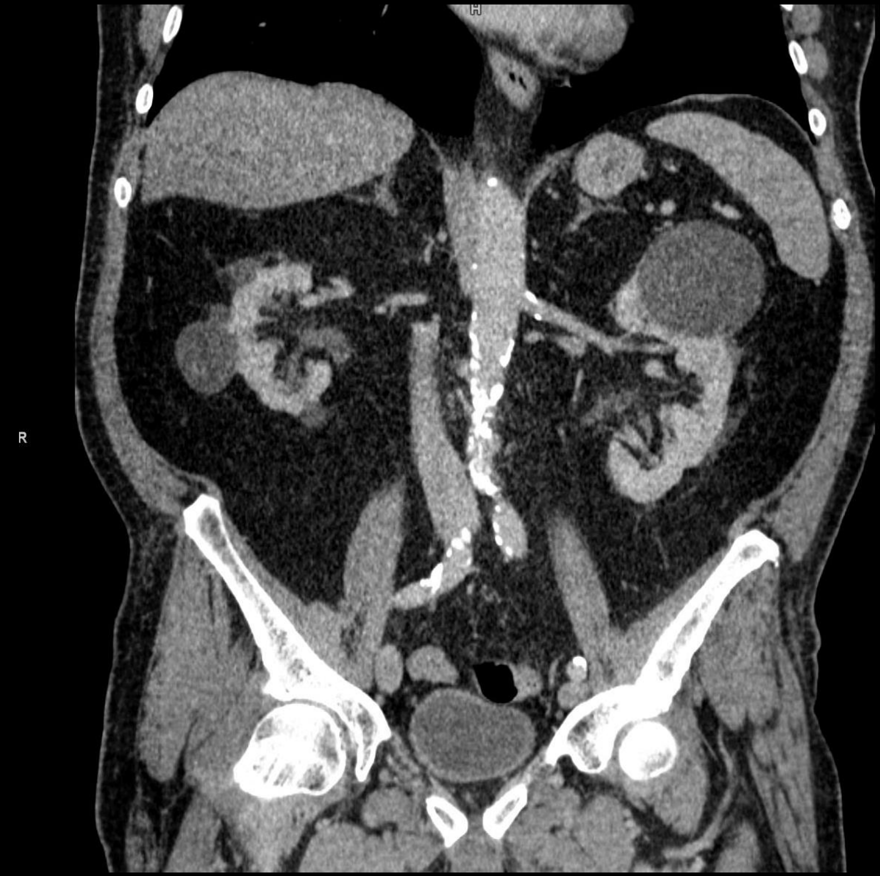

525 views (1050 readings) per rotation in 0.25 s

2·96×(920+640) two-byte channels per view

1,200 MB/s data transfer rate

up to 4 GB rawdata, 2 GB volume size typical

EMI parallel beam scanner (1972)

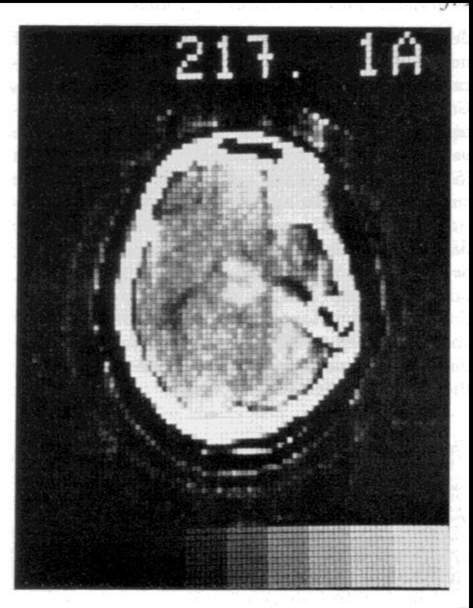

180 views per rotation in 300 s

2×160 positions per view

384 B/s data transfer rate

113 kB data size

dkfz.


@mayo

Canon Aquilion ONE Genesis

GE Revolution Apex

Philips Spectral CT 7500

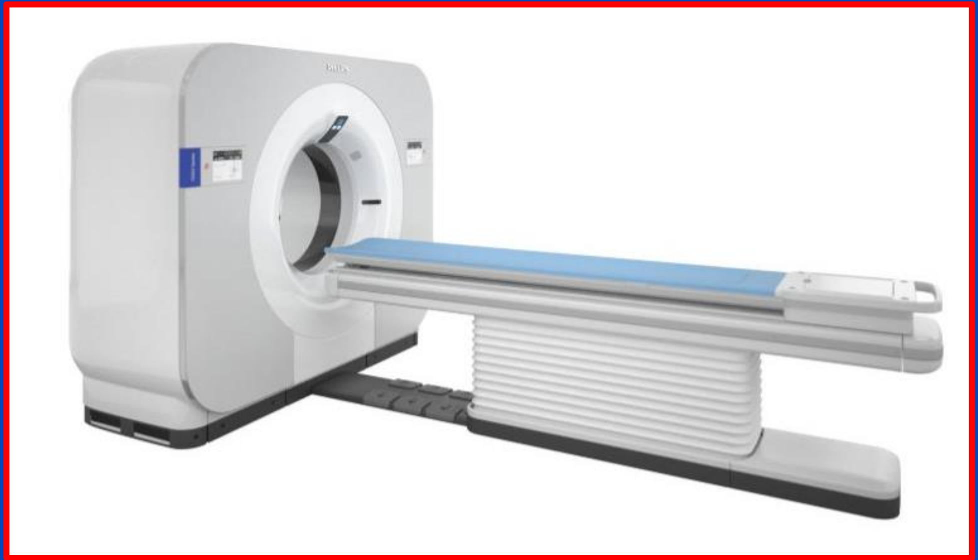

Siemens Naeotom Alpha

What does CT Measure?

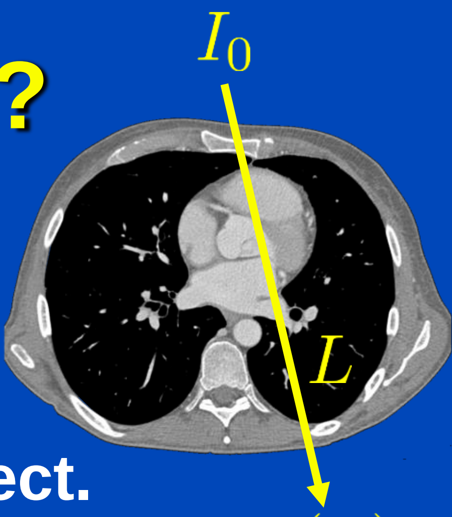

- X-rays are generated in an x-ray tube.
- The polychromatic radiation is attenuated in the patient. X-ray photon attenuation is dominated by the photo and the Compton effect.
- Detectors measure the x-ray intensity after the rays have passed through the patient along several lines *L*.
- The log intensity is the so-called x-ray transform:

$$q(L) = -\ln \frac{I(L)}{I_0} = -\ln \int dE\, w(E) e^{-\int dL \mu(\boldsymbol{r}, E)}$$

- Often, the follwing monochromatic approximation is used:

$$q(L) \approx p(L) = \int dL \mu(\boldsymbol{r}, E_{\text{eff}})$$

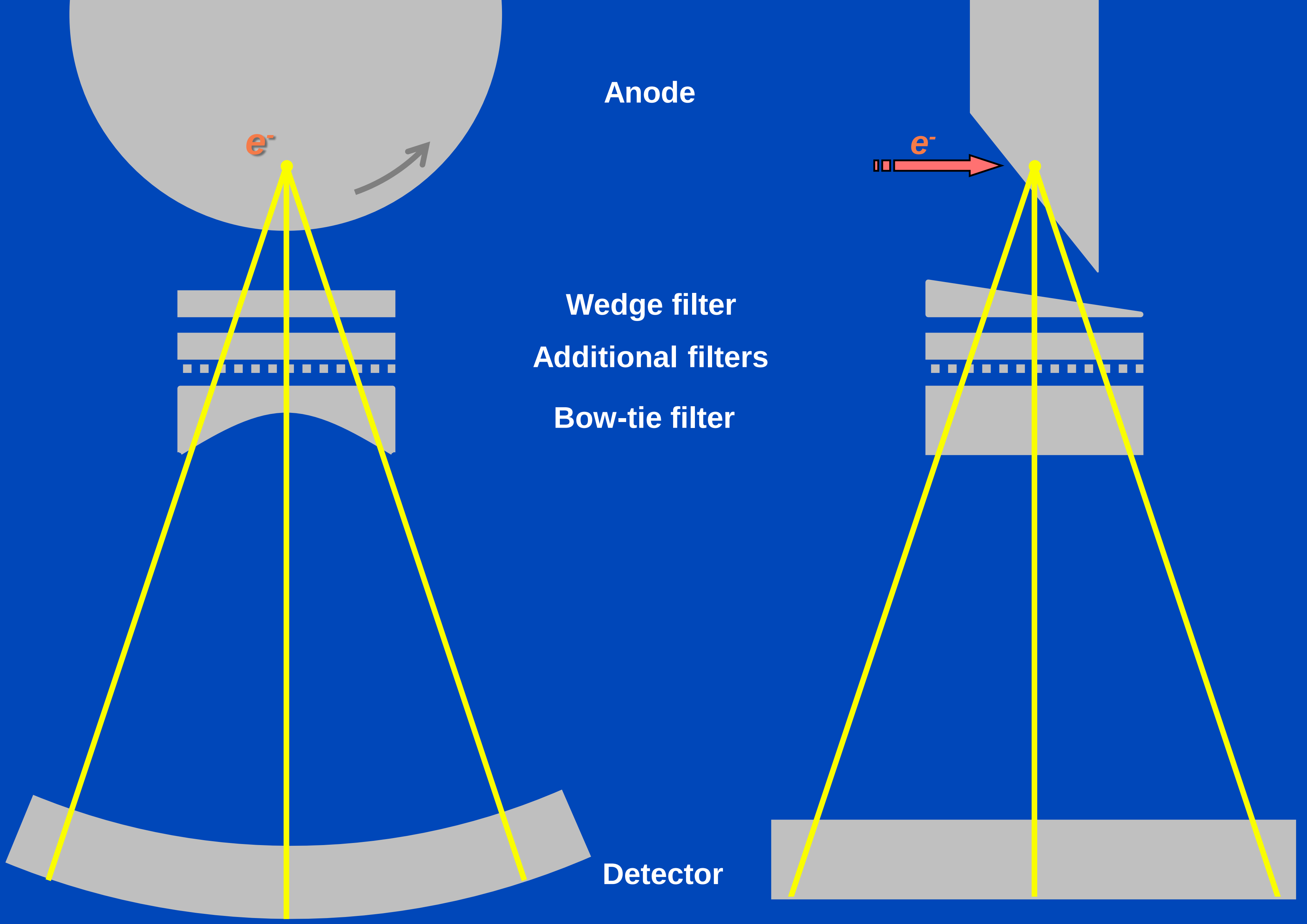

Figure not drawn to scale. Type and order of prefiltration may differ from scanner to scanner.
Depending on the selected protocol filters are changed automatically (e.g. small bowtie for pediatric scans).

Heel Effect

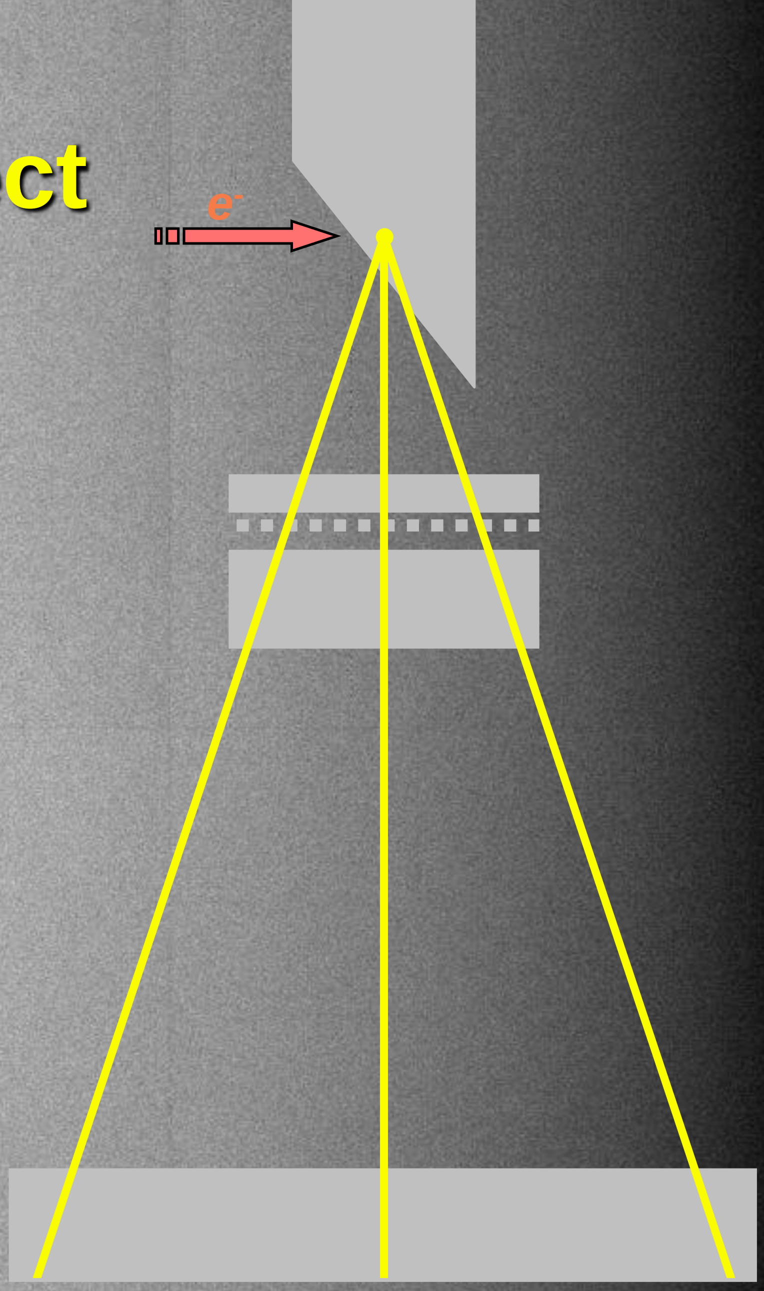

Offset-corrected image (40 kV, 1.39 mA, 23 ms, Ziehm Imaging CMOS)

120 kV + 0 mm water with and without prefilter

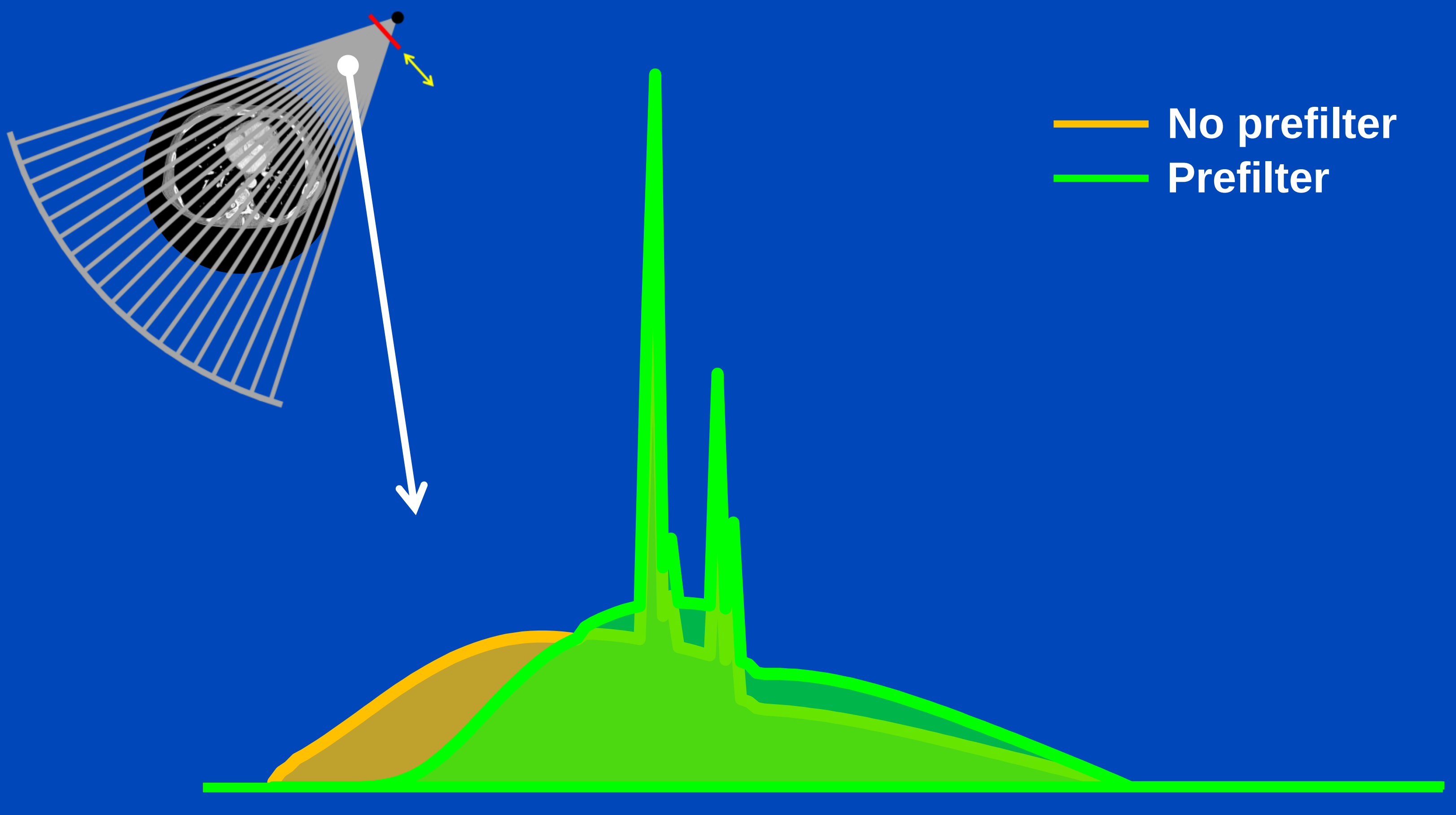

dkfz.

120 kV + 320 mm water with and without prefilter

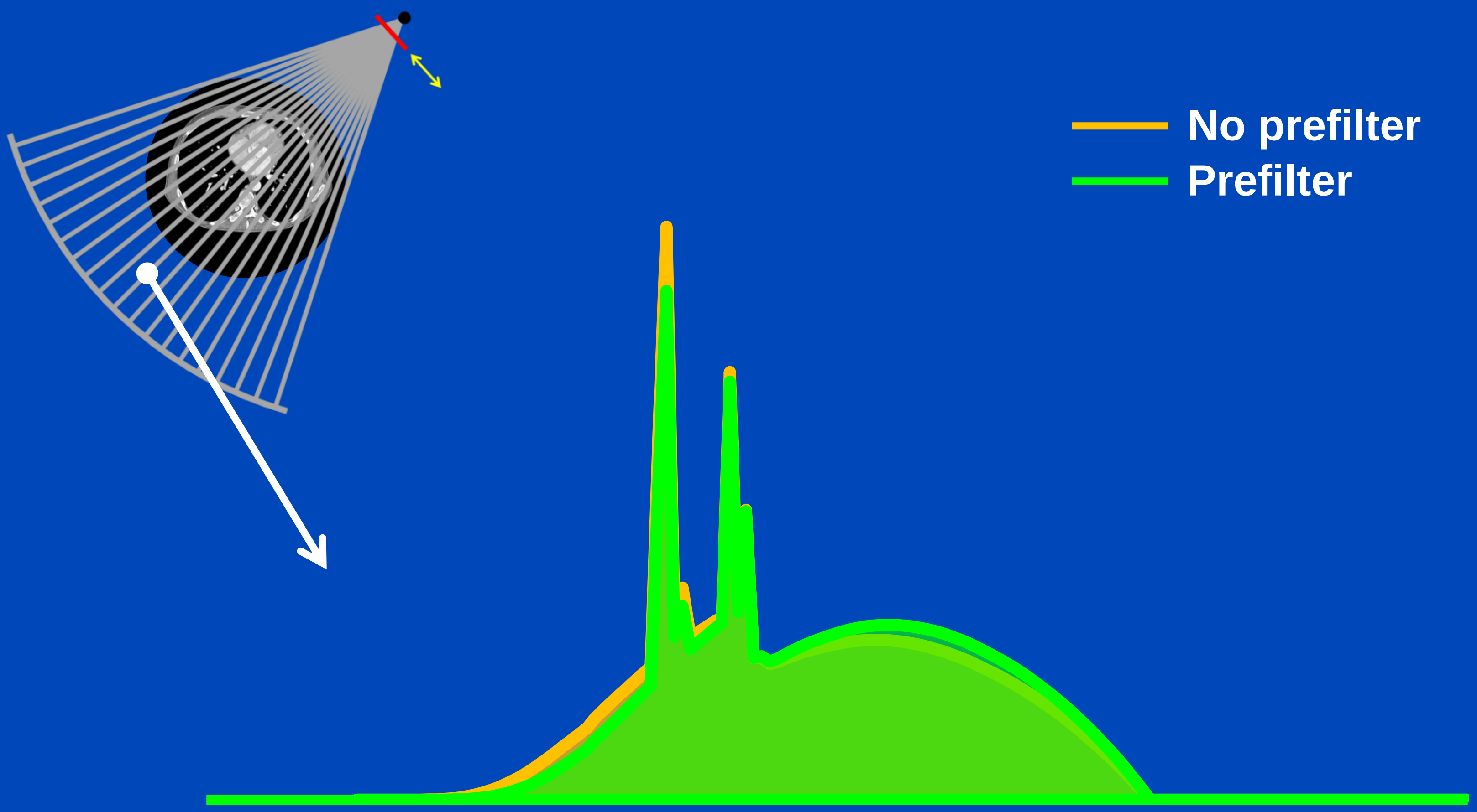

Removable Prefilters in Use Today

- 0.4 mm Sn for Siemens‘ Somatom Flash, Drive, go.Now, go.Up and go.all
- 0.6 mm Sn for Siemens‘ Somatom Force, Edge Plus, go.Top and Definition Edge
- 0.4 mm and 0.7 mm Sn for Siemens‘ Somatom X.cite
- ≈ 0.5 mm Au for Canon‘s Aquilion ONE Prism Edition
- ≈ 1 mm Cu for topograms only (!) in GE‘s Revolution Apex systems

Reference	Topic	Dose Reduction	Assessment	Recon
Agostini et al., 2021	chest, DECT, COVID-19	89%	subjective, different pitch values	iterative
Apfaltrer et al., 2018	coronary artery calcium scoring	73%	subjective	FBP
Axer et al., 2022	urolithiasis	20%	subjetive	iterative
Dewes et al., 2016	abdomen, urinary stones	22%	subjective	iterative
Gordic et al., 2014	chest, pulmonary nodules, phantom	95%	subjective	iterative
Grunz et al., 2022	urinary stone	18% - 38%	subjective, objective	iterative
Hasegawa et al., 2022	chest, detectability index, phantom	22% - 25%	objective	FBP
Jeon et al., 2019	DECT, gout diagnosis	65%	subjective, different scanners	iterative
Kimura et al., 2022	colorectal cancer	89%	subjective	iterative, FBP
Kunz et al., 2022	urinary tract	62%	frequency of calculi detection	iterative
Leyendecker et al., 2019	abdomen	81%	subjective, objective	iterative
Martini et al., 2016	chest, pulmonary nodules	97%	subjective	iterative
Rajendran et al., 2020	sinus, temporal bone	67% - 85%	objective, EICT and PCCT	FBP
Saltybaeva et al., 2019	topogram	80%	effect on TCM	-
Schabel et al., 2018	thoracic aorta calcification	92%	subjective	iterative
Schüle et al., 2022	pelvis	90%	subjective, objective	iterative, FBP
Takemitsu et al., 2022	topogram	80%	effect on TCM	-
Weis et al., 2017	chest, pediatric	77%	subjective, objective	iterative
Wuest et al., 2016	paranasal sinus	73%	subjective, different scanners	FBP
Zhang et al., 2022	guided lung biopsy	73%	subjective	iterative

- Agostini, Andrea, et al. "Third-generation iterative reconstruction on a dual-source, high-pitch, low-dose chest CT protocol with tin filter for spectral shaping at 100 kV: a study on a small series of COVID-19 patients." *La radiologia medica* 126:388–398, 2021.
- Apfaltrer, Georg, et al. "High-pitch low-voltage CT coronary artery calcium scoring with tin filtration: accuracy and radiation dose reduction." *European Radiology* 28(7):3097-3104, 2018.
- Axer, Benedikt, et al. "Comparative evaluation of diagnostic quality in native low-dose CT without and with spectral shaping employing a tin filter in urolithiasis with implanted ureteral stent." *RöFo-Fortschritte auf dem Gebiet der Röntgenstrahlen und der bildgebenden Verfahren* 194(12):1358-1366, 2022.
- Dewes, Patricia, et al. "Low-dose abdominal computed tomography for detection of urinary stone disease - Impact of additional spectral shaping of the x-ray beam on image quality and dose parameters." *European Journal of Radiology* 85(6):1058-1062, 2016.
- Gordic, Sonja, et al. "Ultralow-dose chest computed tomography for pulmonary nodule detection: First performance evaluation of single energy scanning with spectral shaping." *Investigative Radiology* 49(7):465-473, 2014.
- Grunz, Jan-Peter, et al. "Thermoluminescence dosimetry in abdominal CT for urinary stone detection: Effective radiation dose reduction with tin prefiltration at 100 kVp." *Investigative Radiology* 58(3):231-238, 2023.
- Hasegawa, Akira, et al. "A tin filter's dose reduction effect revisited: Using the detectability index in low-dose computed tomography for the chest." *Physica Medica* 99:61-67, 2022.
- Jeon, Ji Young, et al. "The effect of tube voltage combination on image artefact and radiation dose in dual-source dual-energy CT: Comparison between conventional 80/140 kV and 80/150 kV plus tin filter for gout protocol." *European Radiology* 29(3):1248-1257, 2019.
- Kimura, Koichiro, et al. "Dose reduction and diagnostic performance of tin filter-based spectral shaping CT in patients with colorectal cancer." *Tomography* 8(2):1079-1089, 2022.
- Kunz, Andreas Steven, et al. "Tin-filtered 100 kV ultra-low-dose abdominal CT for calculi detection in the urinary tract: A comparative study of 510 cases." *Academic Radiology*, 2022.
- Leyendecker, Pierre, et al. "Prospective evaluation of ultra-low-dose contrast-enhanced 100-kV abdominal computed tomography with tin filter: effect on radiation dose reduction and image quality with a third-generation dual-source CT system." *European Radiology* 29(4):2107-2116, 2019.
- Martini, Katharina, et al. "Evaluation of pulmonary nodules and infection on chest CT with radiation dose equivalent to chest radiography: Prospective intra-individual comparison study to standard dose CT." *European Journal of Radiology* 85(2):360-365, 2016.
- Rajendran, Kishore, et al. "Dose reduction for sinus and temporal bone imaging using photon-counting detector CT with an additional tin filter." *Investigative Radiology* 55(2):91-100, 2020.
- Saltybaeva, Natalia, et al. "Radiation dose reduction from computed tomography localizer radiographs using a tin spectral shaping filter." *Medical Physics* 46(2):544-549, 2019.
- Schabel, Christoph, et al. "Tin-filtered low-dose chest CT to quantify macroscopic calcification burden of the thoracic aorta." *European Radiology* 28:1818-1825, 2018.
- Schüle, Simone, et al. "Low-dose CT imaging of the pelvis in follow-up examinations-significant dose reduction and impact of tin filtration: Evaluation by phantom studies and first systematic retrospective patient analyses." *Investigative Radiology* 57(12):789-801, 2022.

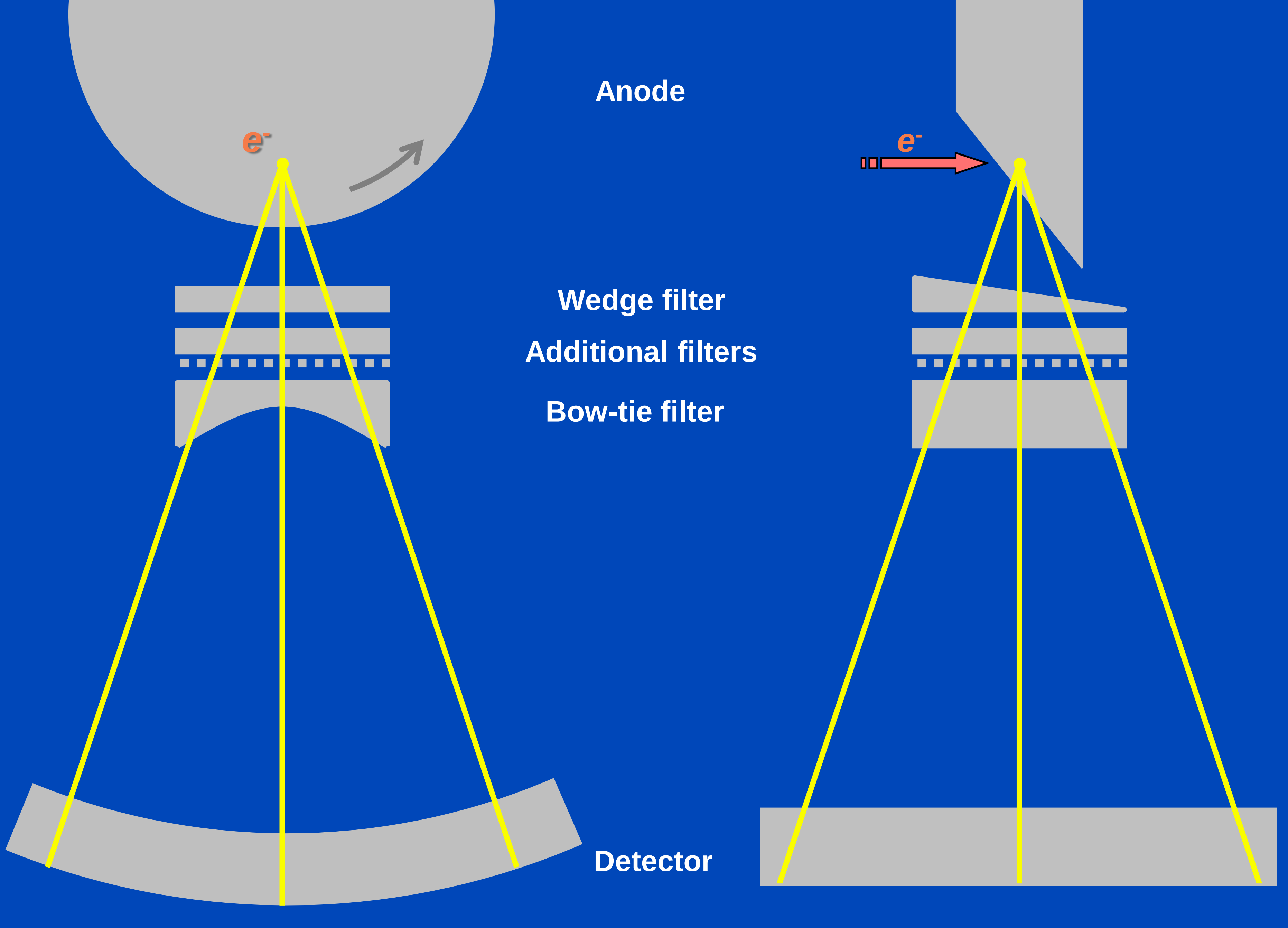

Figure not drawn to scale. Type and order of prefiltration may differ from scanner to scanner.
Depending on the selected protocol filters are changed automatically (e.g. small bowtie for pediatric scans).

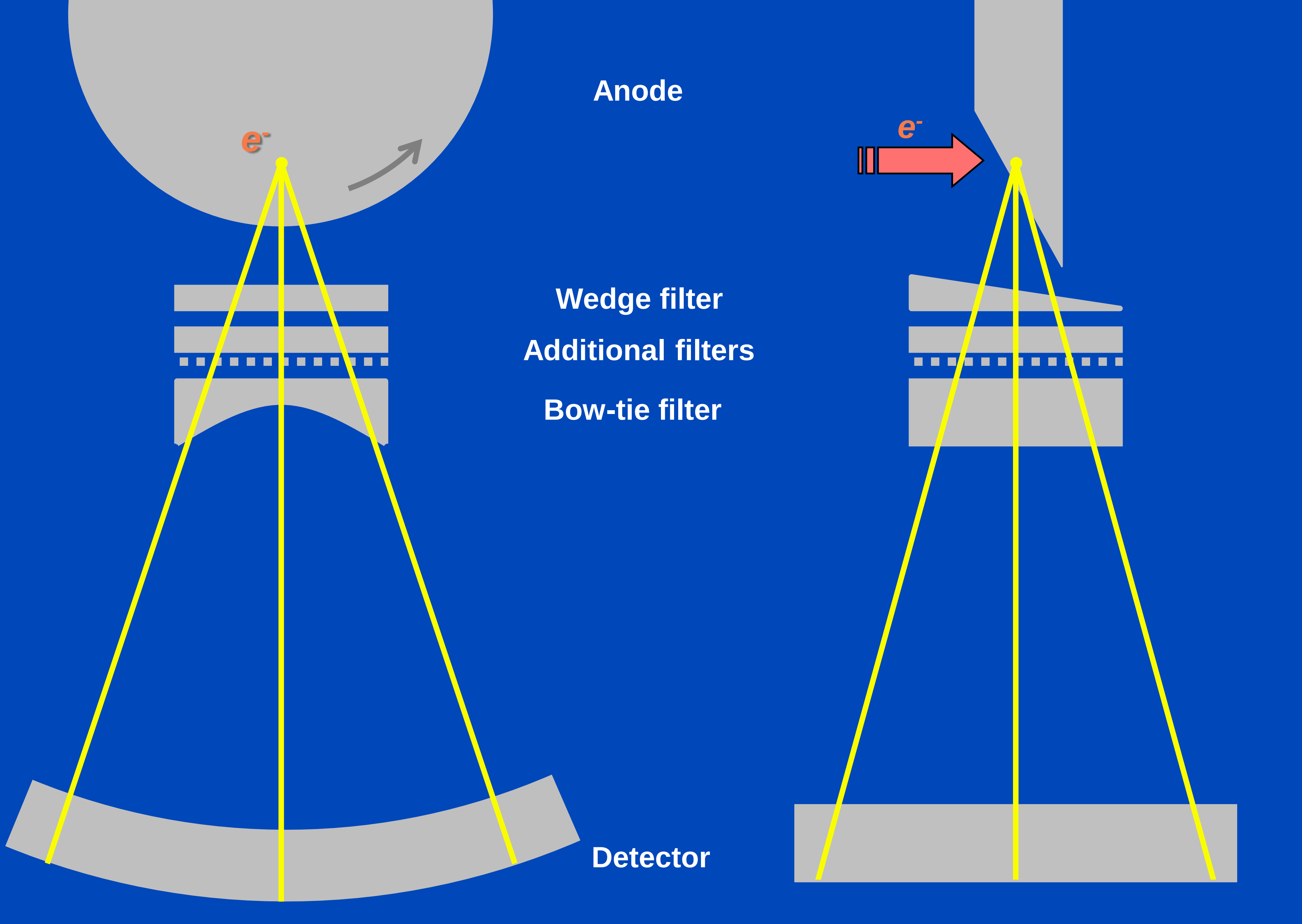

Figure not drawn to scale. Type and order of prefiltration may differ from scanner to scanner.
Depending on the selected protocol filters are changed automatically (e.g. small bowtie for pediatric scans).

Narrow Cone = High Tube Power

Wide Cone = Low Tube Power

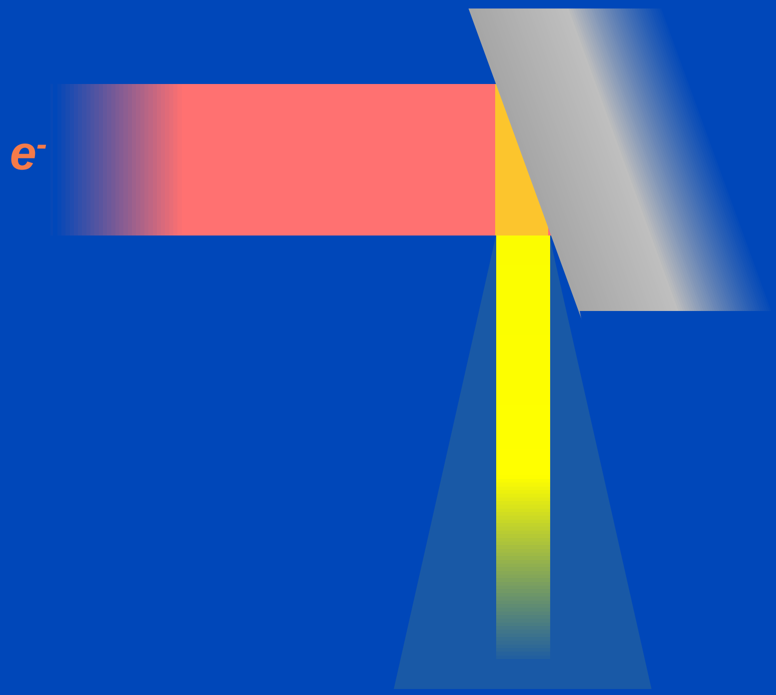

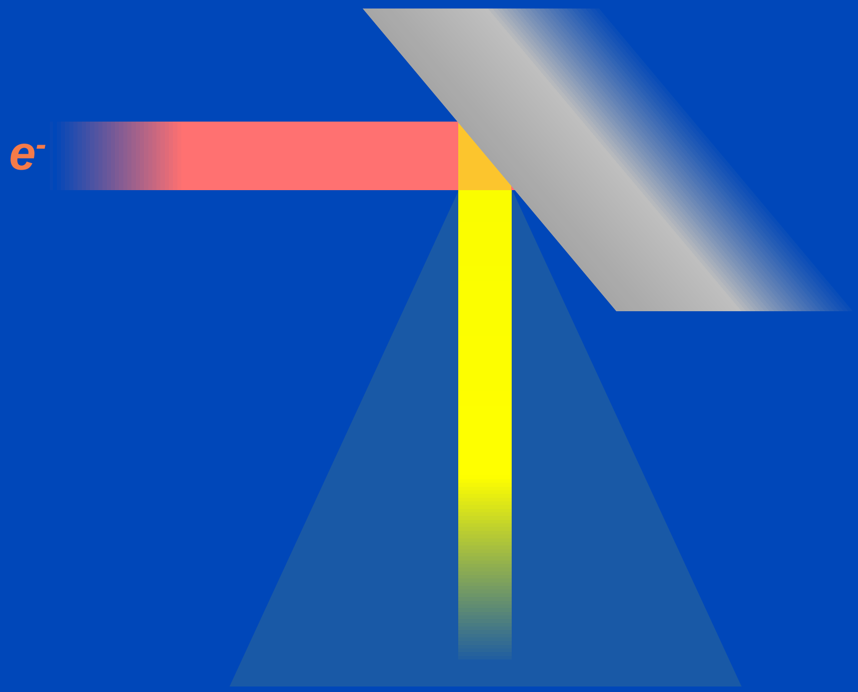

… at the same spatial resolution

Onset of target melting (rule of thumb)[1]: 1 W/µm

[1] D.E. Grider, A. Writh, and P.K. Ausburn. Electron Beam Melting in Microfocus X-Ray Tubes. J. Phys. D: Appl. Phys 19:2281-2292, 1986

What is Displayed?

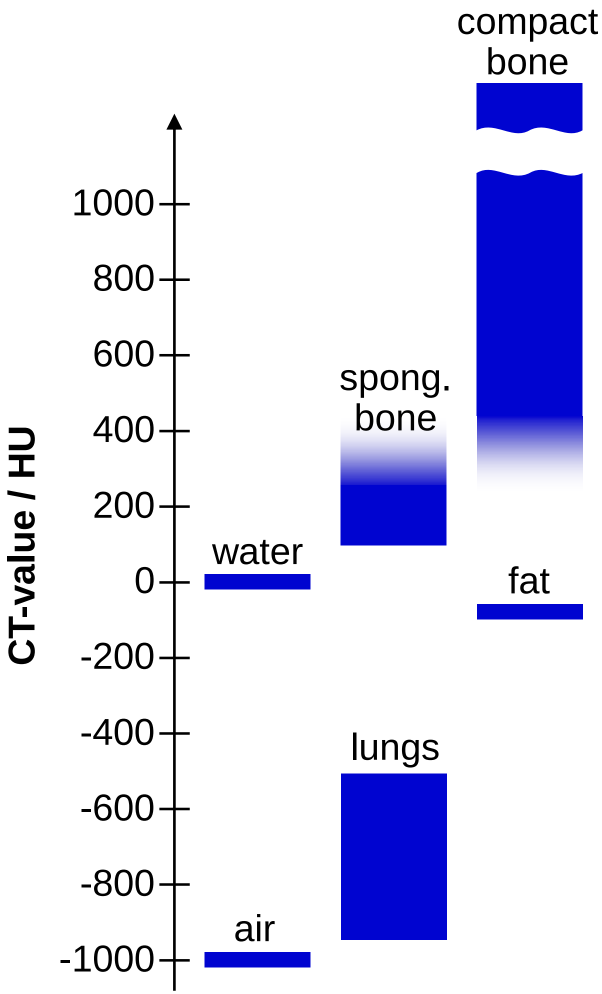

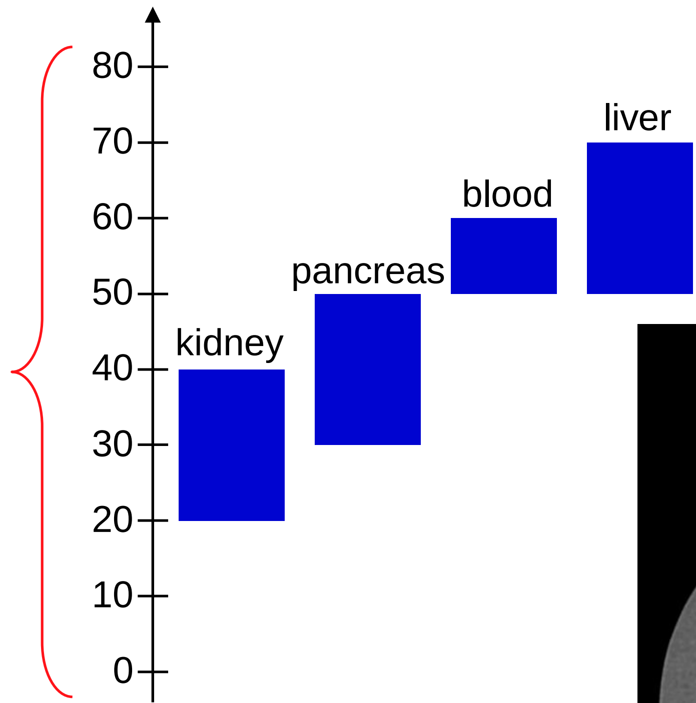

$$CT(\boldsymbol{r}) = \frac{\mu(\boldsymbol{r}) - \mu_{\text{Water}}}{\mu_{\text{Water}}} \cdot 1000 \text{ HU}$$

Fan-Beam Geometry (transaxial / in-plane / x-y-plane)

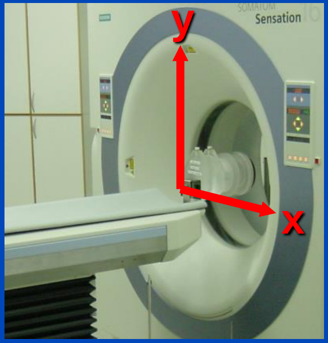

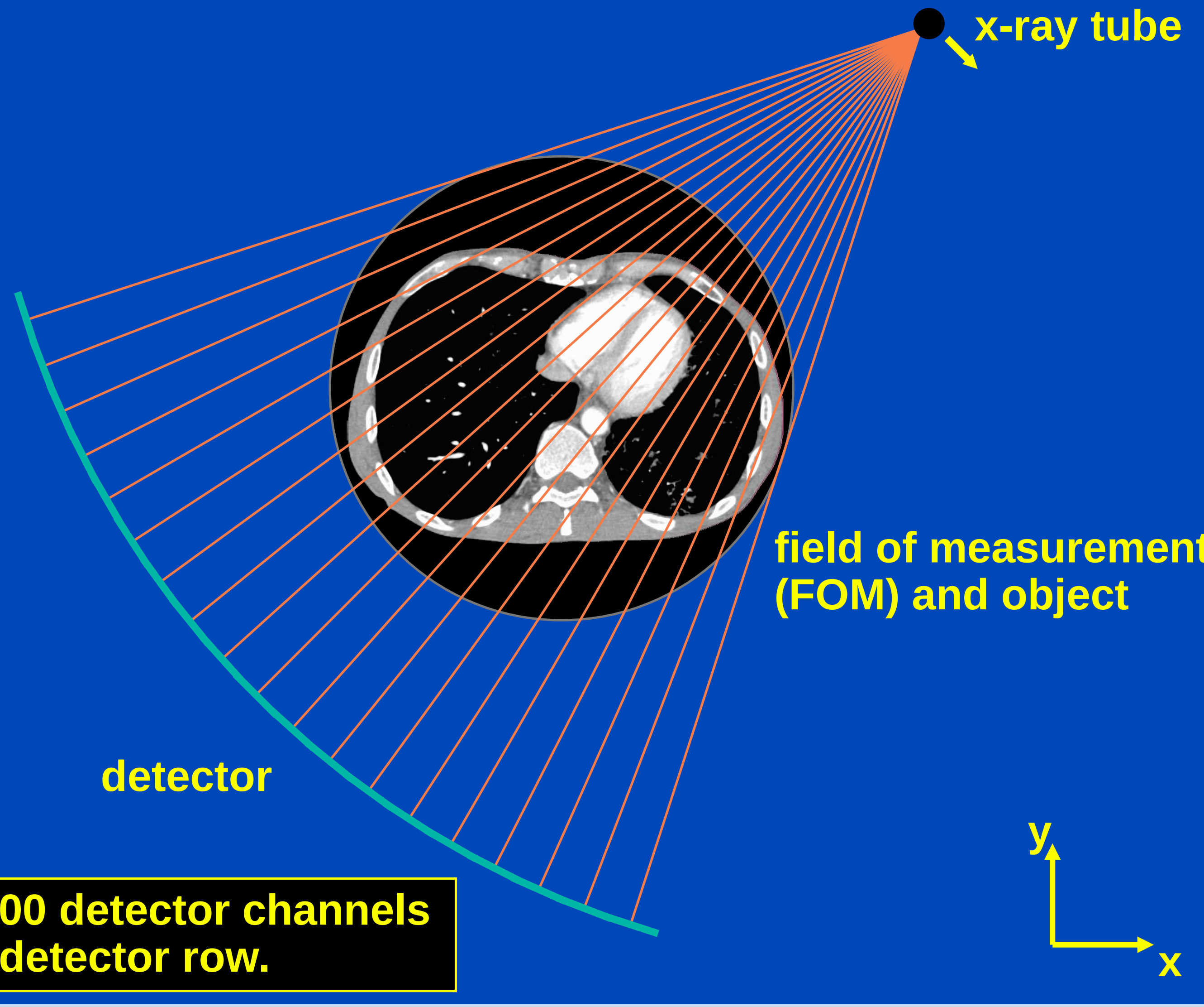

In the order of 1000 detector channels are available per detector row.

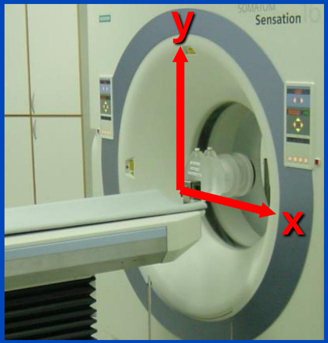

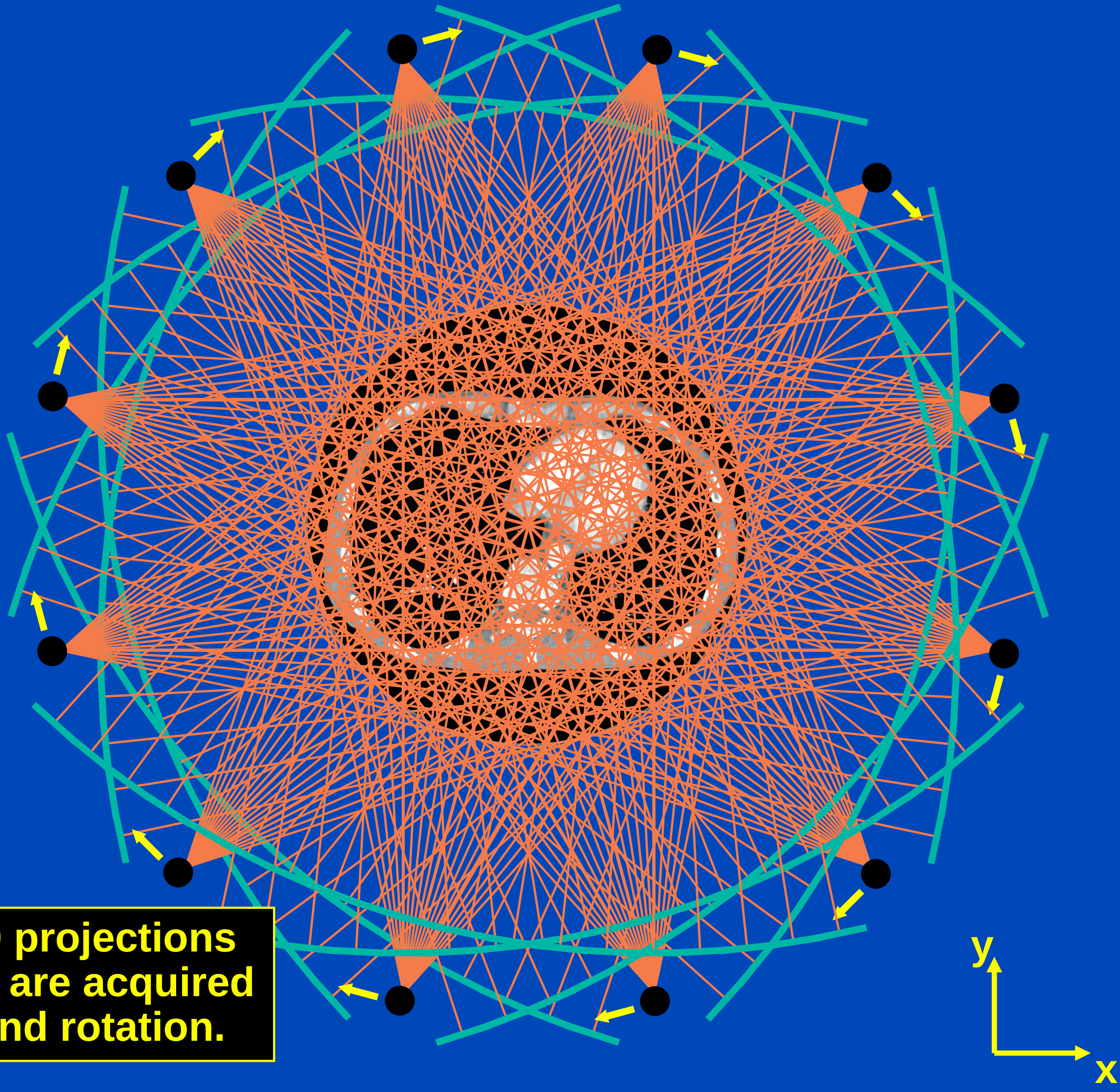

In the order of 1000 projections with 1000 channels are acquired per detector slice and rotation.

Data Completeness

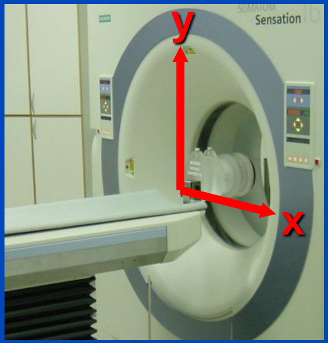

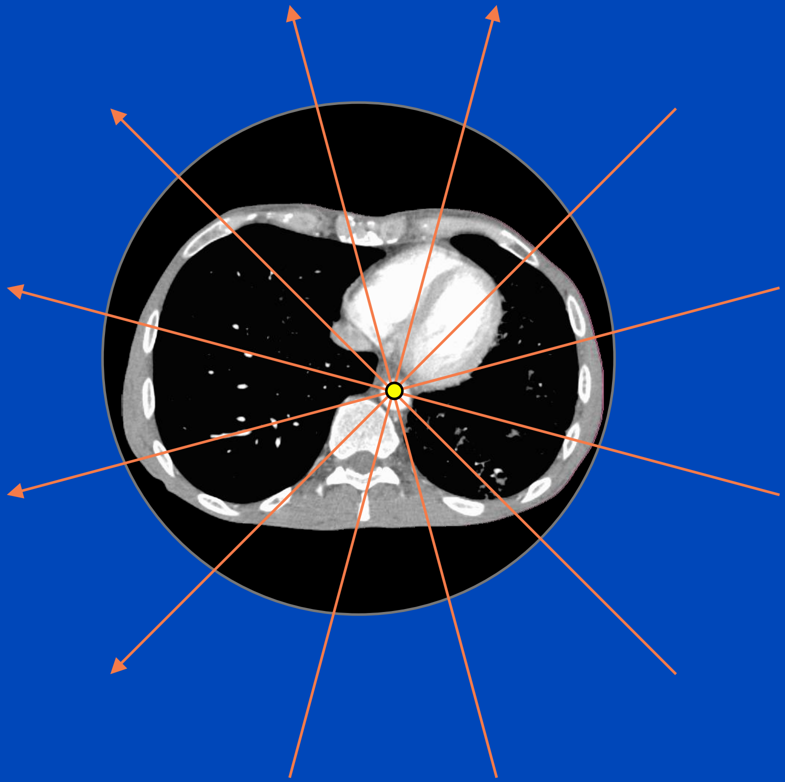

Each object point must be viewed by an angular interval of 180° or more. Otherwise image reconstruction is not possible.

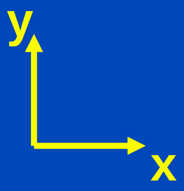

Axial Geometry (z-Direction)

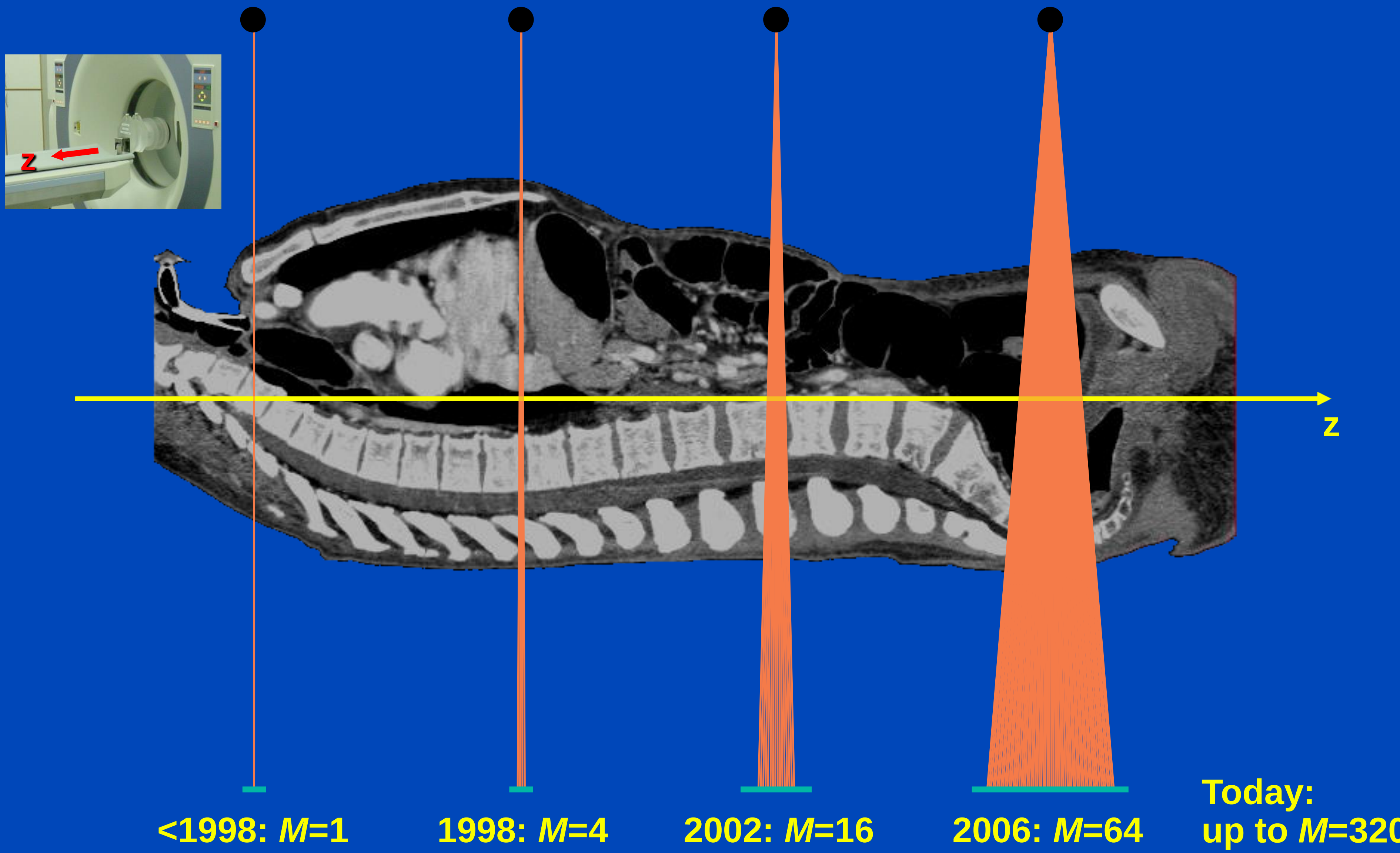

CBCT Geometry

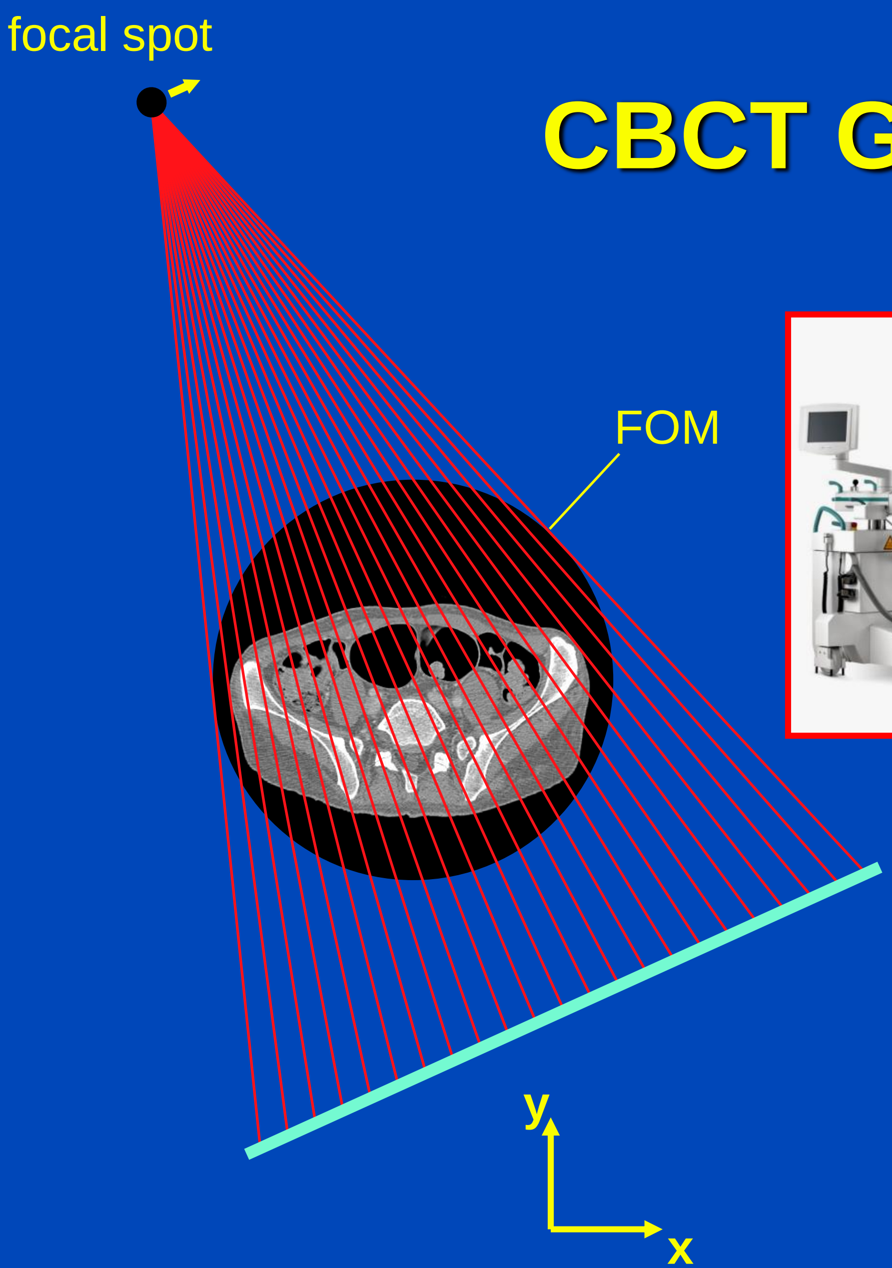

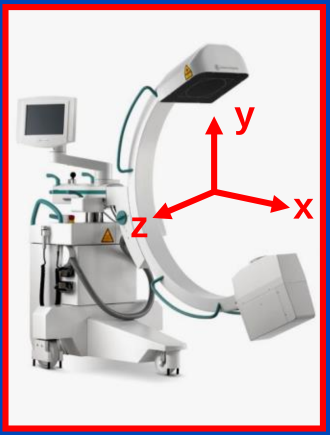

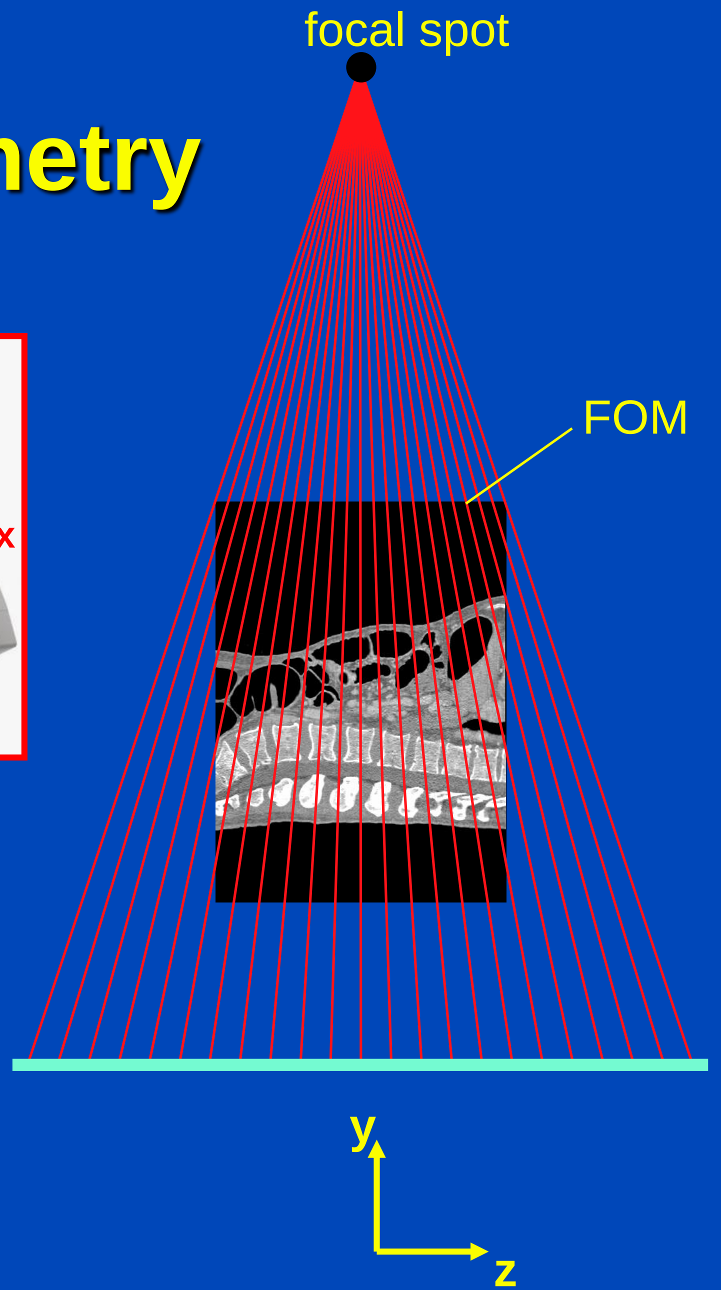

Detector: 1000×1000 to 4000×4000 elements, typically

CBCT Geometry

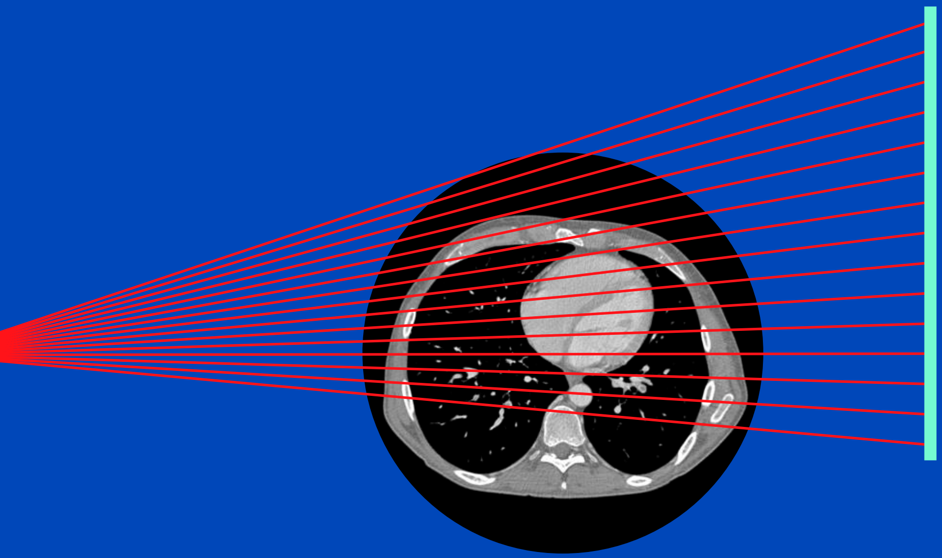

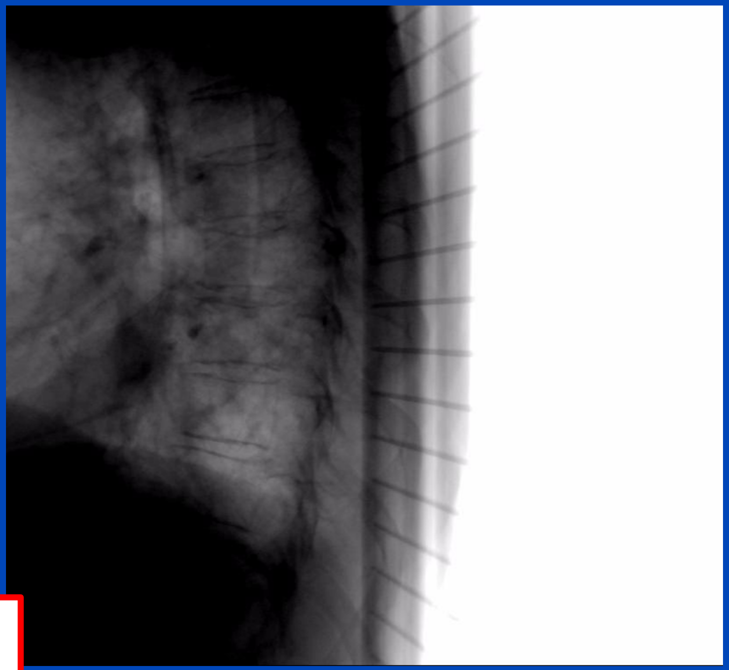

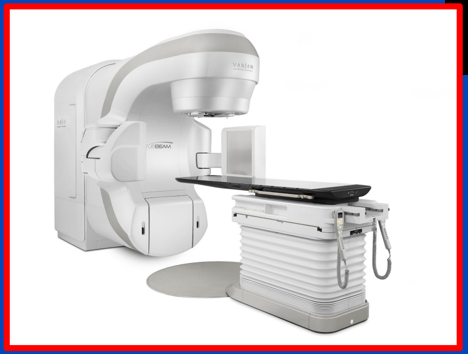

CT Equipment Technology

Canon Aquilion ONE Vision

GE Revolution CT

Philips IQon Spectral CT

Siemens Naeotom Alpha

In-plane resolution: 0.2 … 0.7 mm

Nominal slice thickness: S = 0.2 … 1.5 mm

Tube (max. values): 120 kW, 150 kV, 1300 mA

Effective tube current: mAs_{eff} = 10 mAs … 1000 mAs

Rotation time: T_{rot} = 0.25 … 0.5 s

Simultaneously acquired slices: M = 16 … 320

Table increment per rotation: d = 1 … 183 mm

Scan speed: up to 73 cm/s

Temporal resolution: 50 … 250 ms

Canon Megacool Vi

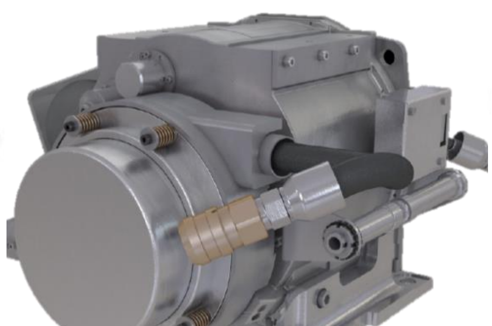

GE Performix HDw

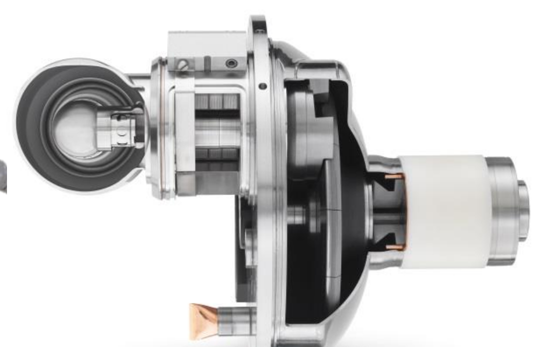

Philips iMRC

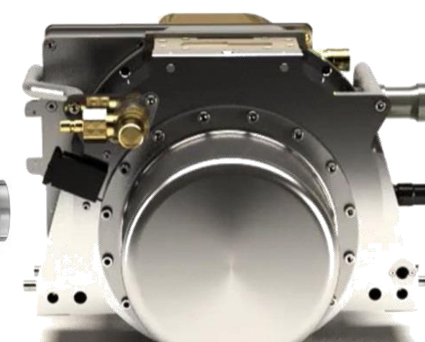

Siemens Vectron

Very Fast Scanning: no Sedation, no Motion Artifacts

Procedure:
Transcatheter aortic valve implantation (TAVI)

Patient age: 80 years

Tube voltage: 80 kV
Current: 340 ref mAs/rot

Rotation time: 0.25 s
Pitch: 3.2
Slice thickness: 0.75 mm
Scan length: 557 mm
Scan time: 0.76 s
Scan speed: 737 mm/s

Kernel : B40
Recon: ADMIRE 3

CTDIvol: 2.7 mGy
DLP: 162 mGy·cm
Effective dose: 2.3 mSv

Case information

Axial slices, *C* = 0 HU, *W* = 1500 HU

Volume rendering

Demands on the Mechanical Design

- Continuous data acquisition (spiral, fluoro, dynamic, …)
- Able to withstand very fast rotation
  - Centrifugal acceleration at 550 mm with 0.5 s: $a = 9\,g$
  - with 0.4 s: $a = 14\,g$
  - with 0.3 s: $a = 25\,g$
  - with 0.2 s: $a = 55\,g$
- Mechanical accuracy better than 0.1 mm
- Compact and robust design
- Short installation times
- Long service intervals
- Low cost

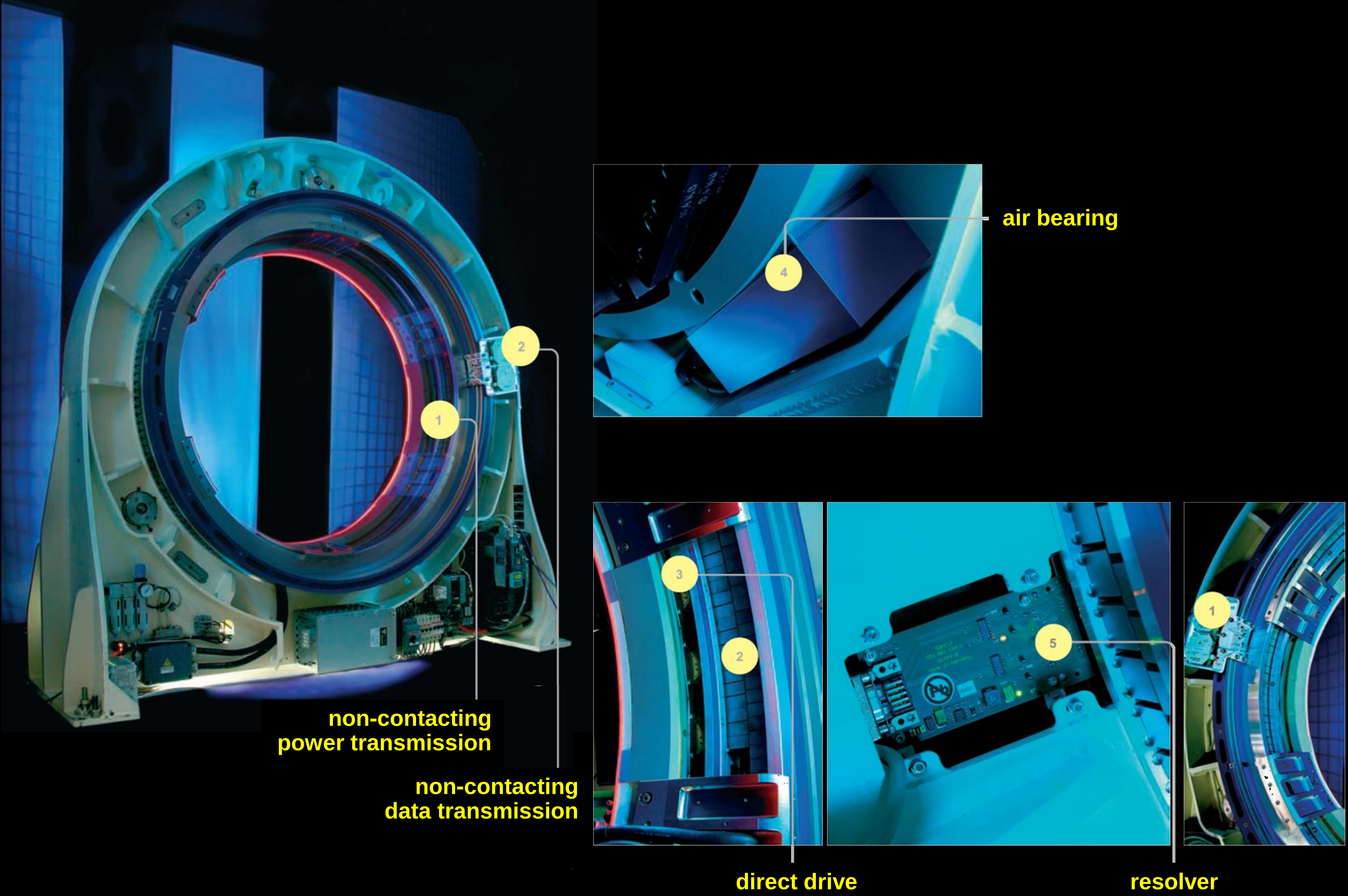

Data courtesy of Schleifring GmbH, Fürstenfeldbruck, Germany
and of rsna2011.rsna.org/exbData/1678/docs/Gantry_Subsystem.pdf

dkfz.

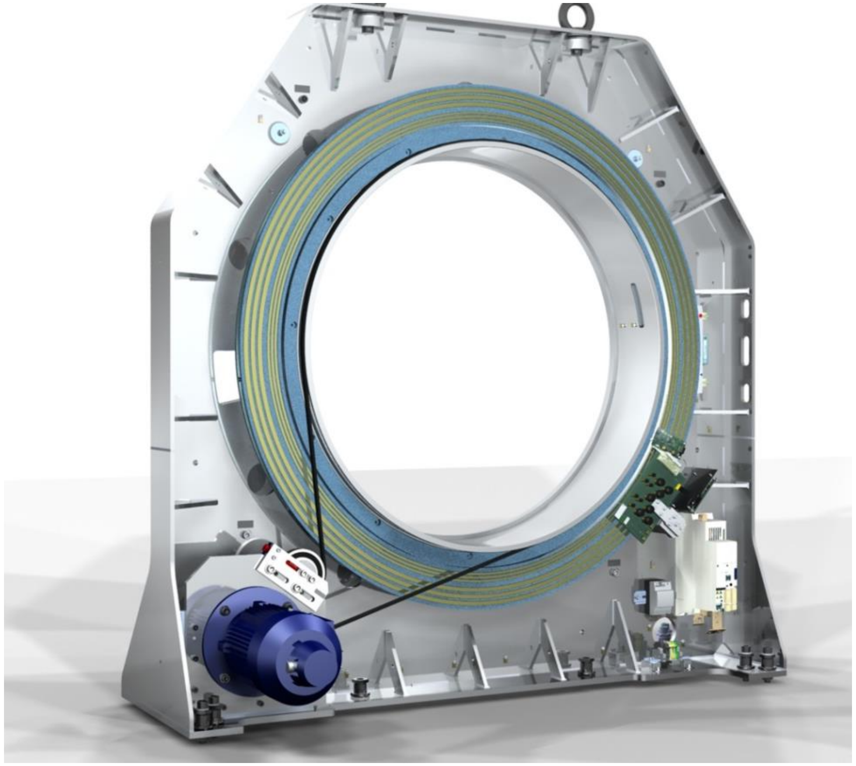

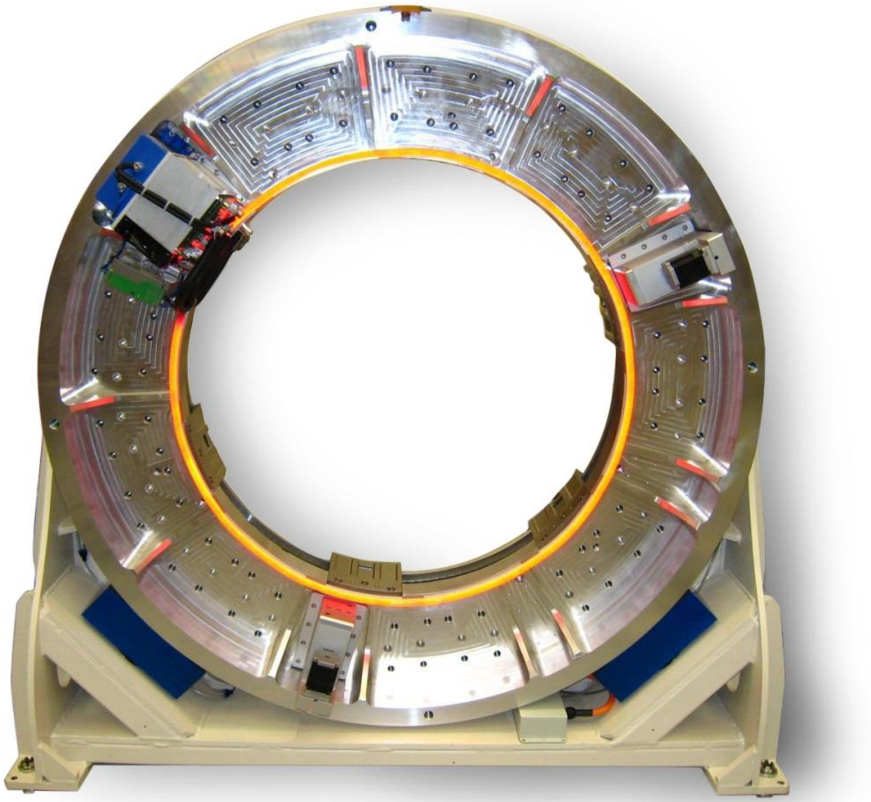

Demands on X-Ray Sources

- Tube voltages from 70 to 150 kV in steps of 10 kV
- High instantaneous power levels (typ. 50 to 120 kW)
- High tube currents at low kV (good for Iodine contrast)
- High continuous power levels (typ. > 5 kW)
- High cooling rates (typ. about 25 kW ≈ 1 MHU/min*)
- High tube current variation (low inertia)
- Must withstand centrifugal forces
  - Centrifugal acceleration at 550 mm with 0.5 s: $a = 9\,g$
  - with 0.4 s: $a = 14\,g$
  - with 0.3 s: $a = 25\,g$
  - with 0.2 s: $a = 55\,g$
- Compact and robust design
- Long service intervals
  - Ball bearings cannot be lubricated and wear out early
  - Liquid bearings to be preferred (also due to good heat conduction)

* 1 MHU = $\sqrt{2}$ MJ

Tube Technology

conventional tube

(rotating anode, helical wire emitter)

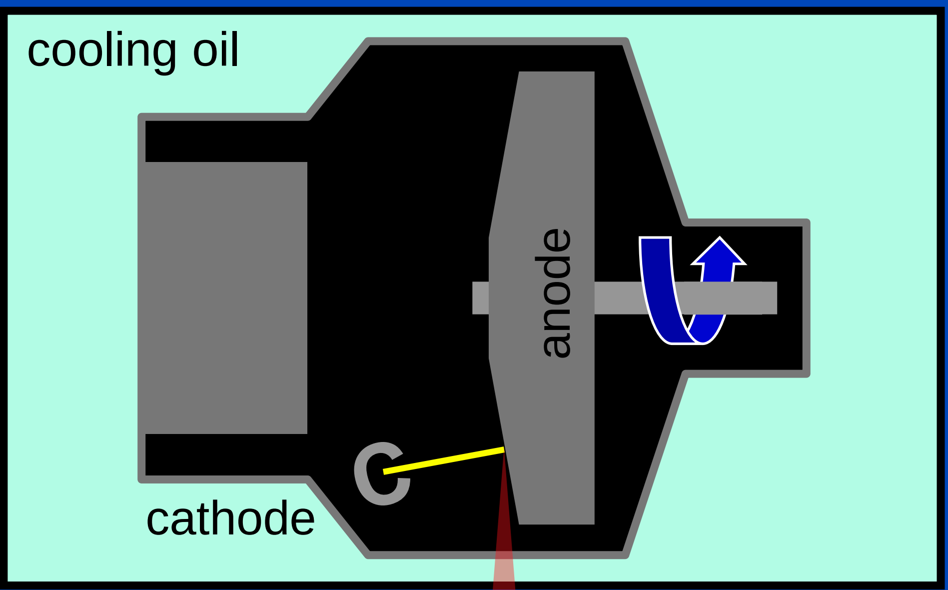

Photo courtesy of GE

Anode at high temperature (>> 1000 °C)

Radiative cooling ($\propto T^4$) is dominant

high performance tube

(rotating cathode, anode + envelope, flat emitter)

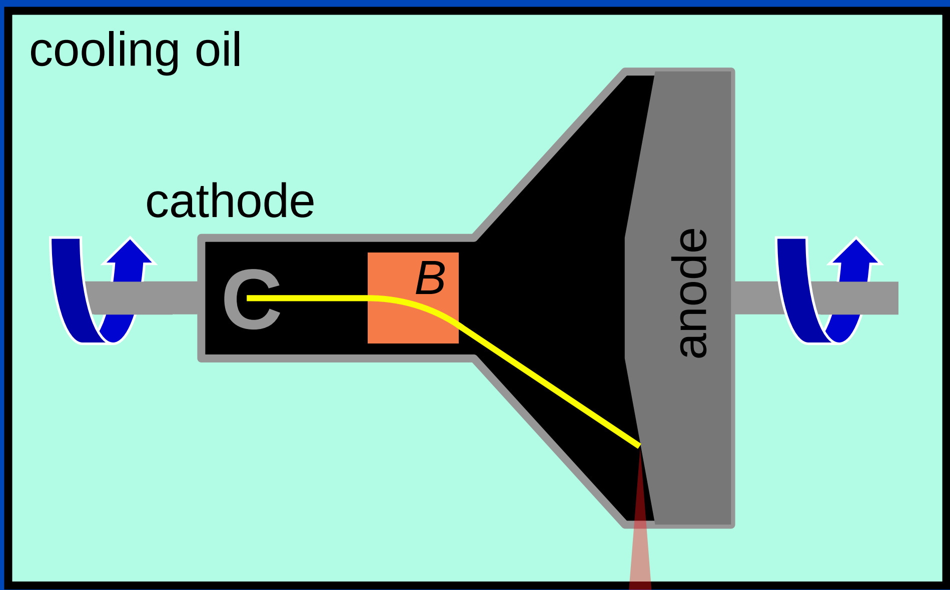

Photo courtesy of Siemens

Anode at low temperature (<< 1000 °C)

Conductive cooling ($\propto T$) is dominant

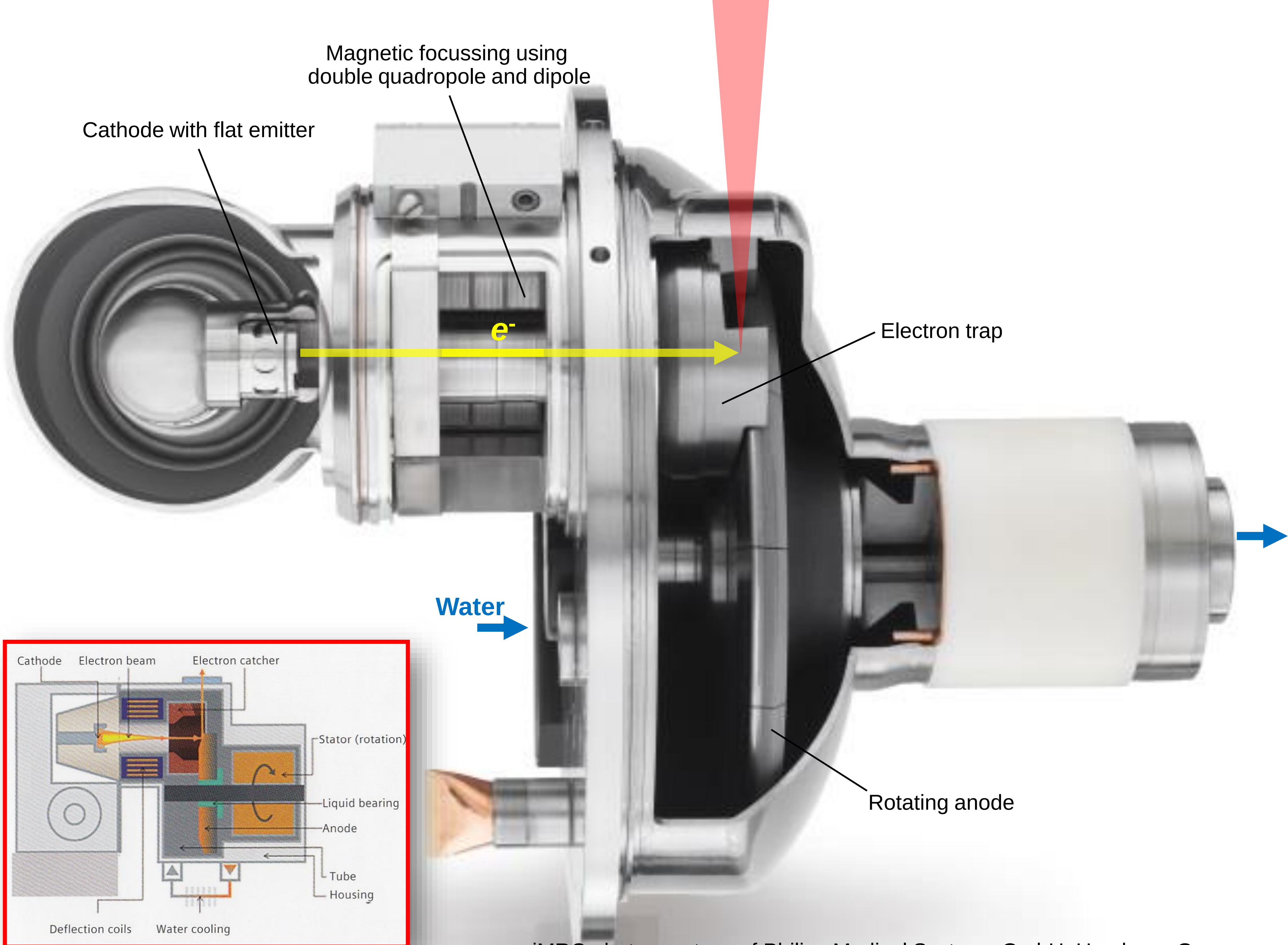

iMRC photo courtesy of Philips Medical Systems GmbH, Hamburg, Germany

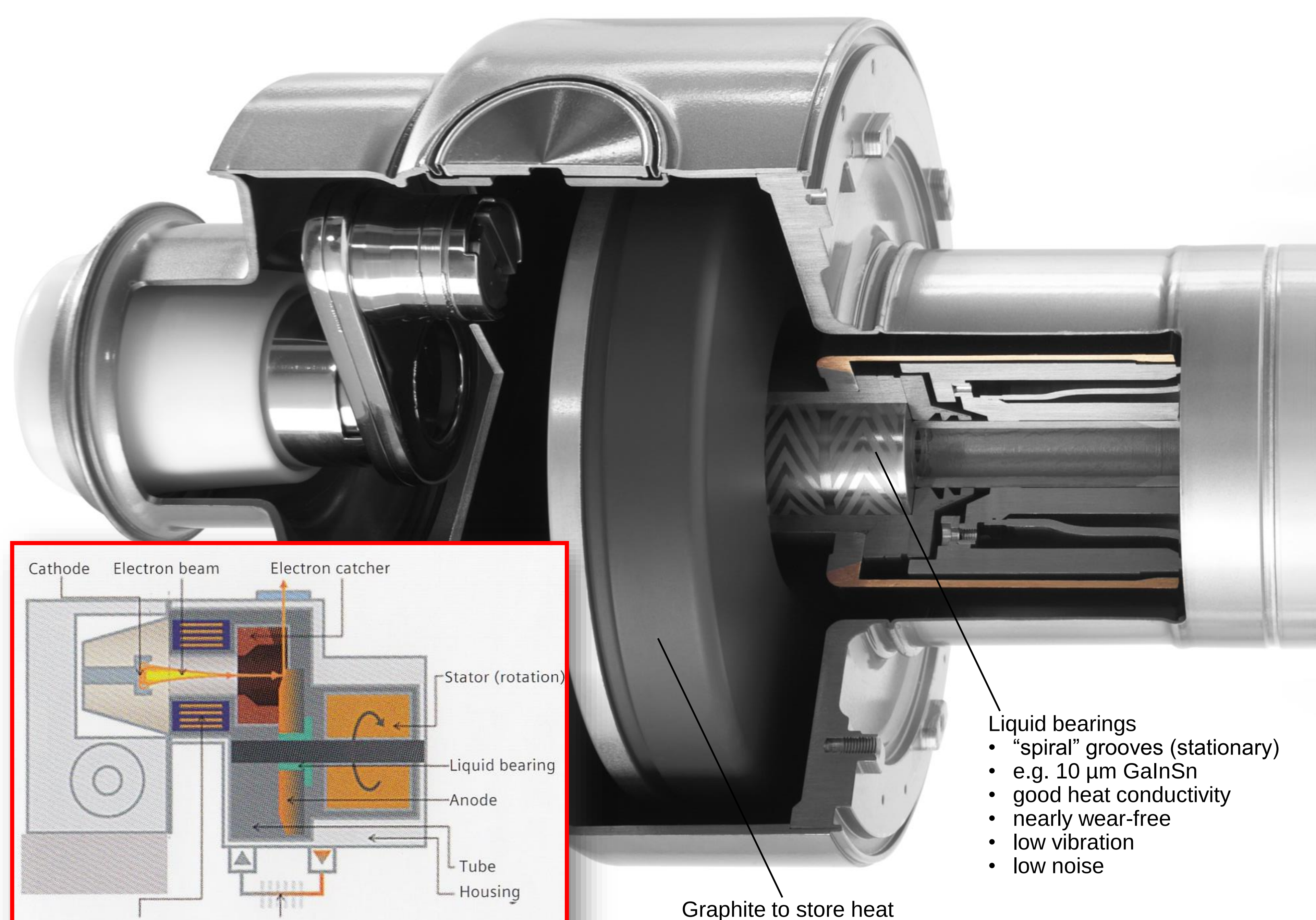

Courtesy of Philips Medical Systems GmbH, Hamburg, Germany

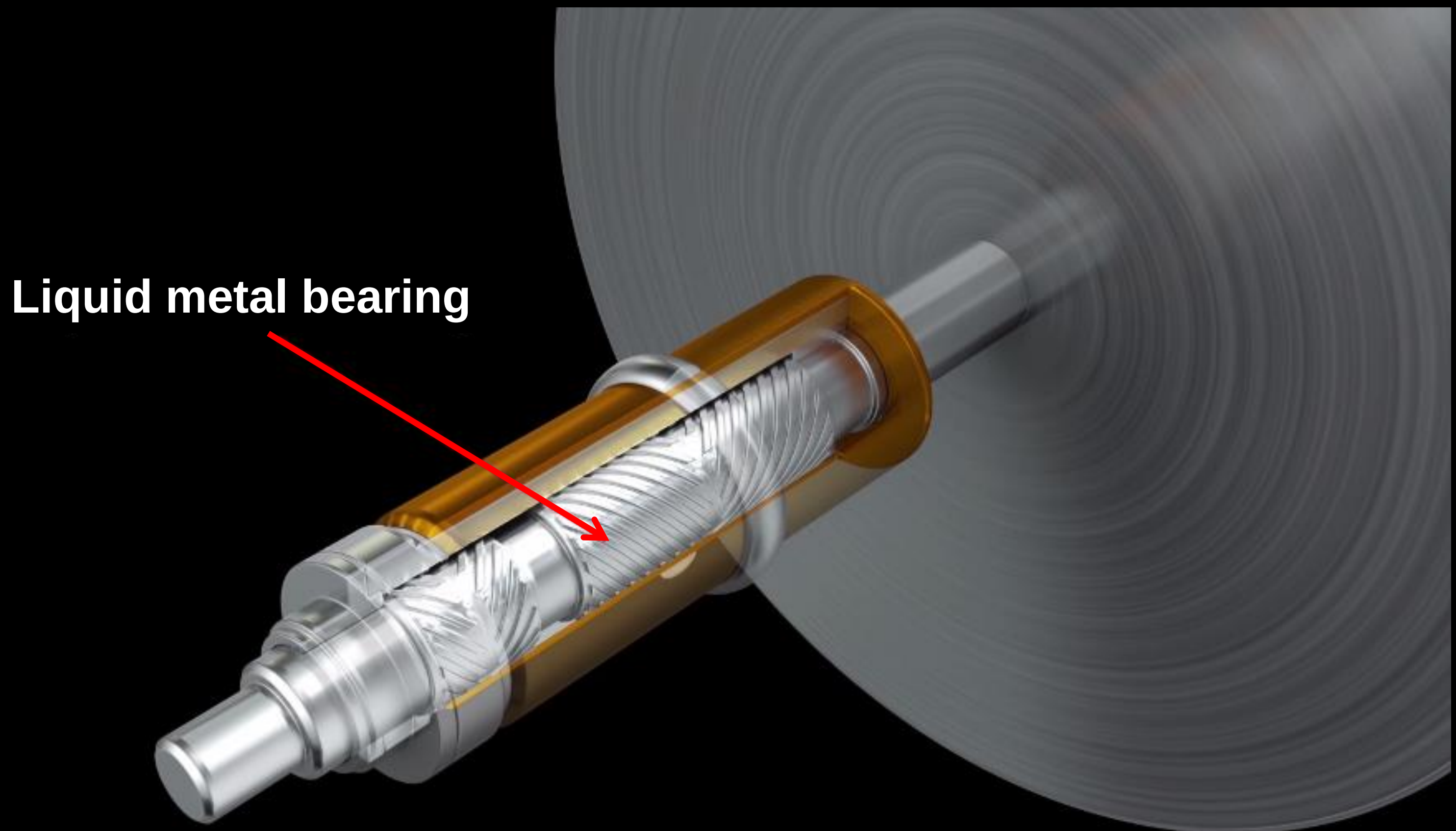

Courtesy of Canon Medical Systems, USA

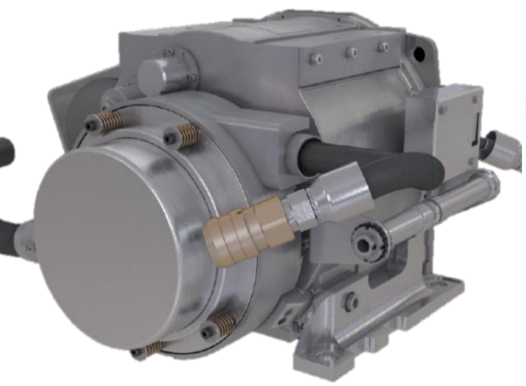

Performix HDw (GE)

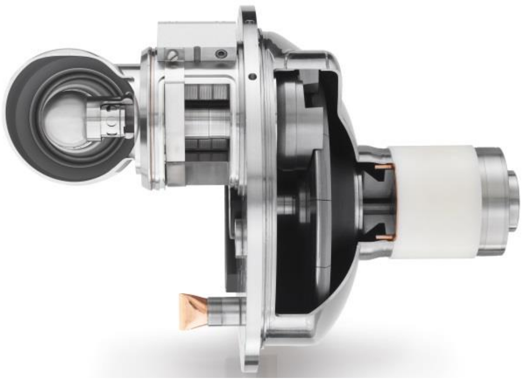

iMRC (Philips)

Straton (Siemens)

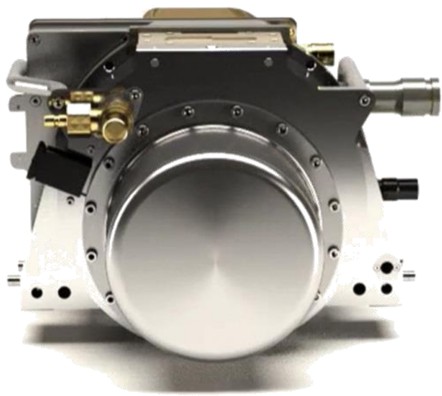

Vectron (Siemens)

Straton vs. Vectron at all kV

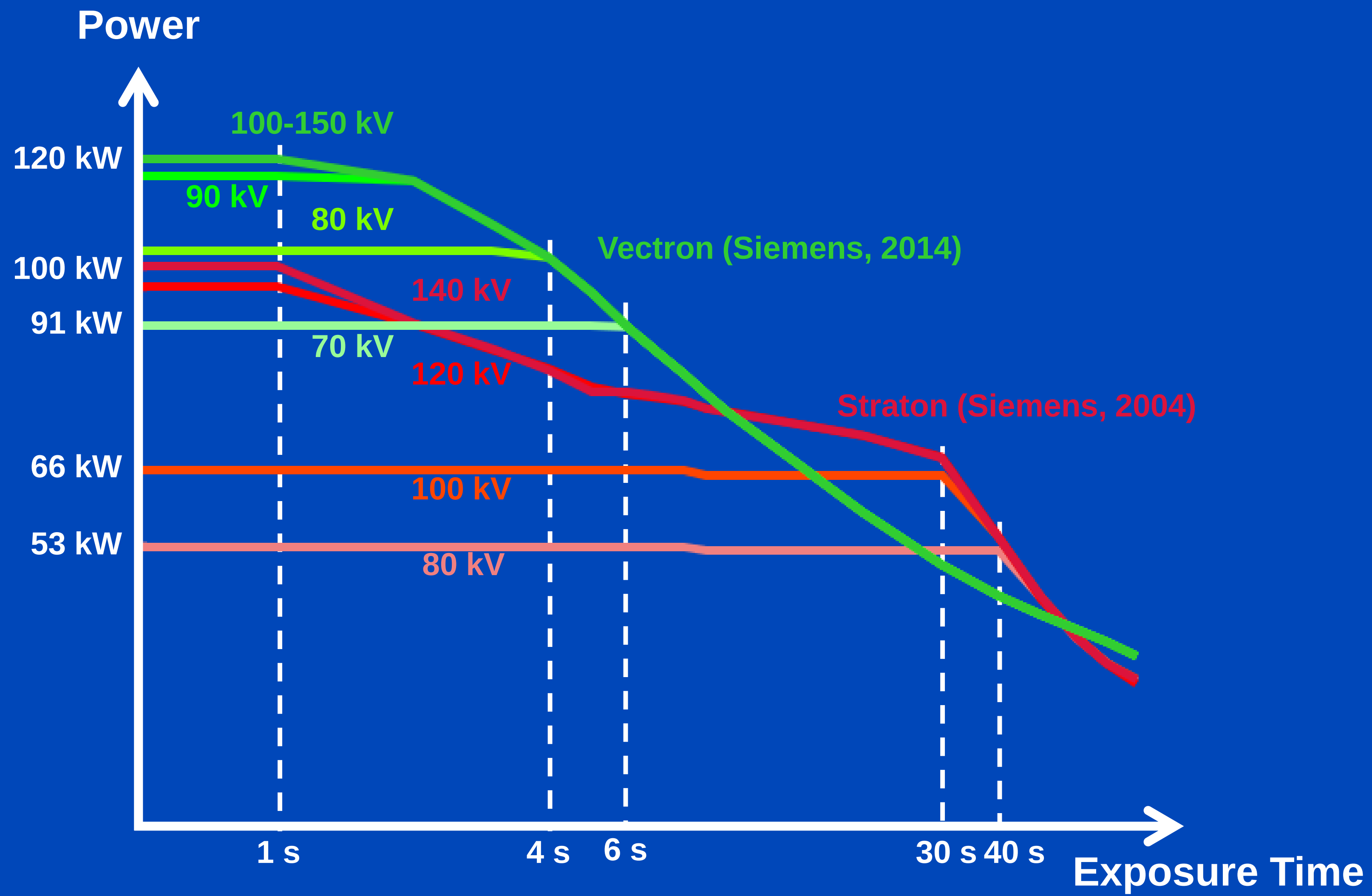

Tube Voltage 80 kV

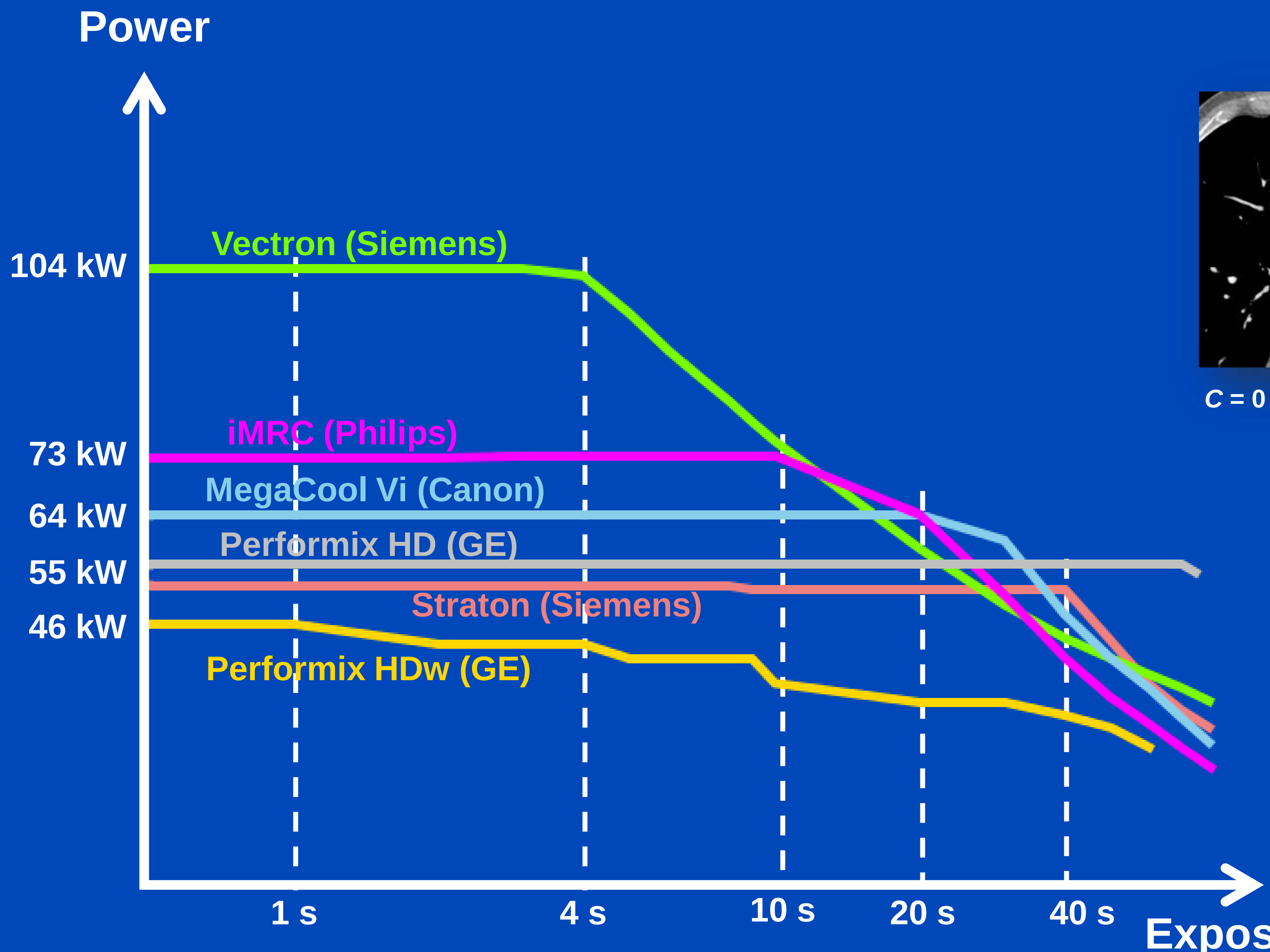

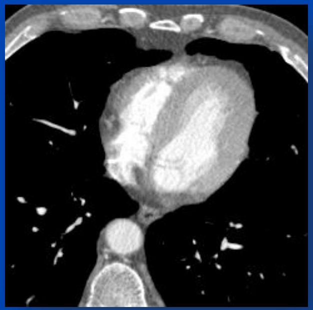

C = 0 HU, *W* = 700 HU

Tube Voltage 120 kV

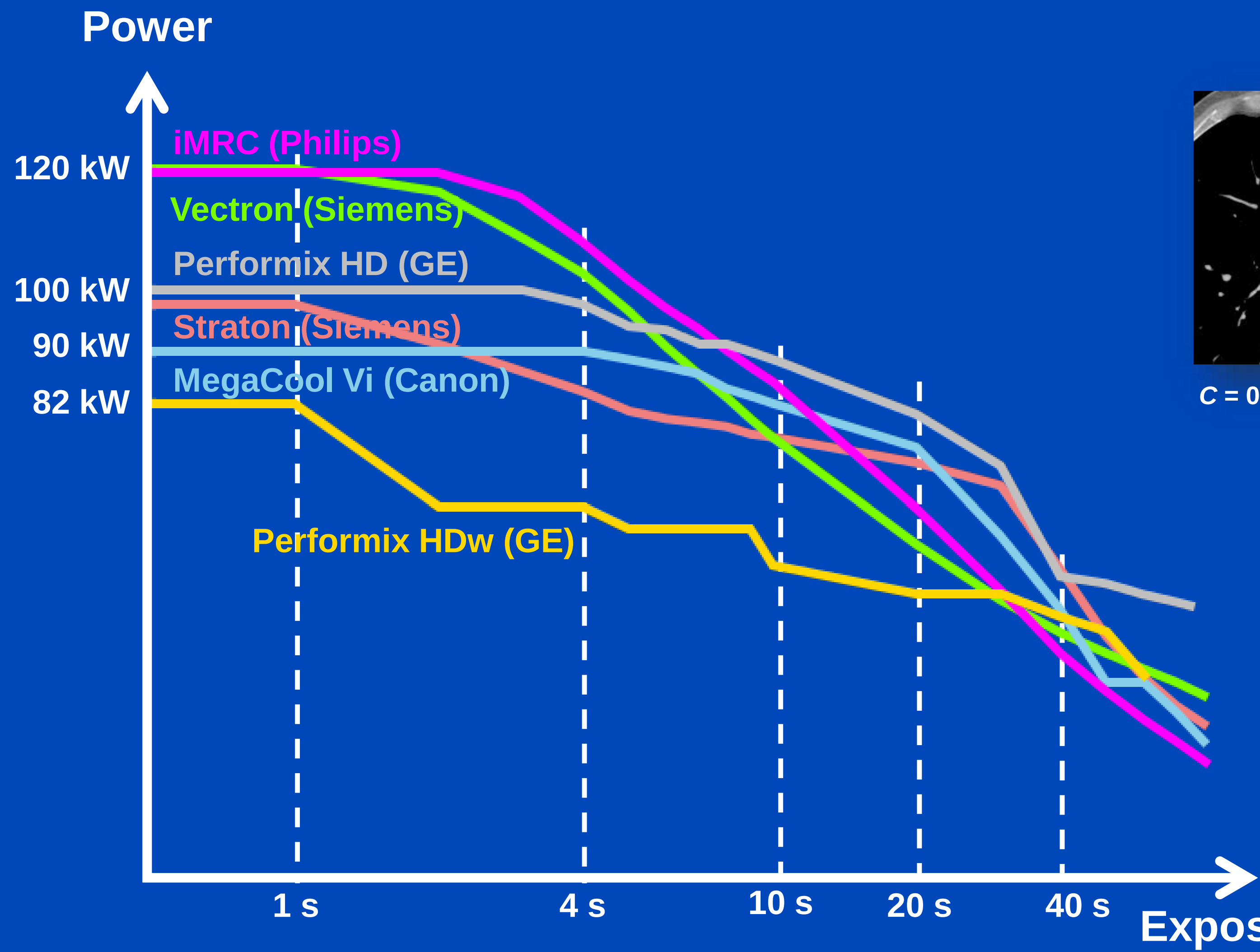

C = 0 HU, W = 700 HU

Naeotom Alpha (Vectron): Std vs. UHR

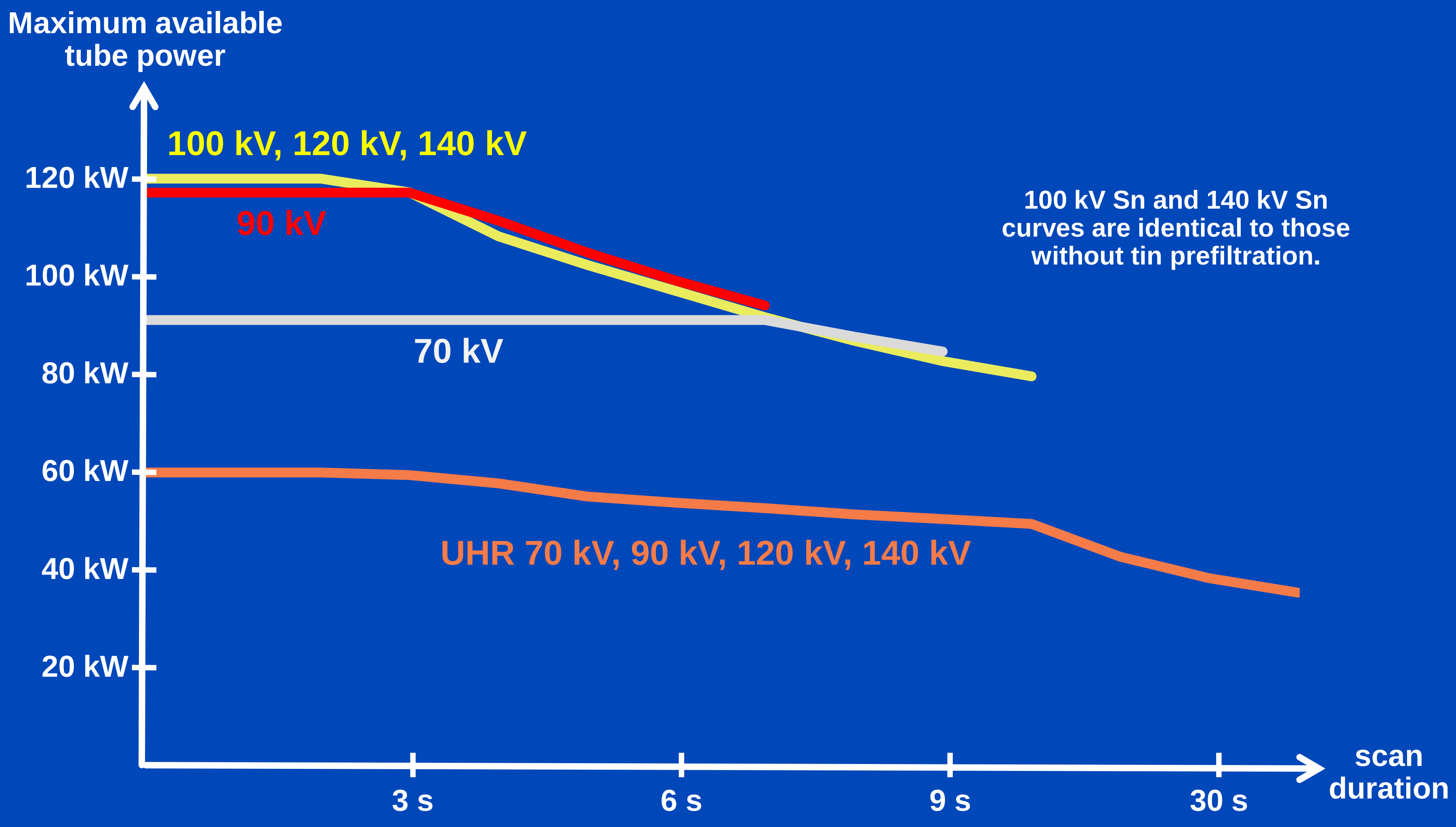

Narrow Cone = High Tube Power

Wide Cone = Low Tube Power

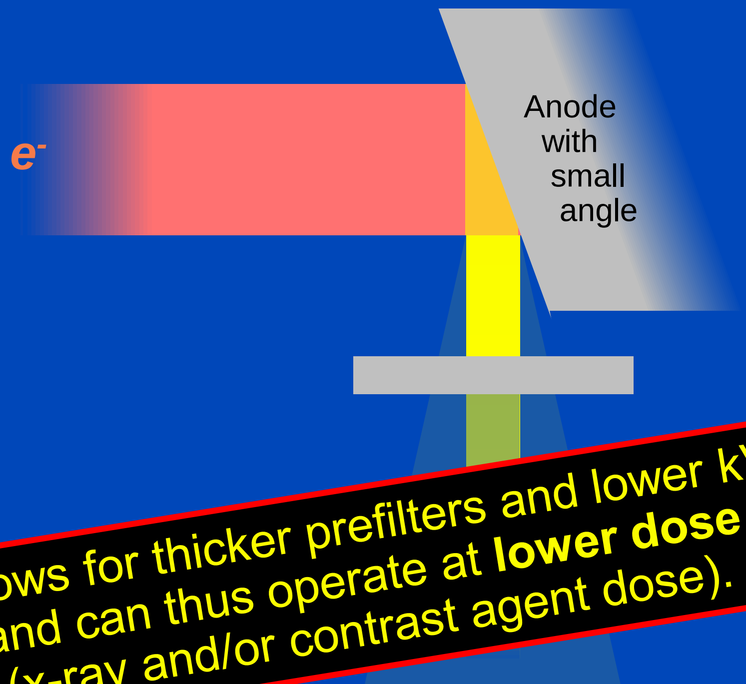

Allows for thicker prefilters and lower kV and can thus operate at **lower dose** (x-ray and/or contrast agent dose).

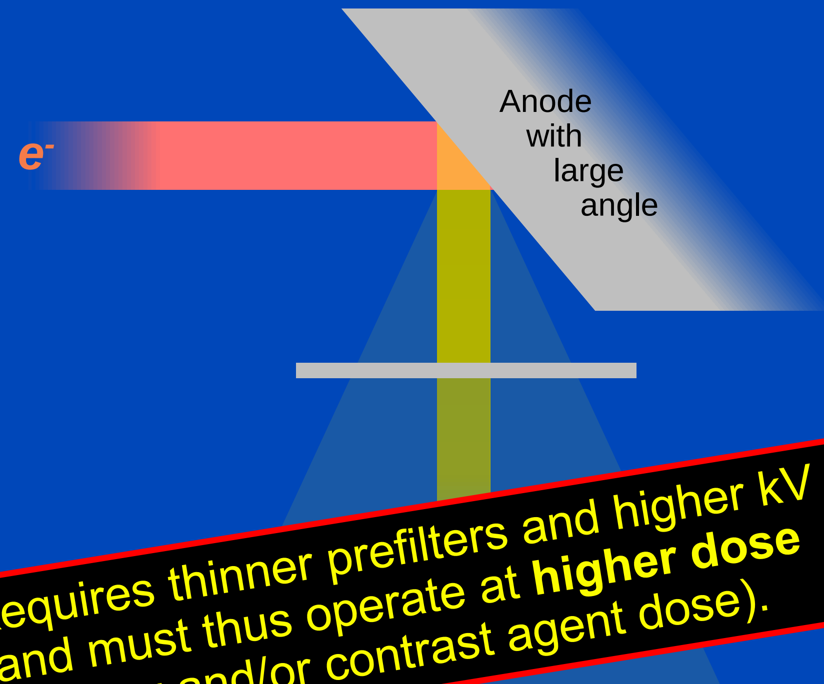

Requires thinner prefilters and higher kV and must thus operate at **higher dose** (x-ray and/or contrast agent dose).

… at the same spatial resolution

Onset of target melting (rule of thumb)[1]: 1 W/µm

[1] D.E. Grider, A. Writh, and P.K. Ausburn. Electron Beam Melting in Microfocus X-Ray Tubes. J. Phys. D: Appl. Phys 19:2281-2292, 1986

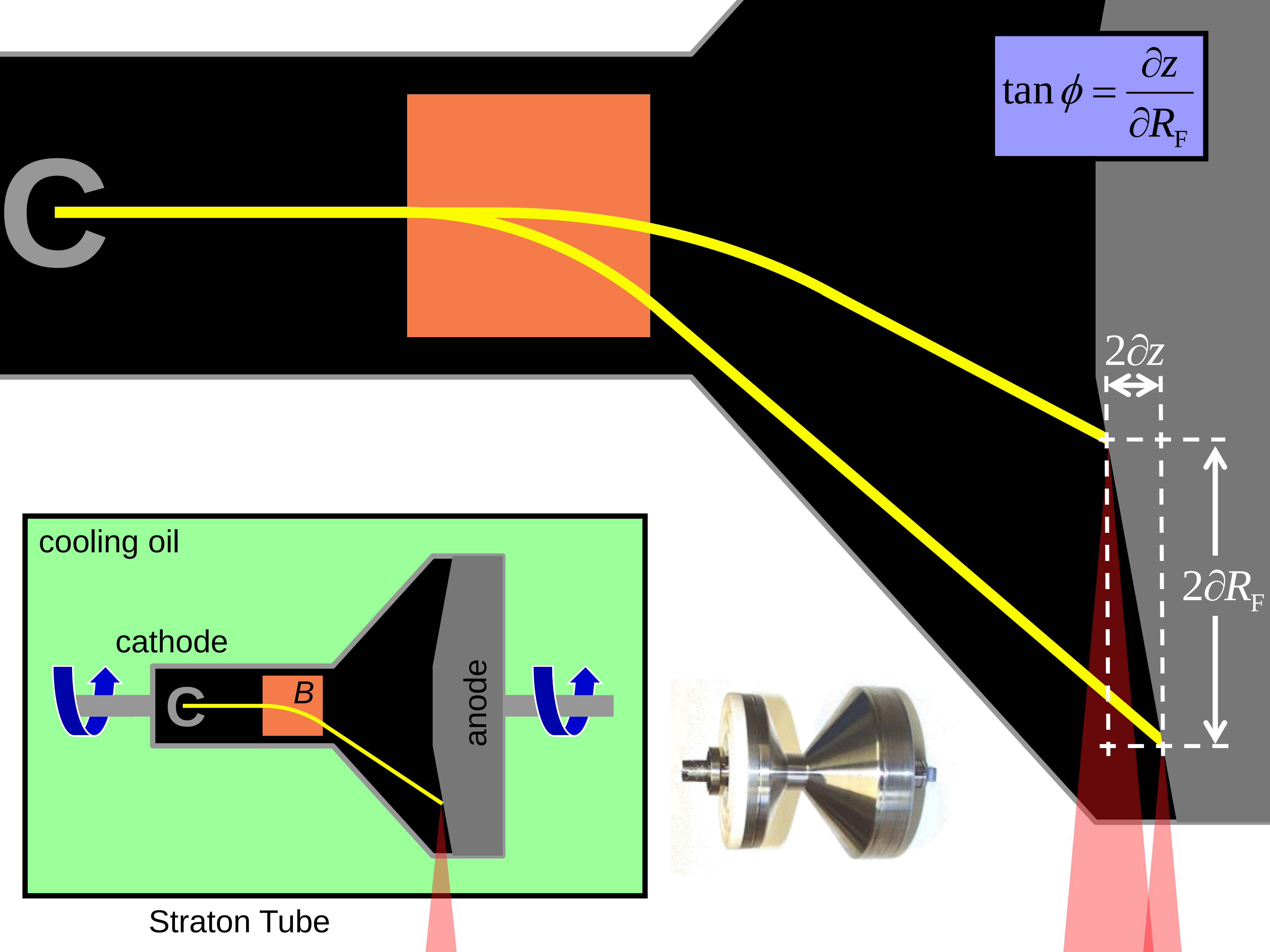

$\tan\phi = \frac{\partial z}{\partial R_F}$
C
$2\partial z$
$2\partial R_F$
cooling oil
cathode
C
B
anode
Straton Tube

αFFS and zFFS

- The flying focal spot (FFS) can be used to improve the in-plane (lateral) sampling as well as the through-plane (longitudinal) sampling.

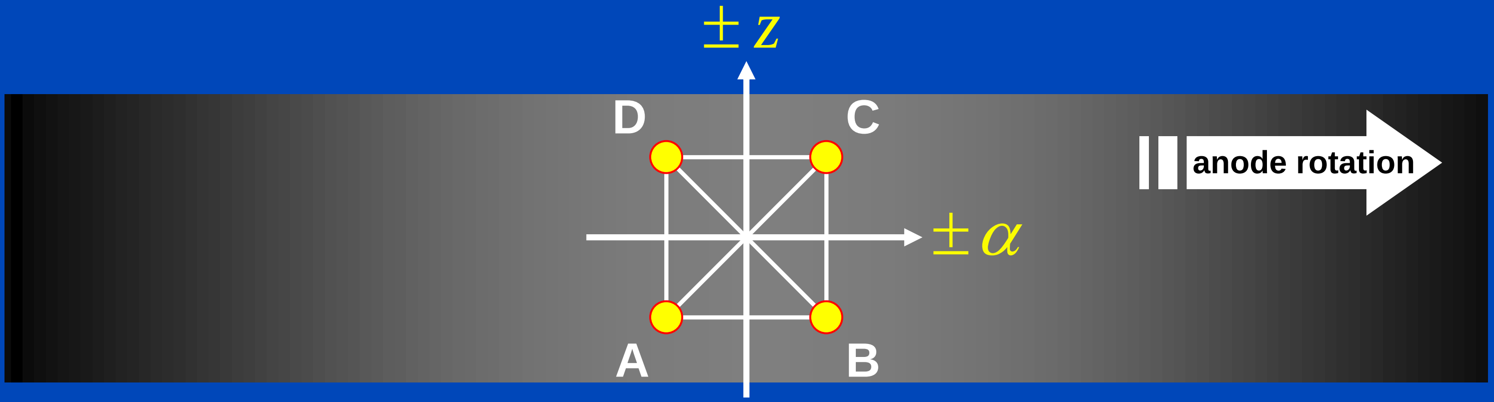

Anode as viewed from the isocenter

αFFS

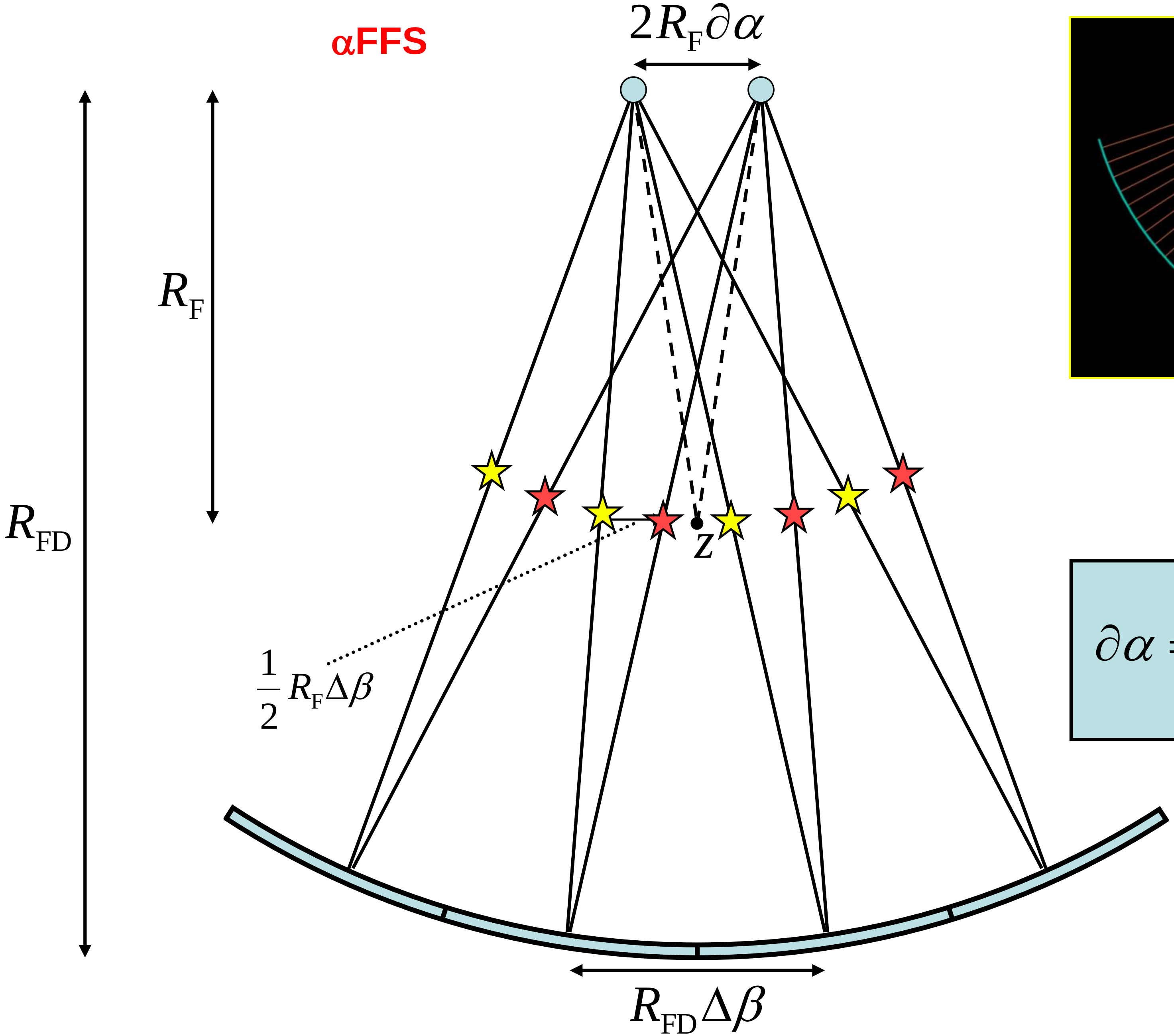

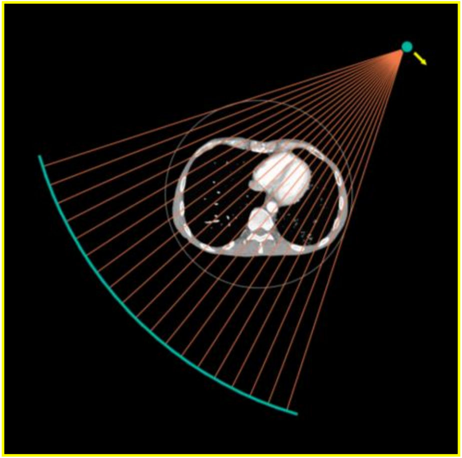

$$\partial\alpha = \frac{1}{4}\Delta\beta\frac{R_{FD}}{R_D}$$

zFFS

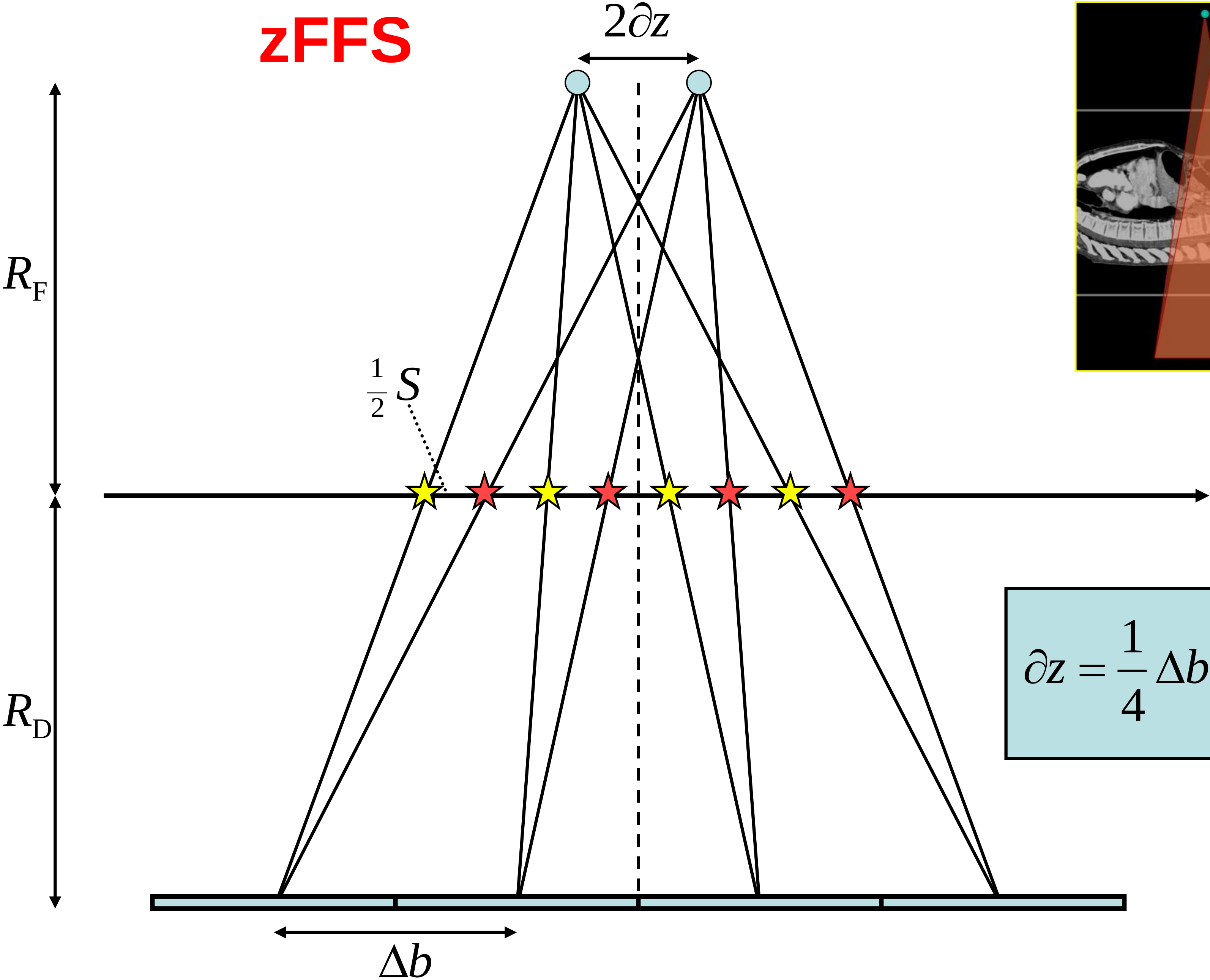

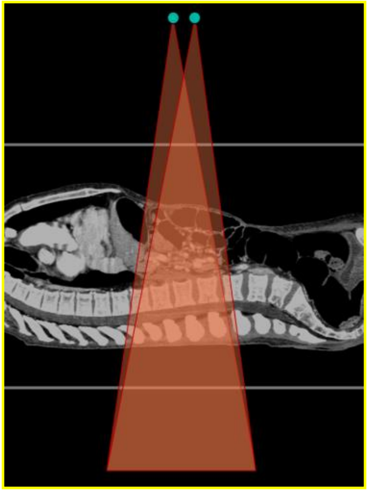

$$\partial z = \frac{1}{4} \Delta b \frac{R_F}{R_D}$$

Rows vs. Slices

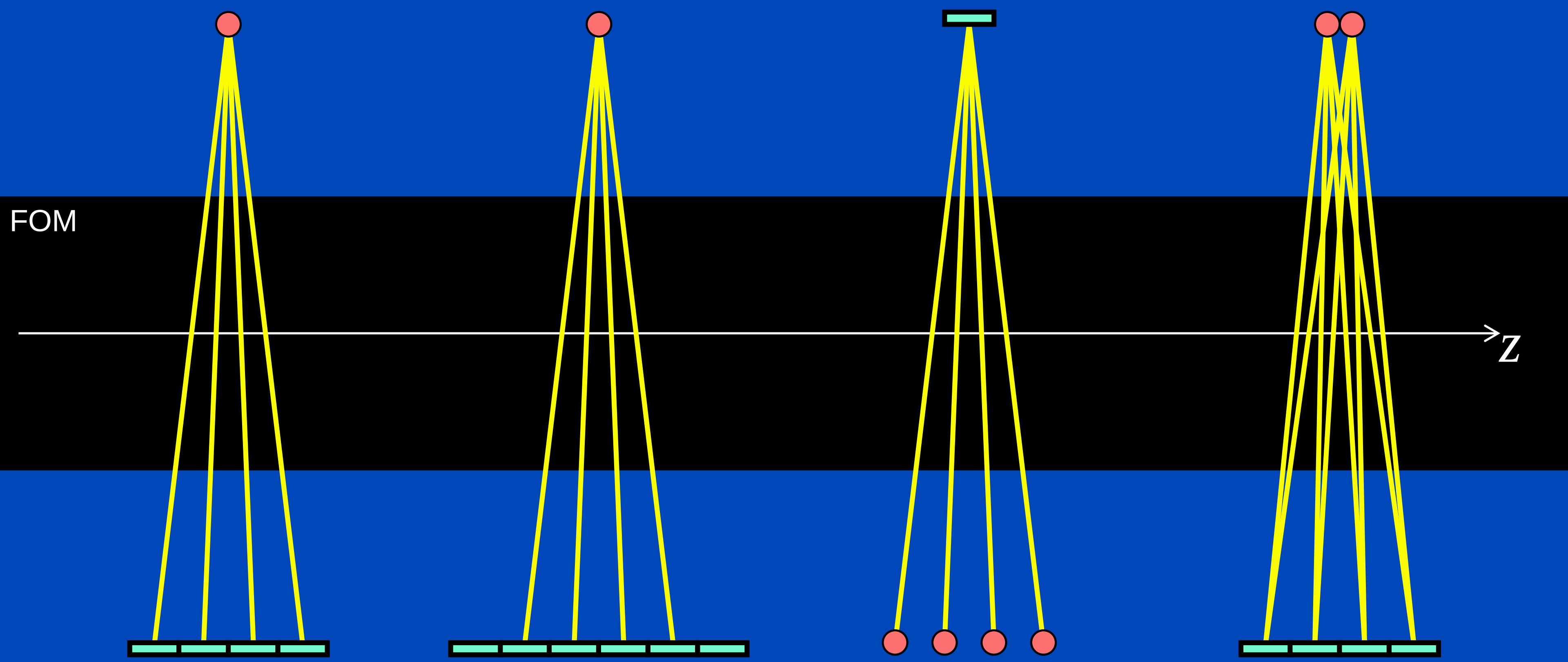

4 Rows
4 Slices

$M = 1 \cdot 4$

6 Rows
4 Slices

$M = 1 \cdot 4$

1 Rows
4 Slices

$M = 4 \cdot 1$

4 Rows
8 Slices

$M = 2 \cdot 4$

CT Detectors

- CT started with scintillation detectors with photomultiplier tubes excited by caesium iodide (CsI) crystals.
- These were replaced during the 1980s by ion chambers containing high-pressure xenon gas.
- These were replaced during the late 1990s by scintillation detectors with photodiodes excited by gadolinium oxysulfide (GOS, Gadox) crystal ceramics.
- These are being replaced since 2021 by direct converting energy-selective photon counting detectors based on cadmium telluride (CdTe) or cadmium zinc telluride (CZT) semiconductor technology.

Xenon Chambers

- High pressure inert gas (typ. xenon, about $25 \cdot 10^5$ Pa)
- Each pair of tungsten plates forms a detector cell
- Bias voltage (around 500 V) set to be below the avalange effect to ensure a linear relationship between the x-ray intensity and the signal.
- If set properly, the amount of ionization is proportional to the energy of the absorbed x-ray photons.
- Pros
  - Low cost
  - No radiation damage
  - Small scatter acceptance angle
- Cons
  - Difficult to have 2D arrays
  - Low quantum efficiency even if the cells are as deep as 10 cm, around 60% or 70% (compared to 99% of solid state detectors, whose geometrical efficiency is 80%)

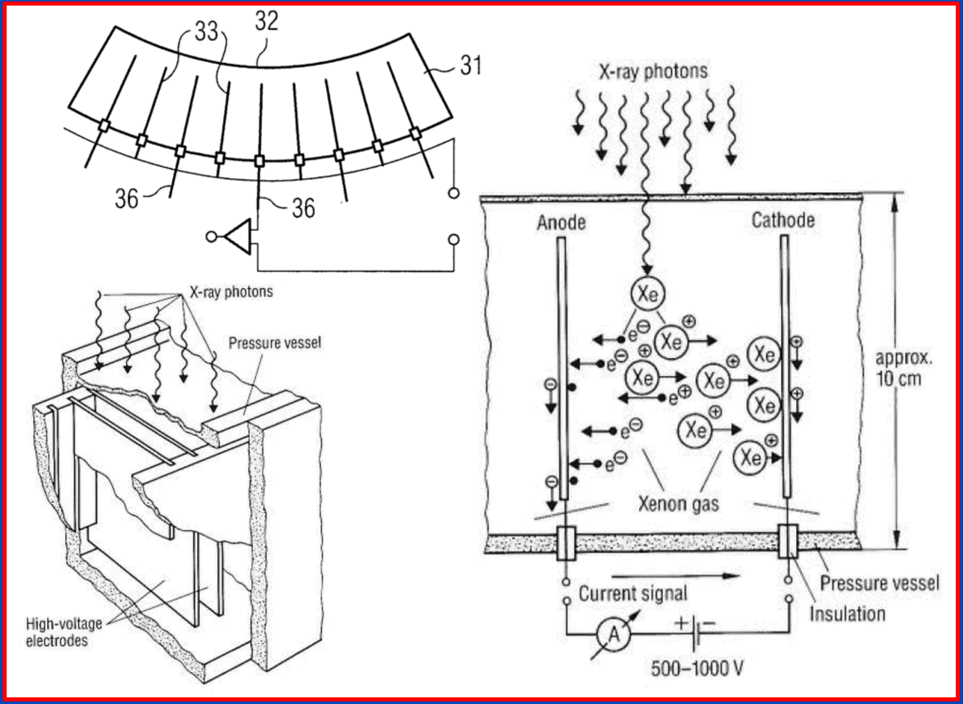

Demands on CT Detector Technology

- Available as multi-row arrays
- Very fast sampling (typ. 300 µs)
- Favourable temporal characteristics (decay time < 10 µs)
- High absorption efficiency
- High geometrical efficiency
- High count rate (up to 10^9 cps*)
- Adequate dynamic range (18 to 22 bit)
- Signal stability (better than 0.1%)

* in the order of 10^5 counts per reading and 10^4 readings per second

Detector Technology

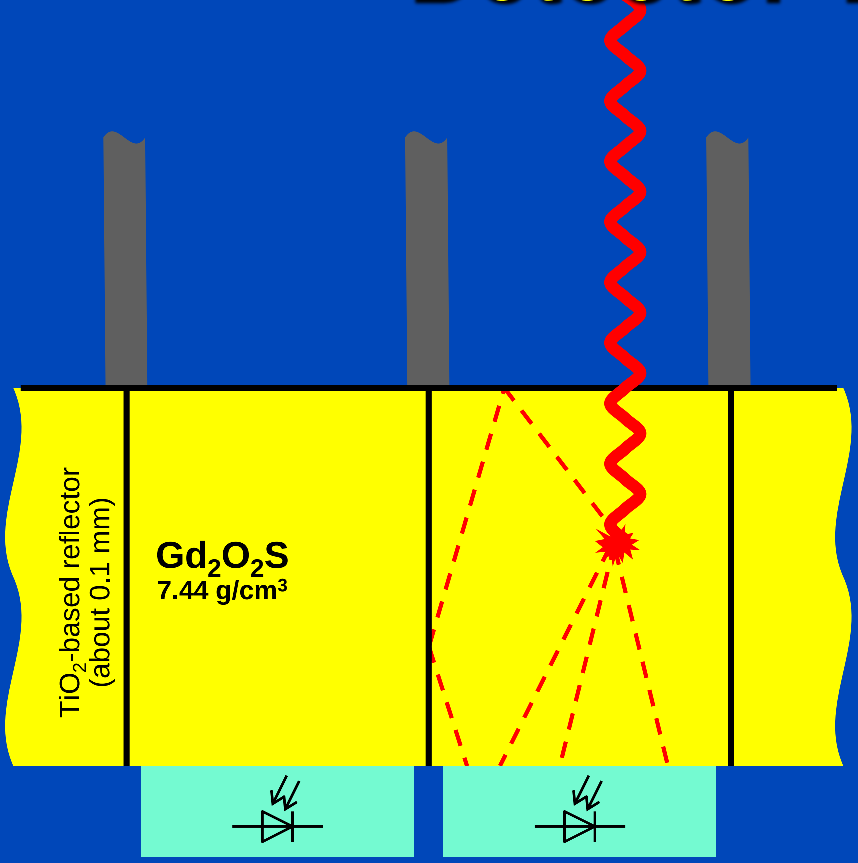

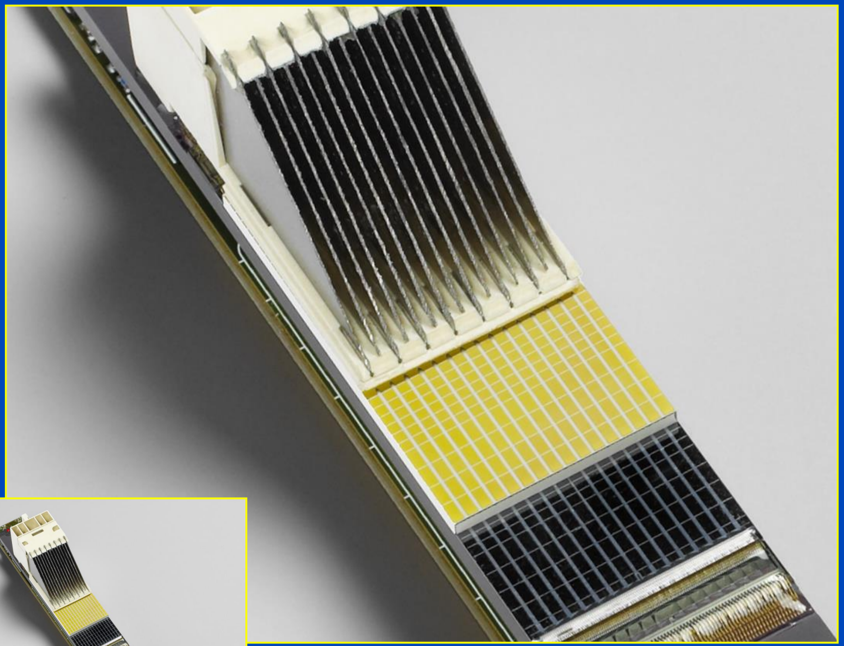

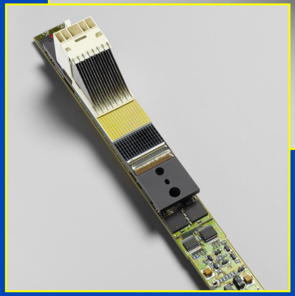

Photo courtesy of Siemens Healthcare, Forchheim, Germany

Clinical CT Detector

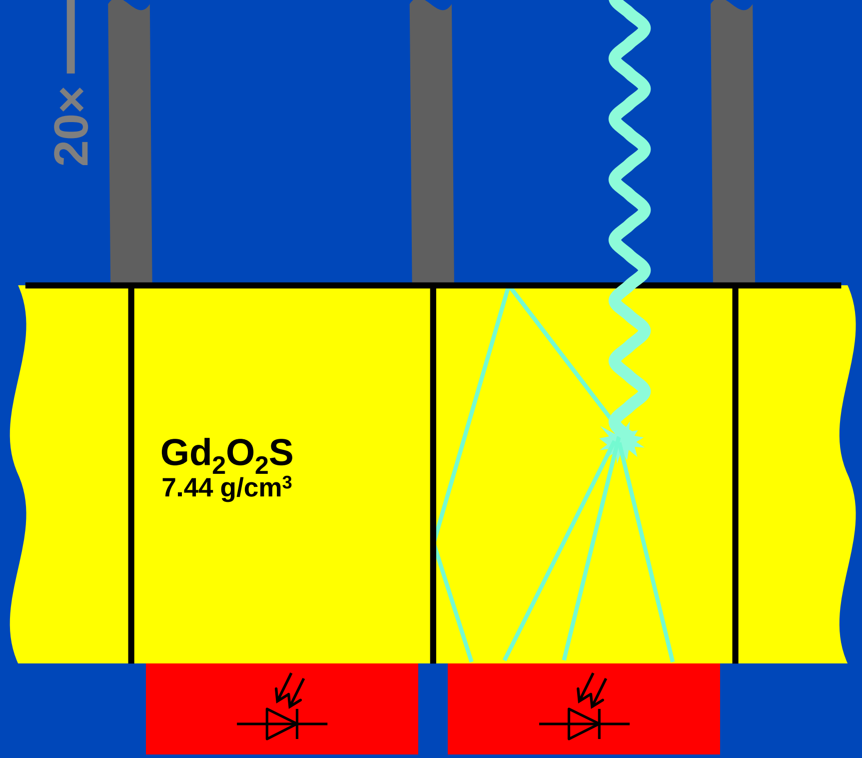

Flat Detector (CBCT)

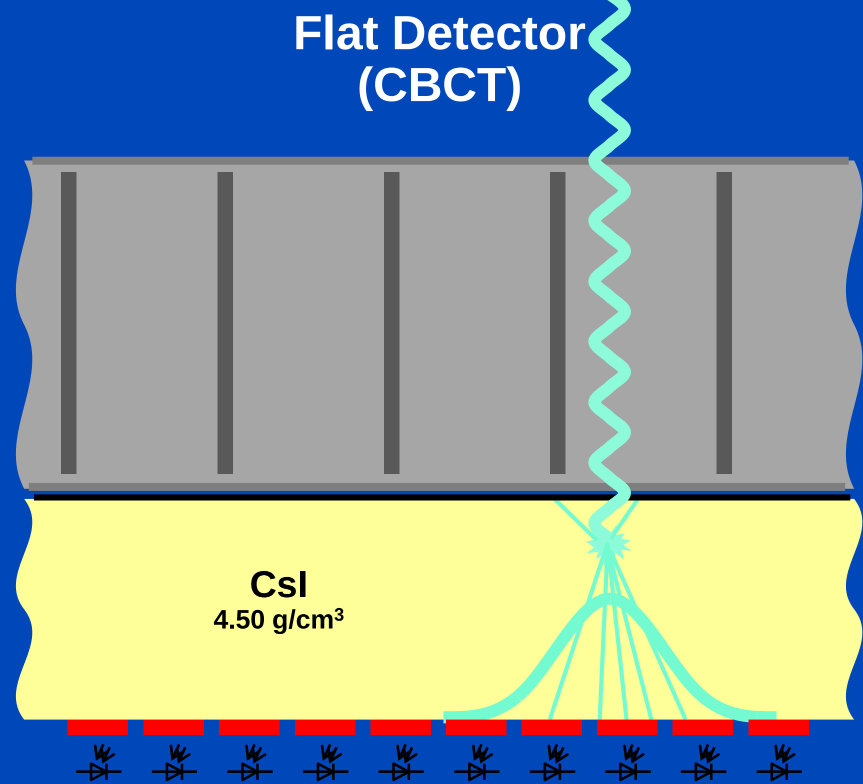

- Anti-scatter grids are aligned to the detector pixels
- Anti-scatter grids reject scattered radiation
- Detector pixels are of about 1 mm size
- Detector pixels are structured, reflective coating maximizes light usage and minimizes cross-talk
- Thick scintillators improve dose usage
- Gd_2O_2S is a high density scintillator with favourable decay times
- Individual electronics, fast read-out (5 kHz)
- Very high dynamic range (10^7) can be realized

- Anti-scatter grids are not aligned to the detector pixels
- The benefit of anti-scatter grids is unclear
- Detector pixels are of about 0.2 mm size
- Detector pixels are unstructured, light scatters to neighboring pixels, there is significant cross-talk
- Thick scintillators decrease spatial resolution
- CsI grows columnar and suppresses light scatter to some extent
- Row-wise readout is rather slow (e.g. 25 Hz)
- Low dynamic range ($<10^3$), long read-out paths

To Grid or not to Grid

- A common misbelieve is that a good or perfect scatter reduction software can be used instead of using anti scatter grids.
- This is wrong, as will be shown in the next slices.
- Facts:
  - Anti scatter grids are beneficial iff the SPR exceeds a certain threshold, i.e. for large cross-sections.
  - Scatter reduction software is always beneficial, with or without anti scatter grid.
  - Noise reduction software is always beneficial, with or without anti scatter grid.

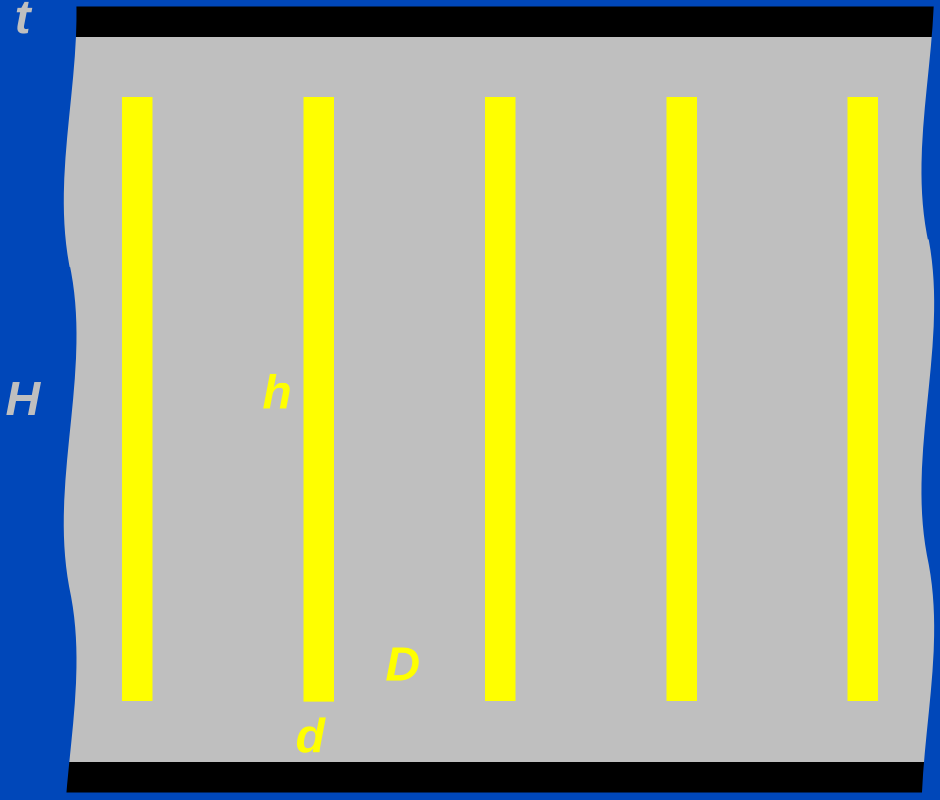

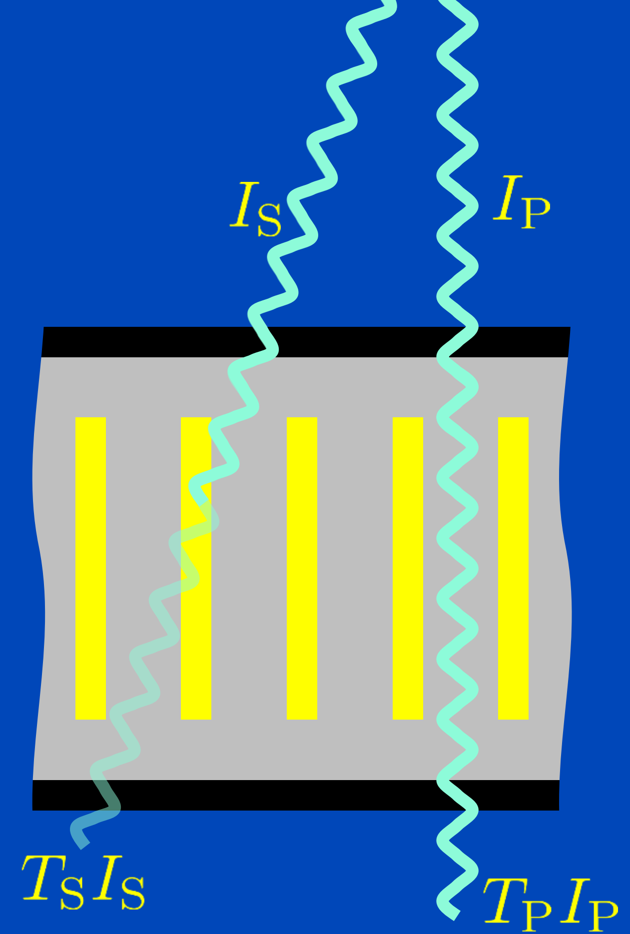

Cover thickness: *t*, e.g. 0.2 mm Al or 0.25 mm C
Height of strips: *h*
Thickness of strips: *d*, e.g. 0.04 mm Pb
Gap between strips: *D*, e.g Al or C-fiber
Grid ratio: *h/D, e.g. 8 or 15*
Grid frequency: 1/(*D*+*d*), e.g. 40/cm
Geometrical efficiency: *D*/(*D*+*d*)
Height of interspace material: *H*

Primary intensity: I_P
Scatter intensity: I_S
Primary transmission: $T_P < 1$, e.g. 75%
Scatter transmission: $T_S > 0$, e.g. 30%

No grid: $T_P = T_S = 1$
Ideal grid: $T_P = 1$, $T_S = 0$

To Grid or not to Grid?

- Only primary counts for the signal, but primary and scatter count for noise. Thus,

$$\mathrm{SNR} = \frac{T_\mathrm{P} I_\mathrm{P}}{\sqrt{T_\mathrm{P} I_\mathrm{P} + T_\mathrm{S} I_\mathrm{S}}}$$

- SNR improvement factor (SNR with grid / SNR no grid)

$$\mathrm{SNR}_\mathrm{if} = T_\mathrm{P} \frac{\sqrt{I_\mathrm{P} + I_\mathrm{S}}}{\sqrt{T_\mathrm{P} I_\mathrm{P} + T_\mathrm{S} I_\mathrm{S}}}$$

- The case $T_\mathrm{S} = 0$ is instructive and yields

$$\mathrm{SNR}_\mathrm{if} \le \sqrt{T_\mathrm{P}}\sqrt{1 + \mathrm{SPR}}$$

  with SPR being the scatter-to-primary ratio.
- Use a grid only for cases with $\mathrm{SNR}_\mathrm{if} \ge 1$.
- Scatter correction and noise reduction algorithms are to be used complementary and not as an alternative to grids!

dkfz.

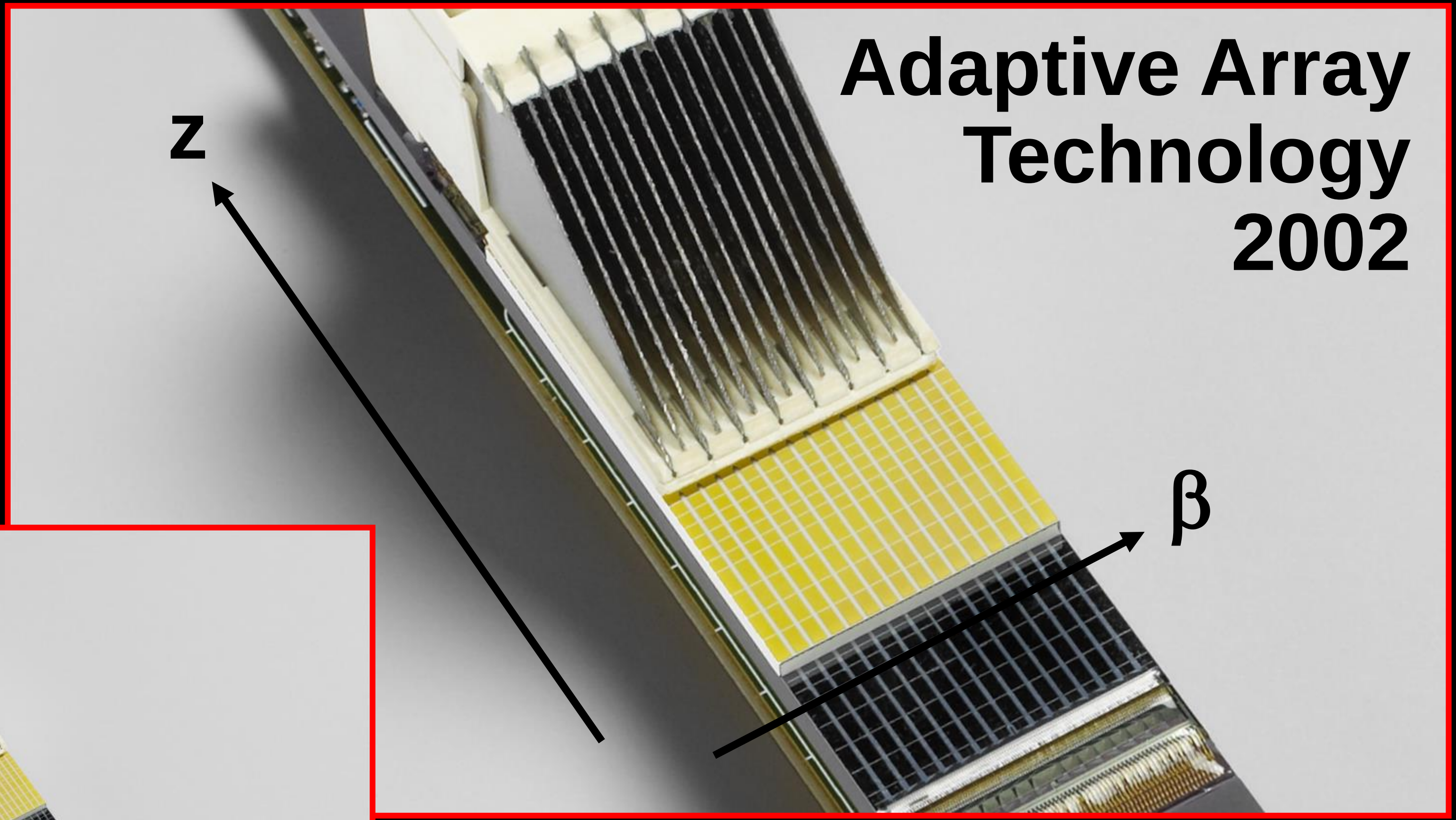

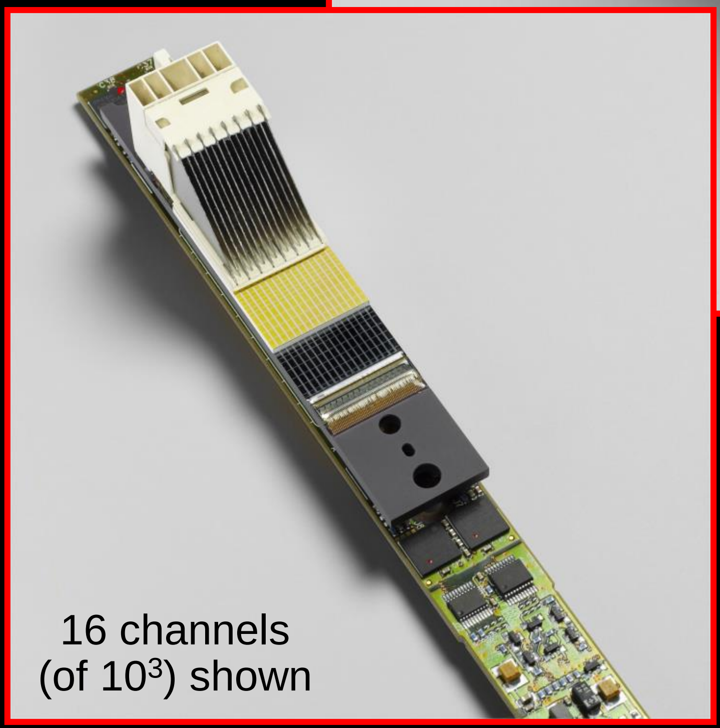

Photo courtesy of Siemens Healthcare, Forchheim, Germany

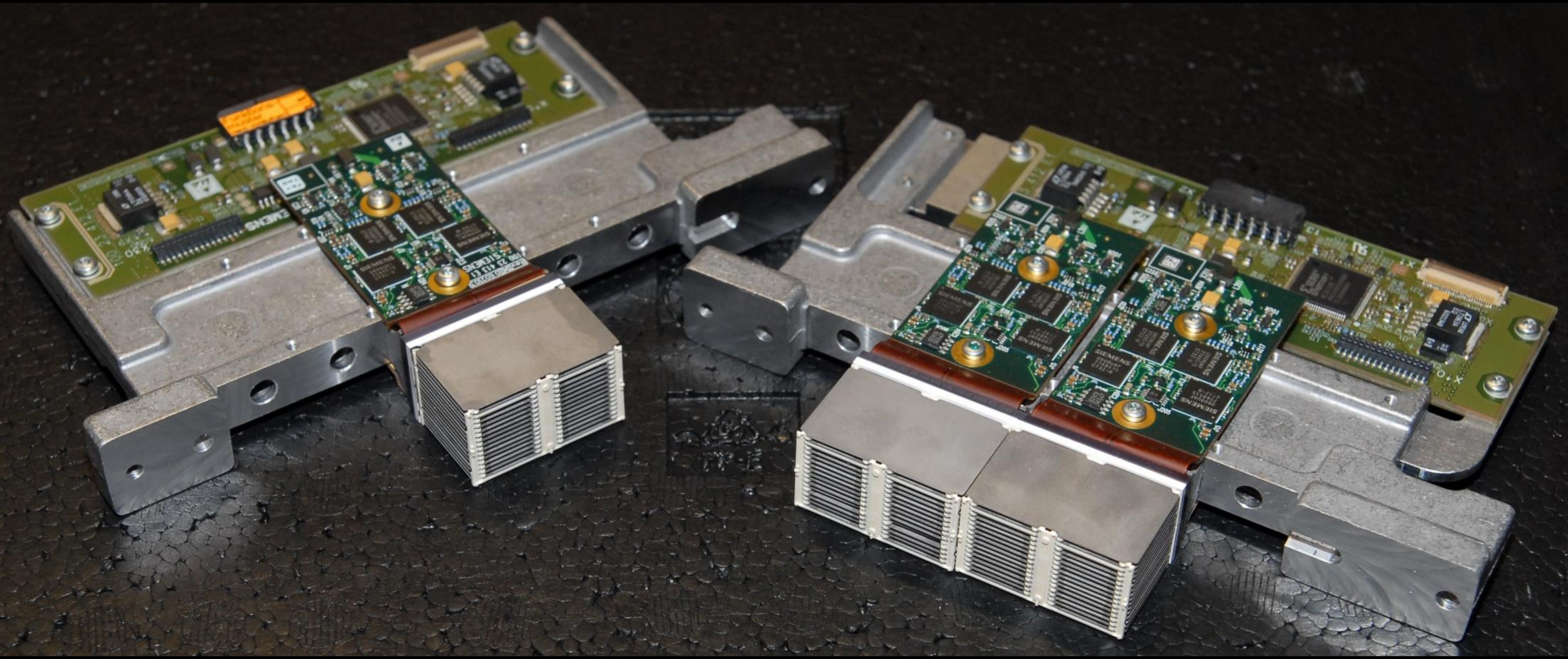

modular and 2D tileable, 1D anti-scatter grid, modules arranged on the surface of a cylinder segment (Photo courtesy by Siemens)

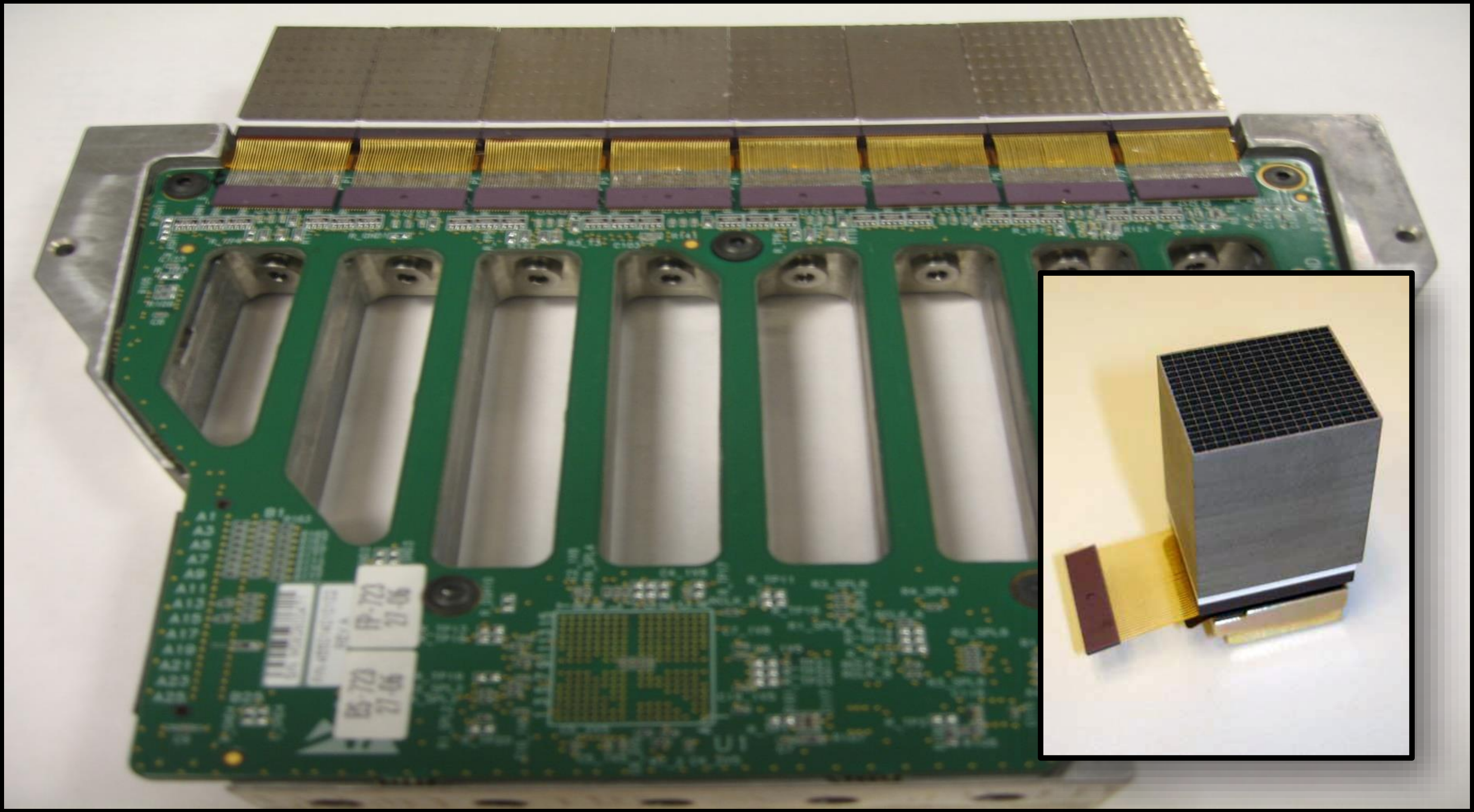

“Nano-panel detectors”, modular and 2D tileable, focussed 2D anti scatter grid
(Photo courtesy by Philips)

Fully Integrated Detector Electronics

- Electronics fully integrated into detector
- Very low electronic noise
- Less dose for infants, better images for obese

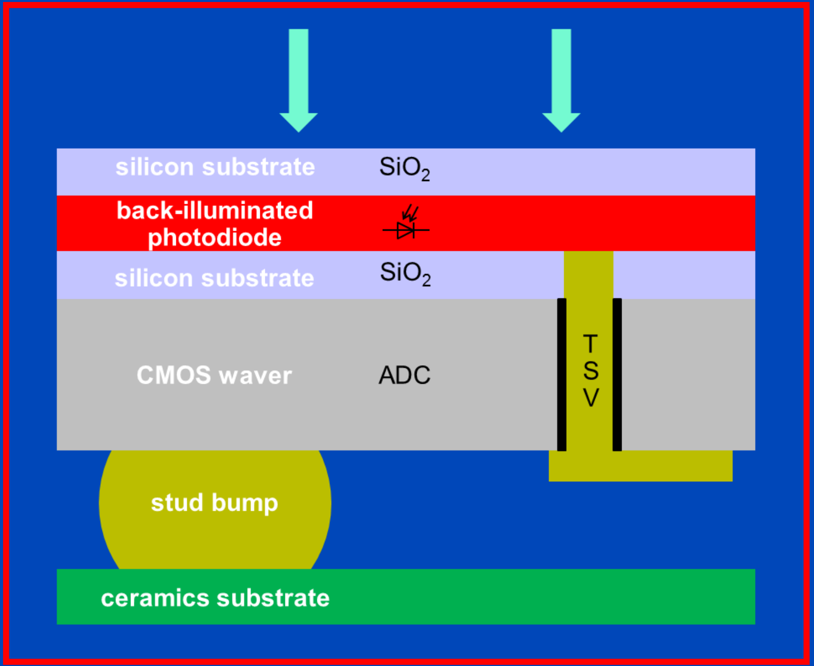

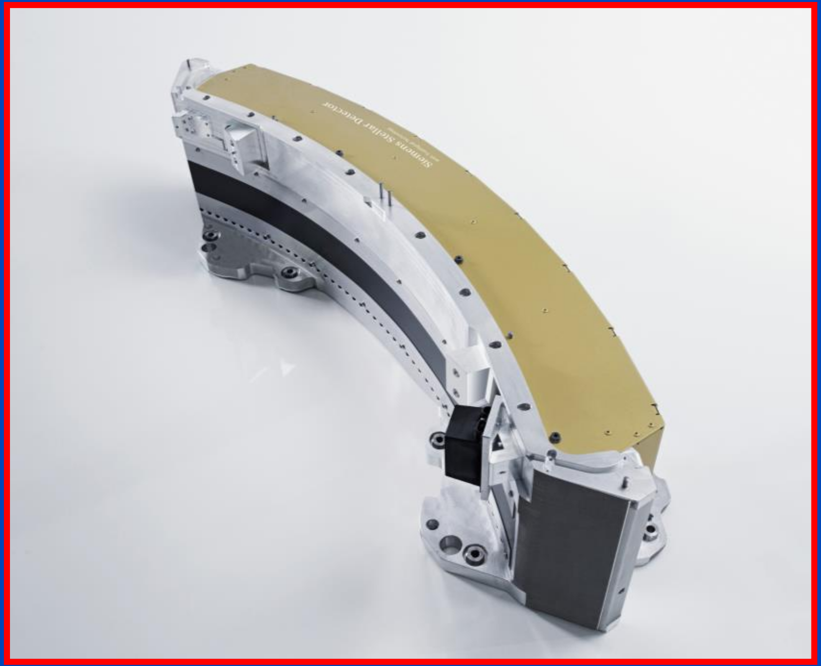

"Stellar detector", modular and 2D tileable, focussed 2D anti scatter grid. Photo courtesy by Siemens.

“Stellar detector”, modular and 2D tileable, focussed 2D anti scatter grid. Photo courtesy by Siemens.

Ultra High Resolution Scans

- With energy integrating detectors UHR requires[1,2]
  - detector comb or detector grid
  - αFFS and/or zFFS
- Realizations
  - Somatom Flash and Force comb (0.61 mm → 0.33 mm)
  - Somatom Flash grid (0.61 mm → 0.33 mm and 0.56 mm → 0.53 mm)
- Dose loss
  - about 50% with comb (46% + penumbra for Flash or Force)
  - about 75% with grid (66% + penumbra for Flash)
- Dose penalty
  - about two-fold dose needed with comb
  - about three-fold dose needed with grid

Flash (0.7 mm × 0.8 mm focus)
- UHR: 1D comb
- zUHR: 2D grid

Force (0.4 mm × 0.5 mm focus)
- UHR: 1D comb
- sUHR: 1D comb + z-deconv

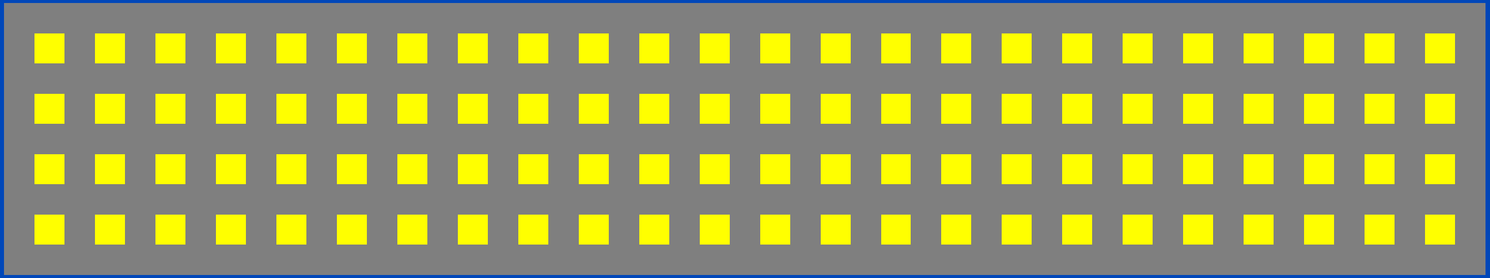

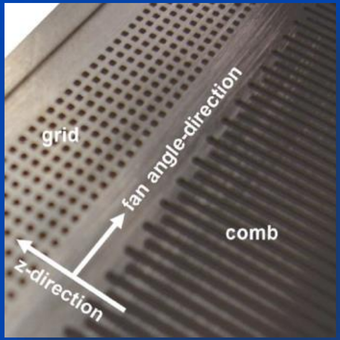

[1]Flohr et al. Novel ultrahigh resolution data acquisition and image reconstruction for multi-detector row CT. Med. Phys. 34(5):1712-1723, May 2007.
[2]Meyer et al. Initial results of a new generation DSCT system using only an in-plane comb filter for UHR temporal bone imaging. Eur Radiol 25:178-185, 2015.

Ultra High Resolution Scans

- Canon offers the Aquilion Precision, a system with dedicated ultra high resolution pixels
  - 0.25 mm pixel size at iso
  - 50% less septa thickness
  - 1792 channels
  - 160 detector rows
  - 1D anti scatter grid
  - 0.4 × 0.5 mm focal spot
  - 10800 rpm anode, liquid metal bearing
  - 512, 1024 or 2048 pixels per image
  - No need for post patient grid or comb: no dose penalty, small pixel effect can be utilized.

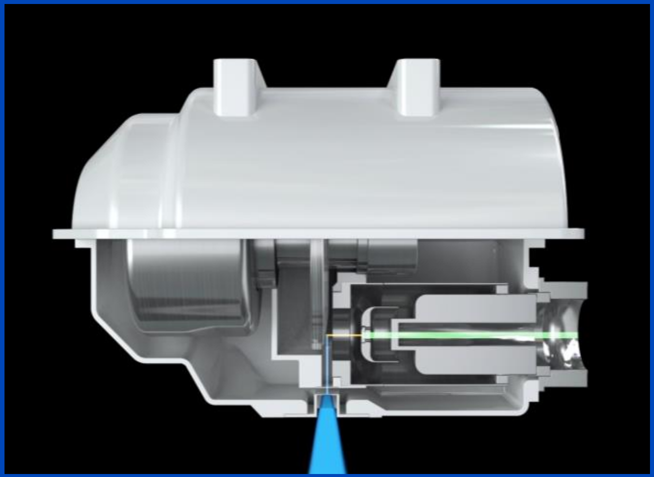

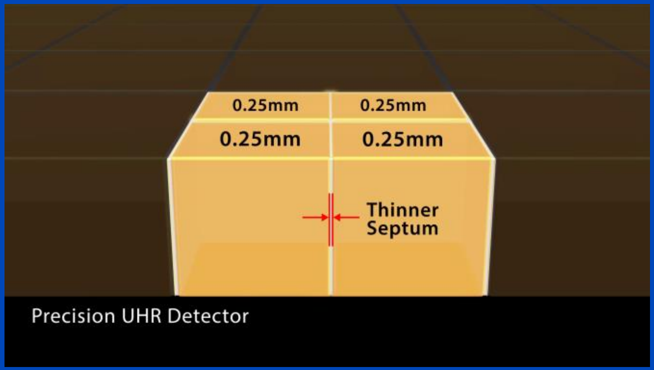

Image courtesy of Canon

Siemens Naeotom Alpha
The World‘s First Photon-Counting CT is a Dual Source PCCT

Alpha PCCT at University Medical Center Mannheim (UMM), Heidelberg University, Germany

Indirect Conversion (Today)

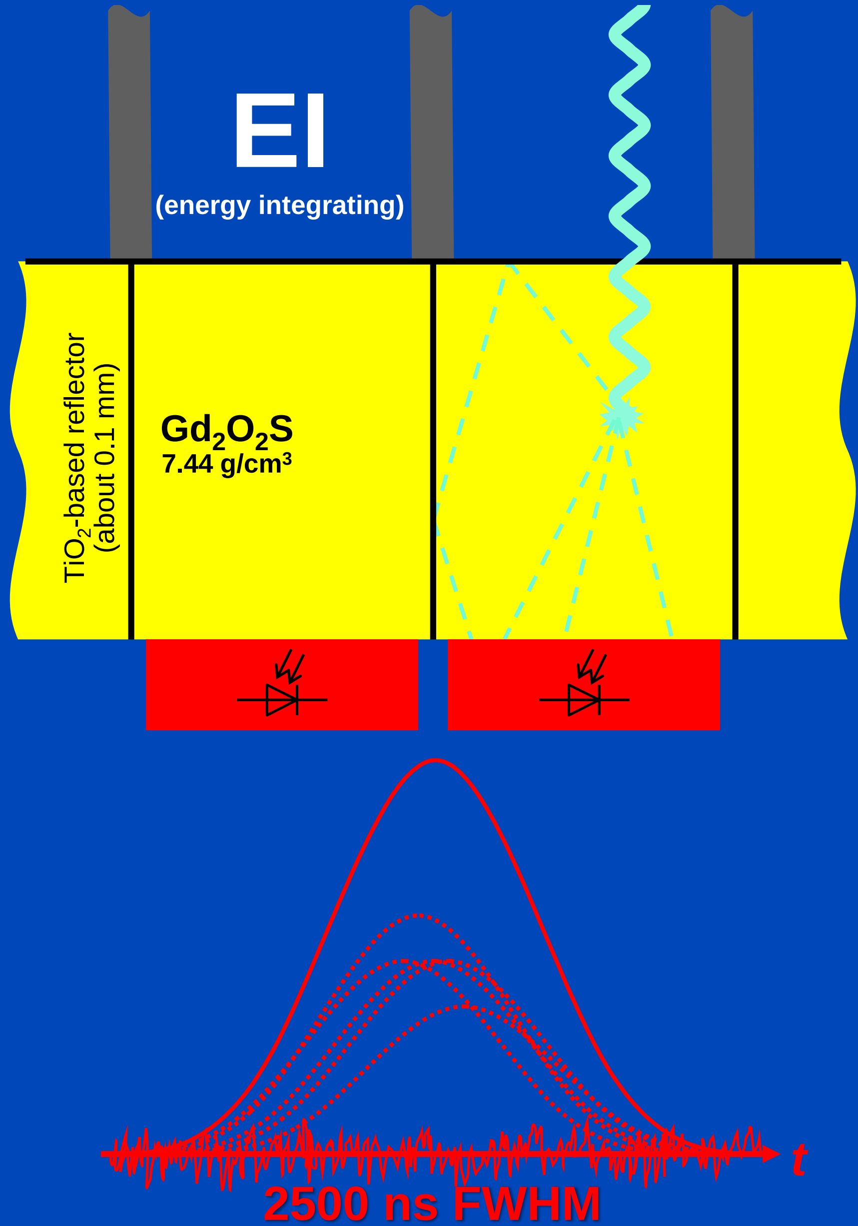

i.e. max $O(40\cdot10^3)$ cps

Direct Conversion (Future)

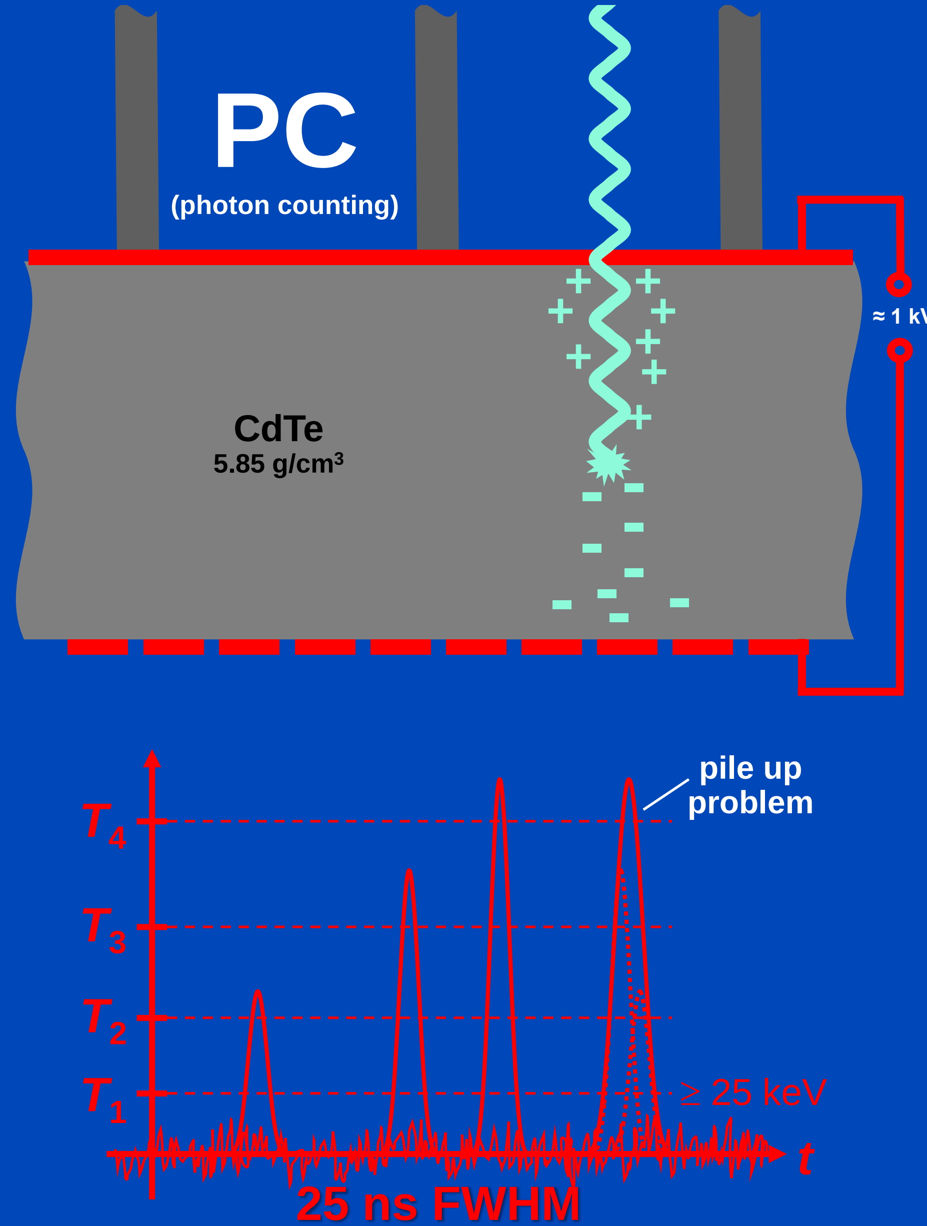

i.e. max $O(40\cdot10^6)$ cps

Requirements for CT: up to 10^9 x-ray photon counts per second per mm^2.
Hence, photon counting only achievable for direct converters.

Evolution of Spatial Resolution

2005: Somatom Flash (B70) | **2014: Somatom CounT (U70)** | **2021: Naeotom Alpha (Br98u)**

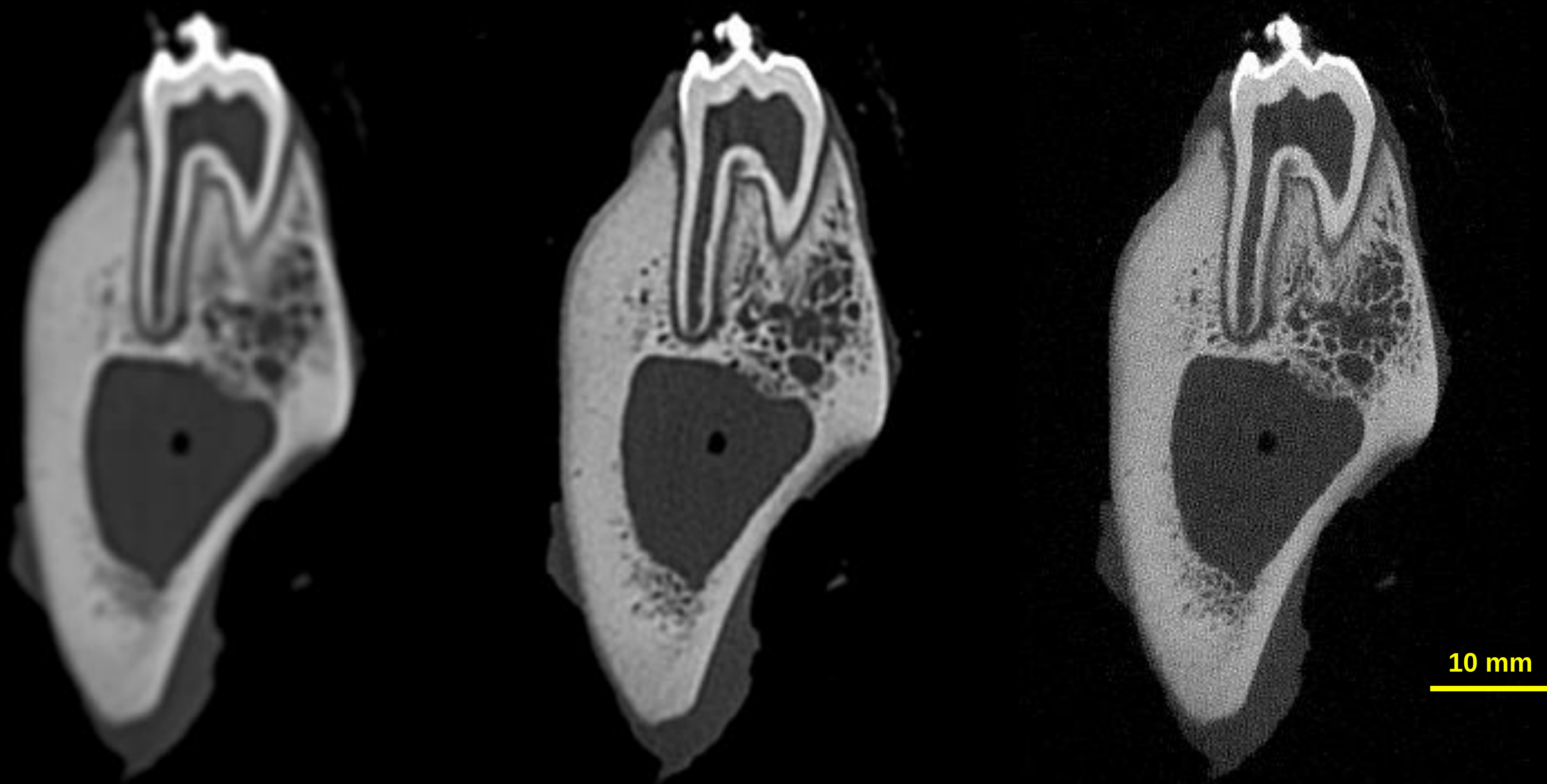

2005:
Pixel size 0.181 mm
Slice Thickness 0.60 mm
Slice Increment 0.30 mm
$MTF_{50\%}$ = 8.0 lp/cm
$MTF_{10\%}$ = 9.2 lp/cm

2014:
Pixel size 0.181 mm
Slice Thickness 0.20 mm
Slice Increment 0.10 mm
$MTF_{50\%}$ = 12.1 lp/cm
$MTF_{10\%}$ = 16.0 lp/cm

2021:
Pixel size 0.181 mm
Slice Thickness 0.20 mm
Slice Increment 0.10 mm
$MTF_{50\%}$ = 39.0 lp/cm
$MTF_{10\%}$ = 42.9 lp/cm

All measurements at Naeotom Alpha, Siemens Healthineers. QIR Reconstructions such that the maximum spatial resolution of Flash, CounT and Alpha is demonstrated on the same sample. *C* = 1200 HU, *W* = 4000 HU

High-End and Mid-Range Systems 2022/2023

CT-System	Rotation, Cone, Coll.	Max. Power, Anode Angle, Name, Max. mA @ low kV	Patient-specific prefilters	Detector Configuration, Type, Name	FOM, Reconstruction Matrix	Special Reconstruction Algorithms	Spectral	
Canon Aquilion ONE Prism Edition	0.275 s, 15°, 160 mm	100 kW, 10°, MegaCool Vi, 600 mA @ 80 kV	Ag, {0, *x*} mm	320 × 0.5 mm, EI, PUREViSION	50 cm, 512	iterative (AIDR 3D), deep (AiCE, PIQE)	fast TVS with DL	H
Canon Aquilion Precision Edition	0.35 s, 3.8°, 40 mm	72 kW, 7°, MegaCool, 600 mA @ 80 kV	none	160 × 0.25 mm, EI, PUREViSION	50 cm, 512, 1024, 2048	iterative (AIDR 3D), deep (AiCE)	2 scans	H
GE Revolution Apex Elite	0.23 s, 15°, 160 mm	108 kW, 10°, Quantix 160, 1300 mA @ 70+80 kV	none	256 × 0.625 mm, EI, GemStone Clarity	50 cm, 512		fast TVS or 2 scans	H
GE Revolution Apex Plus	0.28 s, 7.6°, 80 mm	108 kW, 10°, Quantix 160, 1300 mA @ 70 kV	none	128 × 0.625 mm, EI, GemStone Clarity	50 cm, 512	deep (TrueFidelity), SnapshotFreeze	fast TVS or 2 scans	M
Philips Spectral CT 7500	0.27 s, 7.7°, 80 mm	120 kW, 8°, iMRC, 925 mA @ 80 kV	none	2 · 128 × 0.625 mm, EI, NanoPanel Prism	50 cm, 512, 768, 1024	iterative (iDose)	sandwich	H
Philips Incisive CT	0.35 s, 3.9°, 40 mm	80 kW, vMRC	none	2 · 64 × 0.625 mm, EI	50 cm, 512, 768, 1024	iterative (iDose), deep (Precise Image&Cardiac)		M
Siemens Somatom X.ceed	0.25 s, 3.7°, 38.4 mm	120 kW, 8°, Vectron, 1300 mA @ 70+80+90 kV	Sn, {0, 0.4, 0.7} mm	2 · 64 × 0.6 mm, EI, Stellar	50 cm, 512, 768, 1024	iterative (ADMIRE)	split filter (Twin Beam) or 2 scans (Twin Spiral)	M
Siemens Somatom Force	0.25 s, 5.5°, 57.6 mm	2 · 120 kW, 8°, Vectron, 2 · 1300 mA @ 70+80+90 kV	Sn, {0, 0.6} mm	2 · 2 · 96 × 0.6 mm, EI, Stellar	50 cm/35 cm, 512, 768, 1024	iterative (ADMIRE)	DSCT	H
Siemens Naeotom Alpha	0.25 s, 5.5°, 57.6 mm	2 · 120 kW, 8°, Vectron, 2 · 1300 mA @ 70+90 kV	Sn, {0, 0.4, 0.7} mm	2 · 144×0.4 or 2 · 120×0.2 mm, PC, QuantaMax	50 cm/36 cm, 512, 768, 1024	iterative (QIR)	DSCT and PCCT	H

Premium Recon Algorithms 2022/2023

Vendor	Algorithm	Additional parameters	Sinogram restoration	Image restoration	Full iterations	Deep learning
all	FBP	-	✓	-	-	-
Canon	AIDR-3D enhanced FIRST AiCE PIQE	Body, Bone, Brain, Cardiac, Lung each with Mild, Standard, or Strong ?	✓ ✓ ? ?	✓ ✓ ✓ ✓	- ✓ - -	- - ✓ ✓
GE	ASIR, ASIR-V True Fidelity	0 – 100% (e.g. ASIR 30%) ???	✓ ?	✓ ✓	- -	- ✓
Philips	iDose IMR Precise Image&Cardiac	Levels 1 – 7 Soft, Routine, or SharpPlus ???	✓ ? ?	✓ ? ?	- ? ?	- - ✓
Siemens	IRIS SAFIRE ADMIRE QIR (PCCT-specific)	Strength 1 – 5 Strength 1 – 5 Strength 1 – 5 Strength 1 – 4	✓ ✓ ✓ ✓	✓ ✓ ✓ ✓	- ✓ ✓ ✓	- - - -

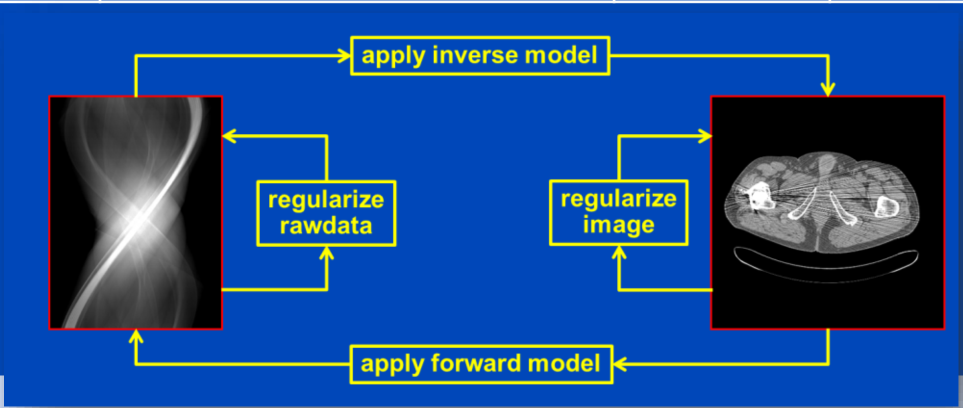

Detector Technology

Clinical CT Detector

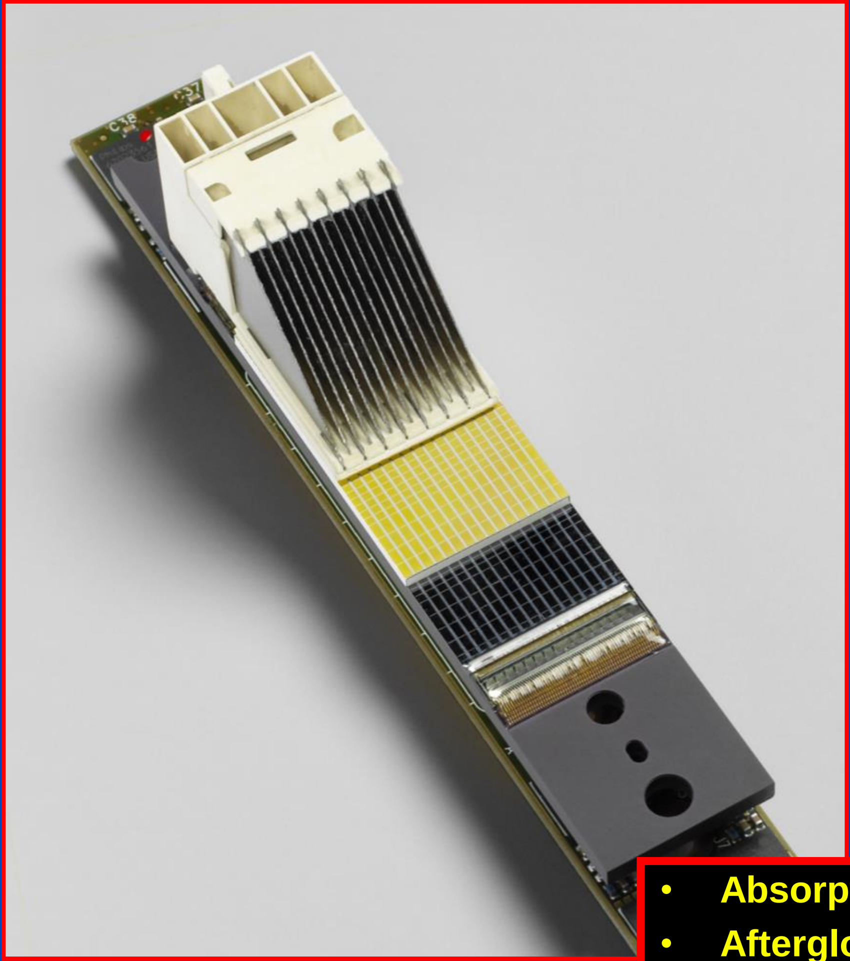

Flat Detector (CBCT)

- Absorption efficiency
- Afterglow
- Dynamic range
- Cross-talk
- Framerate
- Scatter grid

Sensor Dose Efficiency

	Energy-Integrating CT (120 kV)			CBCT (120 kV)			Photon Counting CT (120 kV)		
Material	Gd_2O_2S			CsI			CdTe		
Density	7.44 g/cm^3			4.5 g/cm^3			5.85 g/cm^3		
Thickness	1.4 mm			0.6 mm			1.6 mm		
Manufacturer	Siemens			Varian			Siemens CounT + Alpha		
Water Layer	0 cm	20 cm	40 cm	0 cm	20 cm	40 cm	0 cm	20 cm	40 cm
Photons absorbed	96.2%	92.7%	89.8%	73.5%	59.3%	50.9%	94.5%	88.2%	83.1%
Energy absorbed	94.3%	90.7%	87.9%	66.4%	53.9%	46.6%	91.2%	84.8%	79.9%

Absorption values are relative to a detector of infinite thickness.

The energy absorption coefficient μ_{en} was used to estimate the absorption values.

dkfz.

X-Ray Exposure Dynamic Range *D*

- **D = saturation exposure / quantum-limited exposure**
  - Saturation exposure N_{max}: Exposure where the detector runs into saturation
  - Quantum-limited exposure N_{min}: Exposure where the x-ray quantum noise equals the detector‘s electronic noise.
- **Measurements**[1]
  - Saturation signal: Increase exposure until you obtain $E(S_{max})$ in the offset-corrected reading.
  - Relation $S = k \cdot N$: Evaluate an offset-corrected medium level exposure to obtain a pair of values $\mathrm{Var}(S_{med})$ and $E(S_{med})$. Now, use the relation $\mathrm{Var}(N_{med}) = E(N_{med})$ with $\mathrm{Var}(S_{med}) = k^2 \cdot \mathrm{Var}(N_{med})$ and $E(S_{med}) = k \cdot E(N_{med})$ to find $k = \mathrm{Var}(S_{med}) / E(S_{med})$.
  - Electronic noise: Determine $\mathrm{Var}(S_{min})$ from the subtraction of two dark images.
- **X-ray exposure dynamic range**

$$D = \frac{E(N_{\max})}{E(N_{\min})} = \frac{E(S_{\max})/k}{\mathrm{Var}(S_{\min})/k^2} = \frac{E(S_{\max})\mathrm{Var}(S_{\mathrm{med}})}{E(S_{\mathrm{med}})\mathrm{Var}(S_{\min})}$$

[1]Instead of doing this very simple procedure one may want to use statistically optimal estimates. One may use many readings, and many exposure levels. One may further determine *D* on a pixel-by-pixel basis.

dkfz.

Dynamic Range Required for Diagnostic Image Quality

- **Soft tissue μ = 0.0192/mm object of diameter *D* between D_{min} = 200 mm and D_{max} = 500 mm with a lesion of diameter *d* = 5 mm and contrast δ = 5 HU = 0.005.**
- **Number of photons to be registered at the detector:**

$$I(D, \delta d) = I_0 e^{-\mu D - \mu\delta d}$$

- **Minimal signal difference to be detected:**

$$I(D_{\text{max}}, \delta d) - I(D_{\text{max}}, 0) \approx \mu\delta d I(D_{\text{max}}, 0)$$

- **Maximum signal to be detected:**

$$I(D_{\text{min}}, 0)$$

- **Thus, the dynamic range required in diagnostic CT is in the order of**

$$\frac{I(D_{\text{min}}, 0)}{\mu\delta d\, I(D_{\text{max}}, 0)} \approx 10^6 \approx 2^{20}$$

Dynamic Range in Flat Detectors

	Saturation-to-noise range			X-ray exposure range				Digital range	
	Electronic noise (ADU)	Saturation signal (ADU)	Dynamic range	Quantum limited exposure (μR)	Saturation exposure (μR)	Dynamic range	Eff. bit depth (bits)	Quantization range	Eff. bit depth (bits)
No binning, gain 2	**A1**	**B1**	**B1/A1**	**A2**	**B2**	**C2=B2/A2**	**D2=lb(C2)**	**B1:1**	**lb(B1)**
Dynamic gain switching	5.32	80500	15100	2.75	3550	**1291**	**10.3**	80500:1	16.3
0.5 pF fixed	5.32	14500	2700	2.75	595	**216**	**7.8**	14500:1	13.8
4 pF fixed	3.57	14800	4150	35.7	4200	**118**	**6.9**	14800:1	13.8
2x2 binning, gain 1									
Dual gain readout	4.33	80100	18500	1.00	1800	**1800**	**10.8**	80100:1	16.3
Dynamic gain switching	4.37	84200	19300	1.03	2062	**2002**	**11.0**	84200:1	16.4
0.5 pF fixed	4.37	14300	3300	1.03	311	**302**	**8.2**	14300:1	13.8
4 pF fixed	3.14	14800	4700	15.6	2104	**135**	**7.1**	14800:1	13.8
0.5 pF fixed, gain 2 (fluoroscopy mode)	7.25	12900	1700	0.71	125	**176**	**7.5**	12900:1	13.6

Table 2 4030CB dynamic range in available imaging modes **A2 is defined as the exposure where QuantumNoise=ElectronicNoise.**

$$D = \frac{80500/k}{5.32^2/k^2} = 1291 \quad \text{if} \quad k = 0.45$$

Table taken from [Roos et al. “Multiple gain ranging readout method to extend the dynamic range of amorphous silicon flat panel imagers,” *SPIE Medical Imaging Proc.*, vol. 5368, pp. 139-149, 2004]. Additional values were added, for convenience.

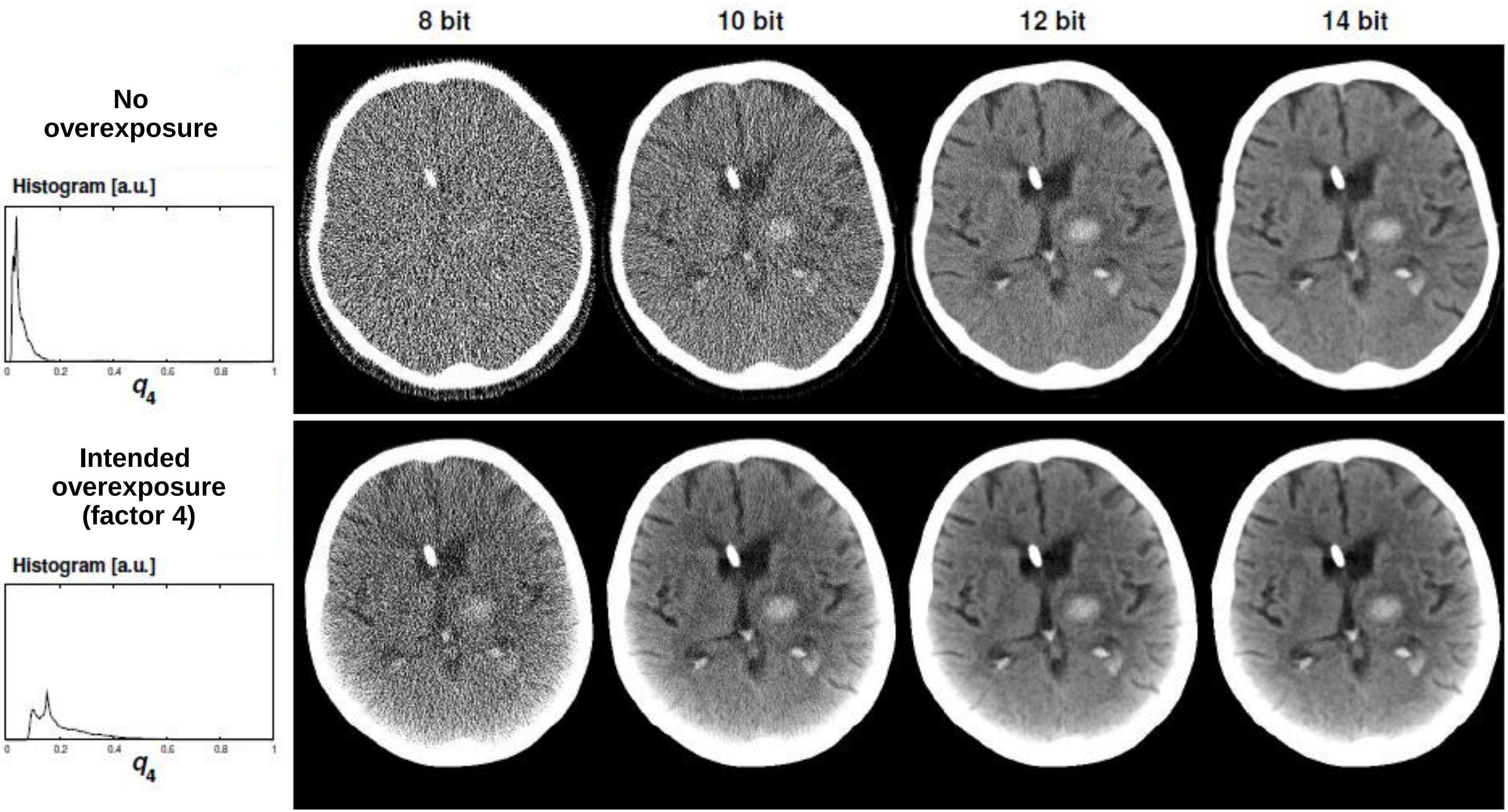

8 bit
10 bit
12 bit
14 bit
No overexposure
Histogram [a.u.]
0
0.2
0.4
0.6
0.8
1
q_4
Intended overexposure (factor 4)
Histogram [a.u.]
0
0.2
0.4
0.6
0.8
1
q_4

Multiple Exposures vs. Long Integration Times

- **Assume a signal *S* can be detected only with an added readout noise *R* of known expectation and variance**

$$\mathrm{E}(S), \mathrm{Var}(S), \mathrm{E}(R) = 0, \mathrm{Var}(R)$$

- **Averaging *T* readouts yields:**

$$\mathrm{Var}\Big(\frac{1}{T}\sum_t (S_t + R_t)\Big) = \frac{1}{T^2}\sum_t \big(\mathrm{Var}S + \mathrm{Var}R\big) = \frac{\mathrm{Var}S}{T} + \frac{\mathrm{Var}R}{T}$$

- **Using the *T*-fold integration time and dividing by *T* yields:**

$$\mathrm{Var}\Big(\frac{1}{T}\big(\sum_t S_t + \hat{R}\big)\Big) = \frac{1}{T^2}\Big(\sum_t \mathrm{Var}S + \mathrm{Var}\hat{R}\Big) = \frac{\mathrm{Var}S}{T} + \frac{\mathrm{Var}\hat{R}}{T^2}$$

dkfz.

Electronic Noise *R* as a Function of Integration Time

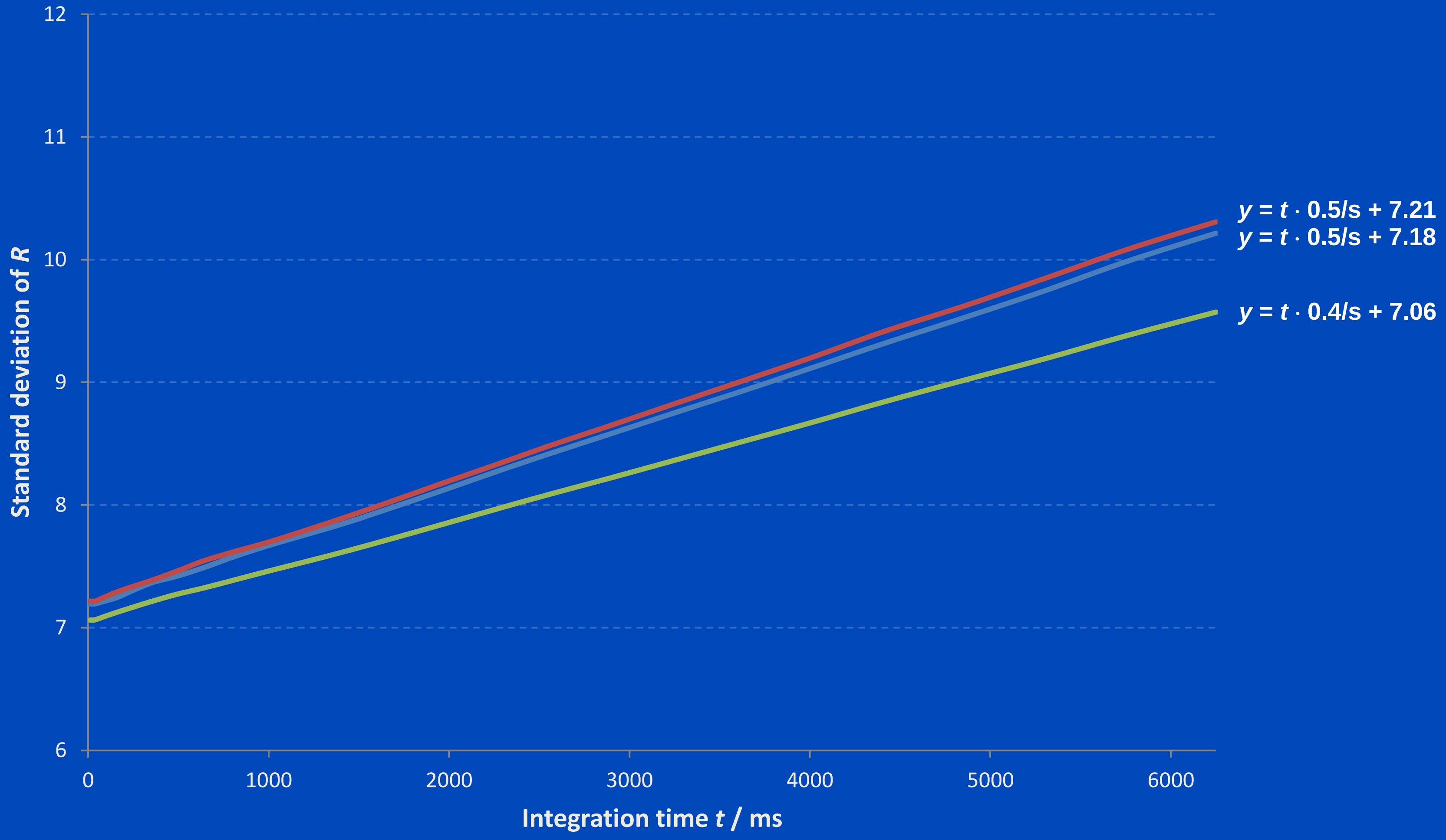

Plots and linear fits for three different modules of a PerkinElmer flat detector Dexela 2923

CT Scan Trajectories

Circle

Sequence

$$p = \frac{d}{MS} \leq 0.9$$

Spiral

$$p = \frac{d}{MS} \leq 1.5$$

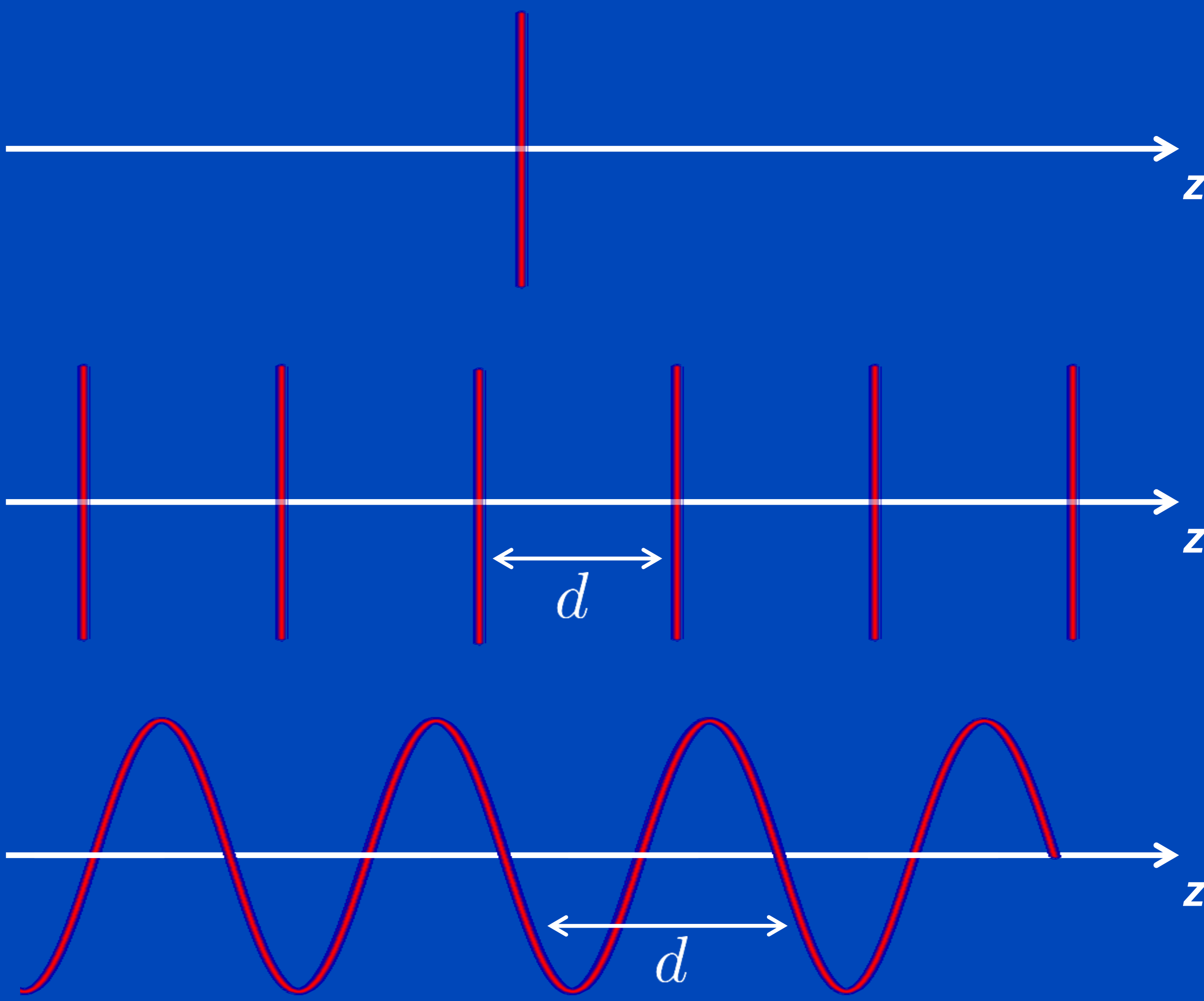

Analytical Image Reconstruction

$$x^2 = y$$

Model

$$x = \sqrt{y}$$

Solution

Filtered Backprojection (FBP)

Measurement: $p(\vartheta,\xi) = \int dxdy\, f(x,y)\delta(x\cos\vartheta + y\sin\vartheta - \xi)$

Fourier transform:

$$\int d\xi\, p(\vartheta,\xi)e^{-2\pi i\xi u} = \int dxdy\, f(x,y)e^{-2\pi i u(x\cos\vartheta + y\sin\vartheta)}$$

This is the central slice theorem: $P(\vartheta,u) = F(u\cos\vartheta, u\sin\vartheta)$

Inversion: $f(x,y) = \int\limits_0^\pi d\vartheta \int\limits_{-\infty}^{\infty} du\, |u| P(\vartheta,u)e^{2\pi i u(x\cos\vartheta + y\sin\vartheta)}$

$$= \int\limits_0^\pi d\vartheta\, p(\vartheta,\xi) * k(\xi)\Big|_{\xi = x\cos\vartheta + y\sin\vartheta}$$

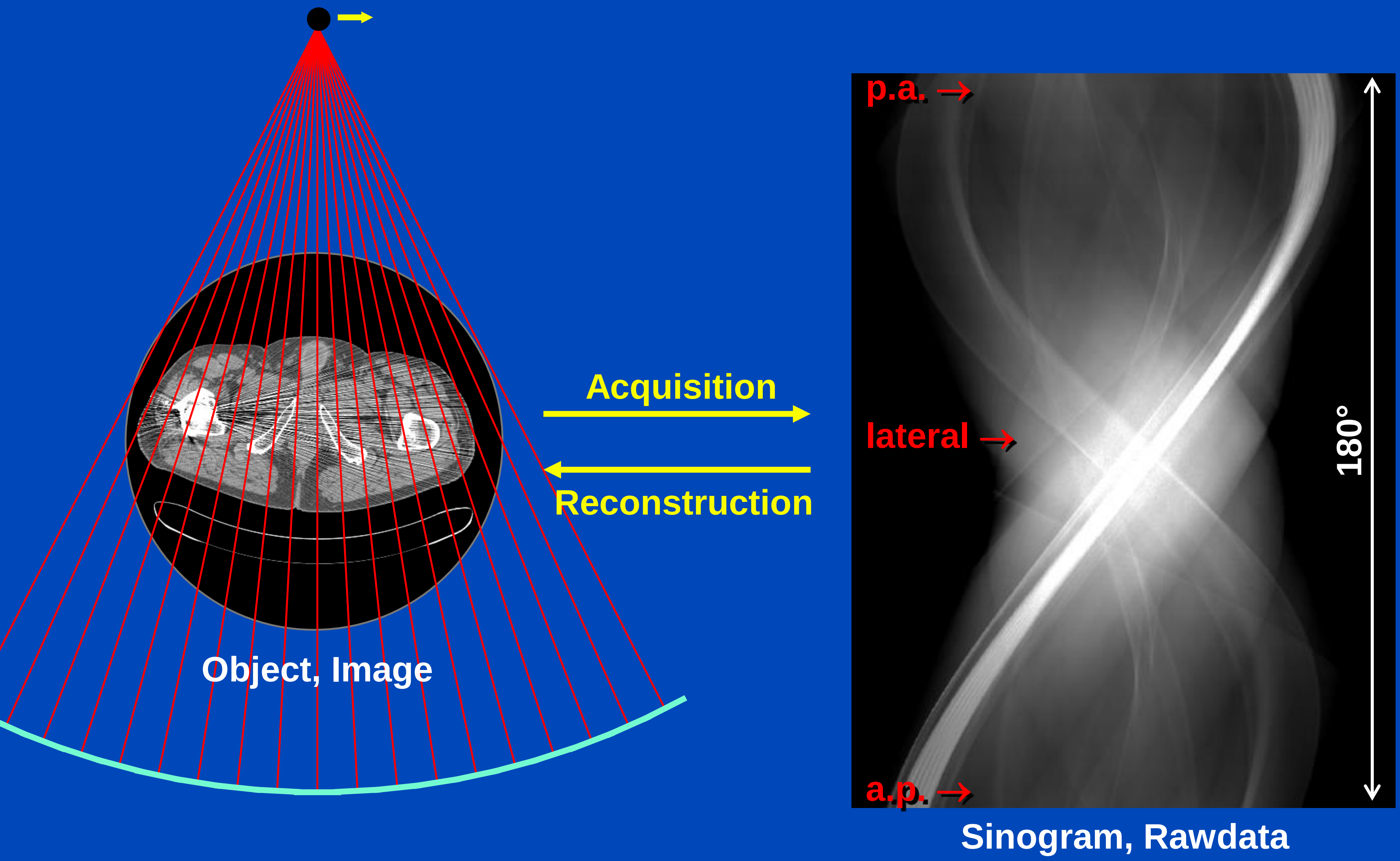

Acquisition
Reconstruction
Object, Image
p.a.
lateral
a.p.
180°
Sinogram, Rawdata

Filtered Backprojection (FBP)

1. Filter projection data with the reconstruction kernel.
2. Backproject the filtered data into the image:

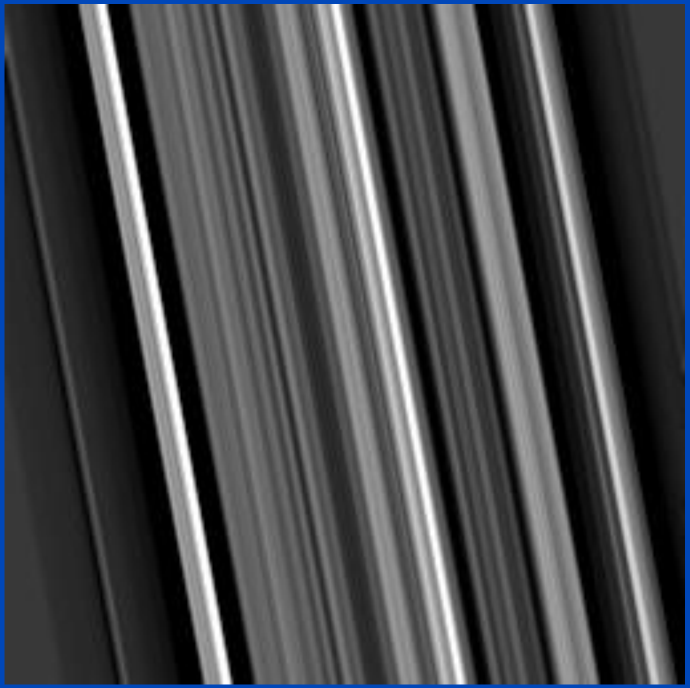

Smooth kernel (e.g. B30)

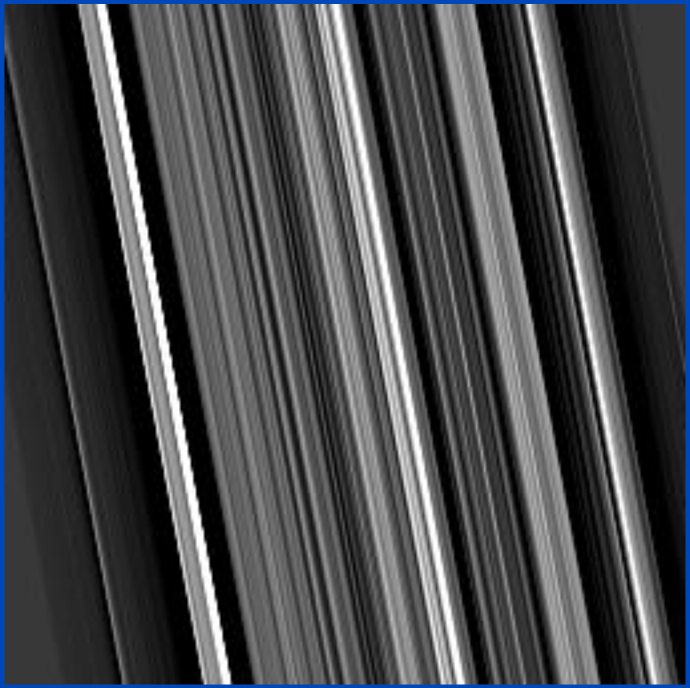

Sharp kernel (e.g. B70)

Reconstruction kernels balance between spatial resolution and image noise.

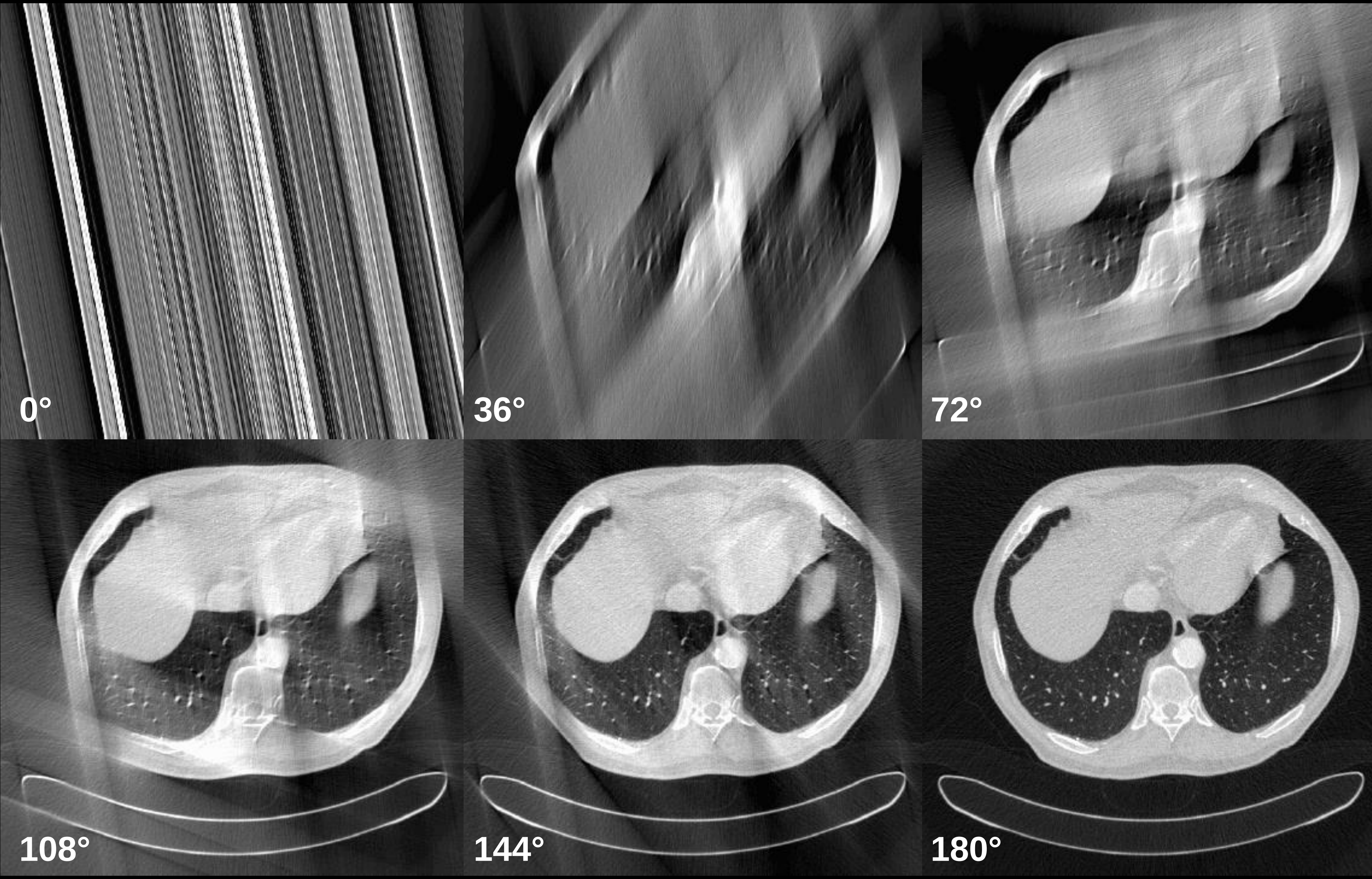
0°
36°
72°
108°
144°
180°

normalized

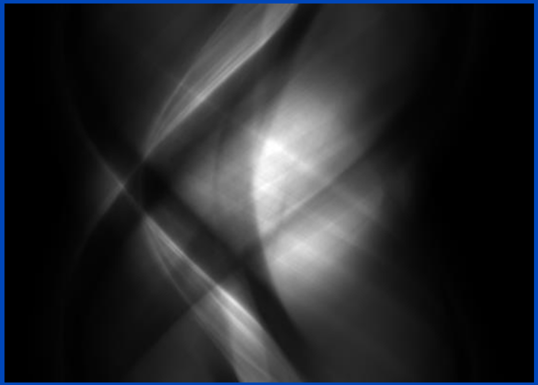

log normalized

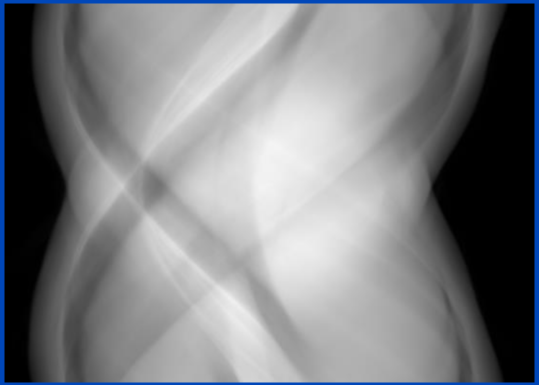

log normalized and convolved

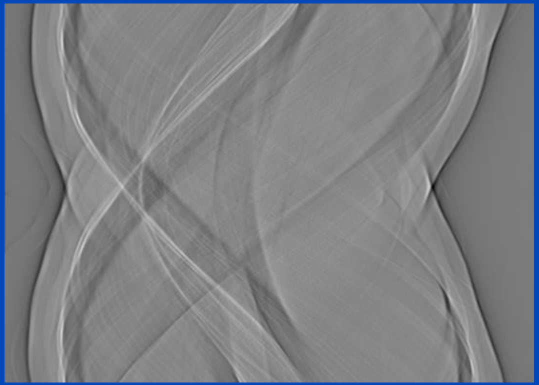

after 36°

after 72°

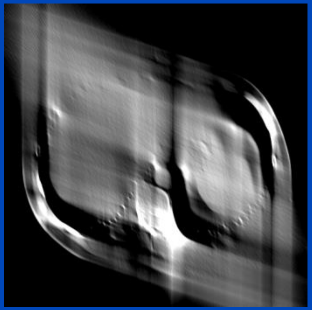

after 108°

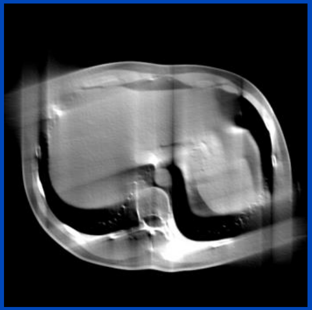

after 144°

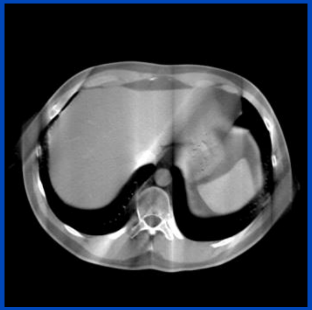

after 180°

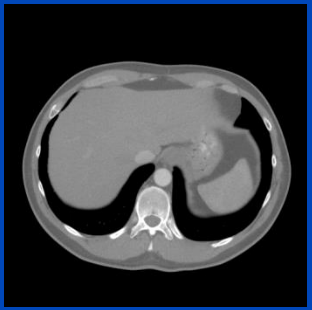

1 projection

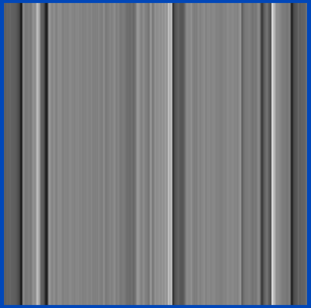

2 projections

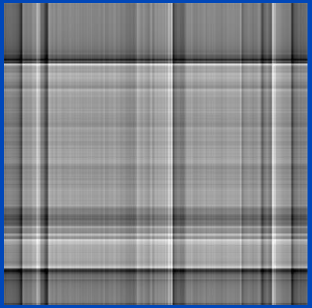

4 projections

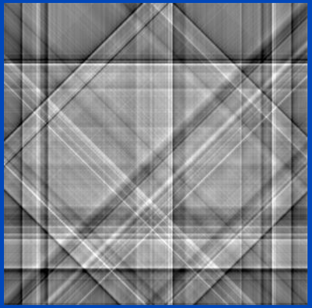

8 projections

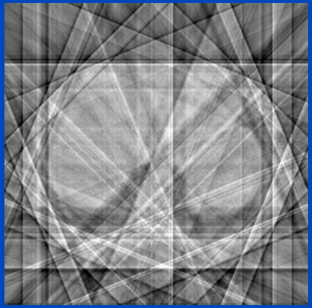

all projections

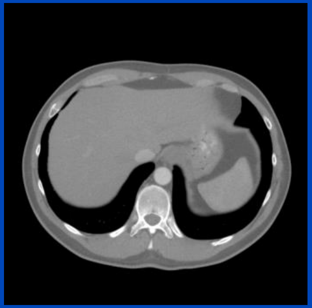

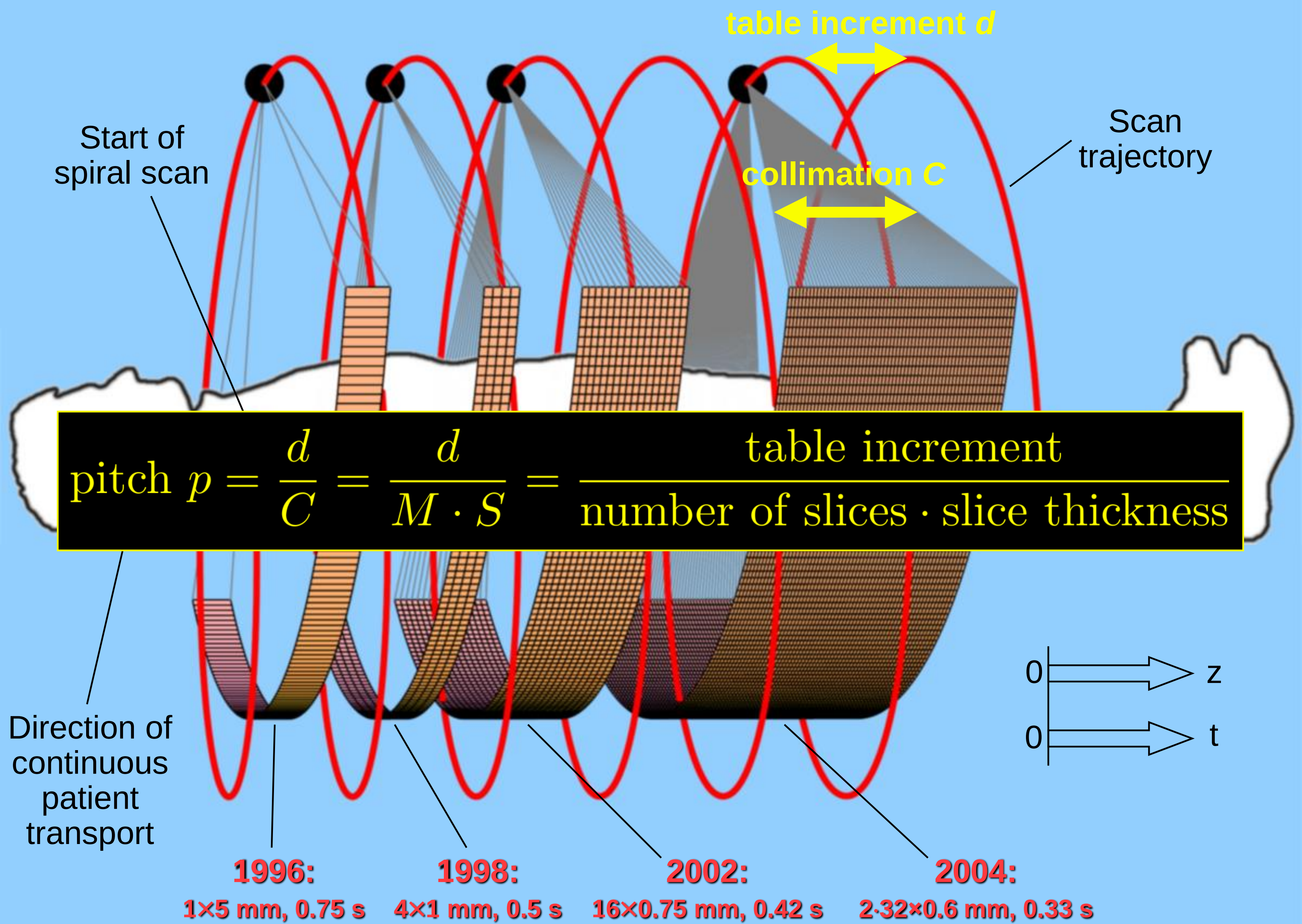

$$\text{pitch } p = \frac{d}{C} = \frac{d}{M \cdot S} = \frac{\text{table increment}}{\text{number of slices} \cdot \text{slice thickness}}$$

Kalender et al., Radiology 173(P):414 (1989) and 176:181-183 (1990)

360° LI Spiral z-Interpolation for Single-Slice CT (M=1)

$$p = \frac{d}{MS} \leq 2$$

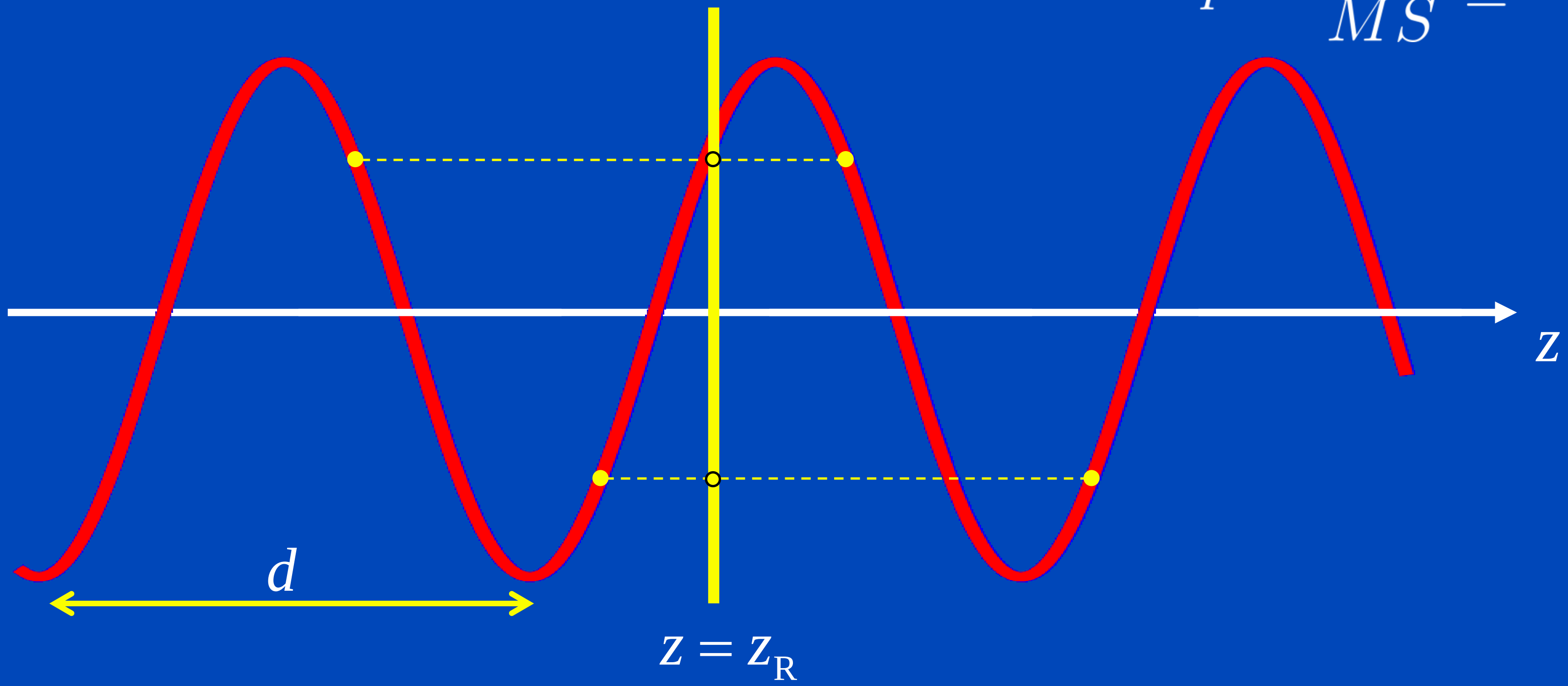

Spiral z-interpolation is typically a linear interpolation between points adjacent to the reconstruction position to obtain circular scan data.

without *z*-interpolation

with *z*-interpolation

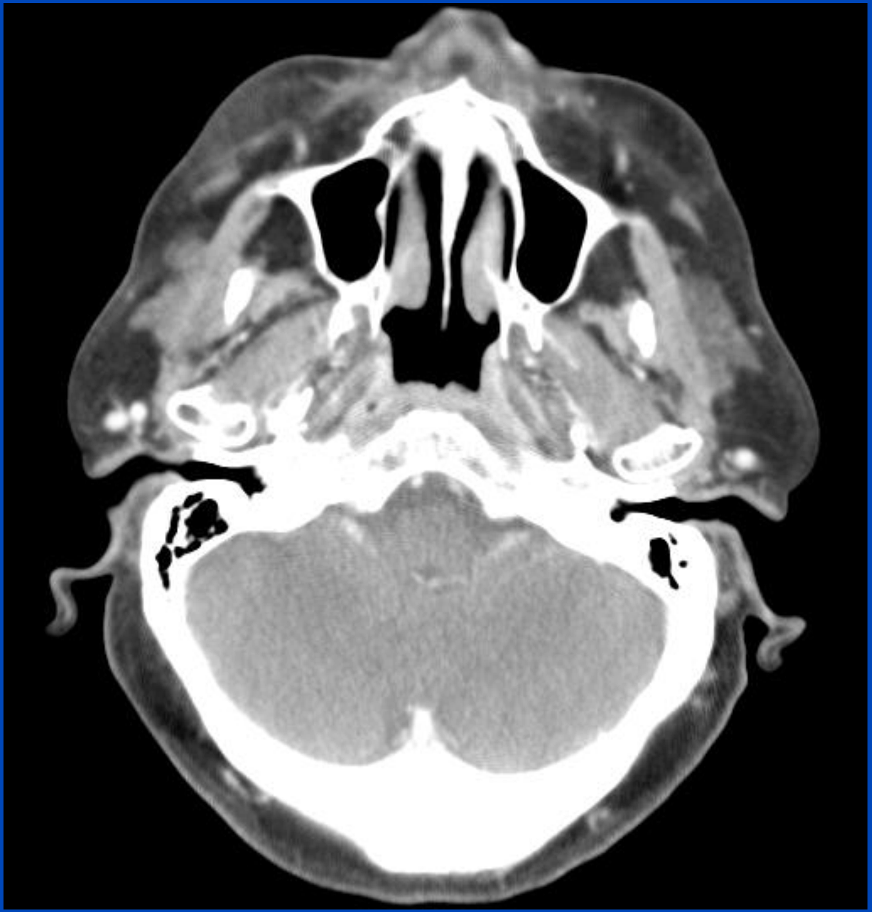

What's so Nice about Spiral CT?

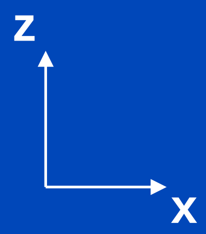

S = 3 mm, *RI* = 3 mm

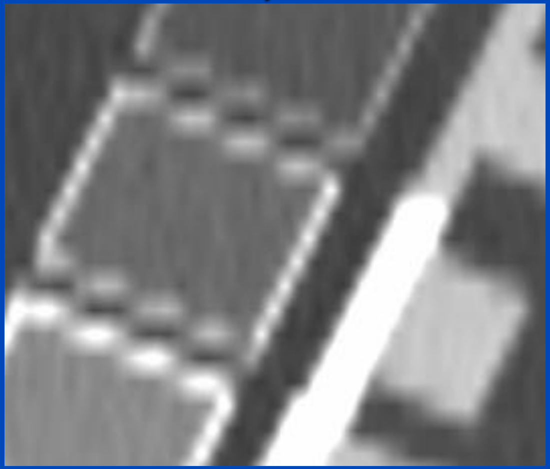

S = 3 mm, *RI* = 1 mm

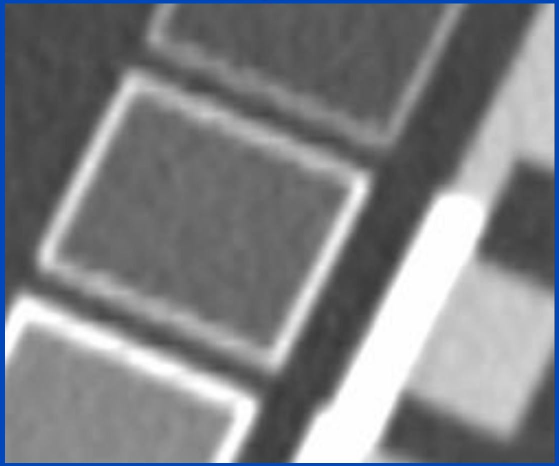

MPR images of the European Spine Phantom (inclined at 25°).

Kalender WA, Polacin A, Süß C. Radiology 1994; 193:170-171

Sampling Artifact

S_{eff} = 3 mm, *RI* = 3 mm

S_{eff} = 3 mm, *RI* = 1 mm

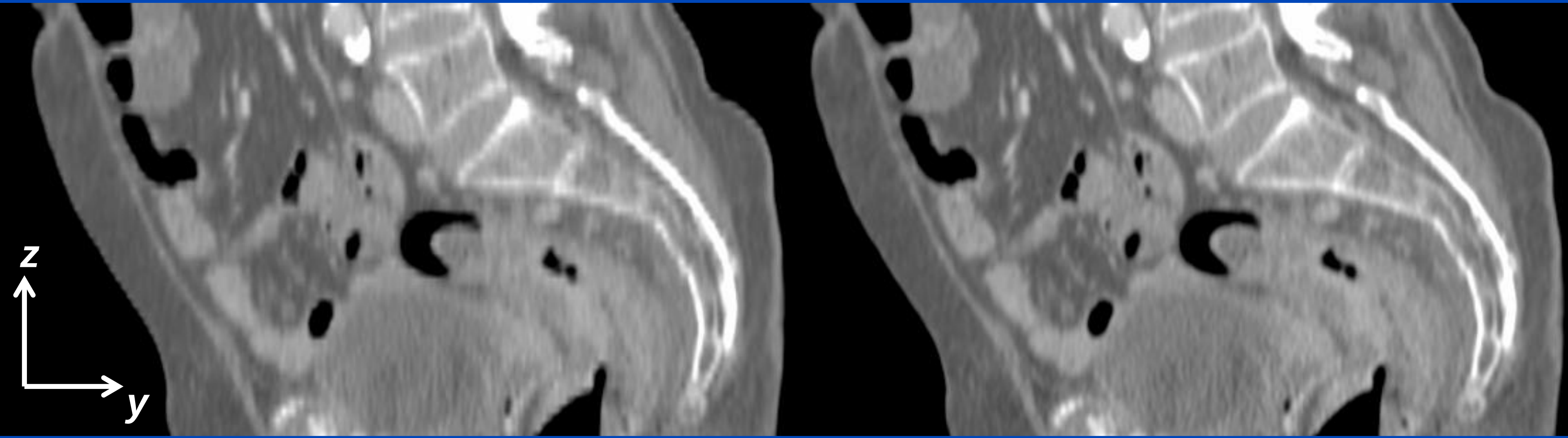

Always perform overlapping recons!

C = 0 HU, *W* = 800 HU

RSNA 1989
SSCT (*M* = 1)

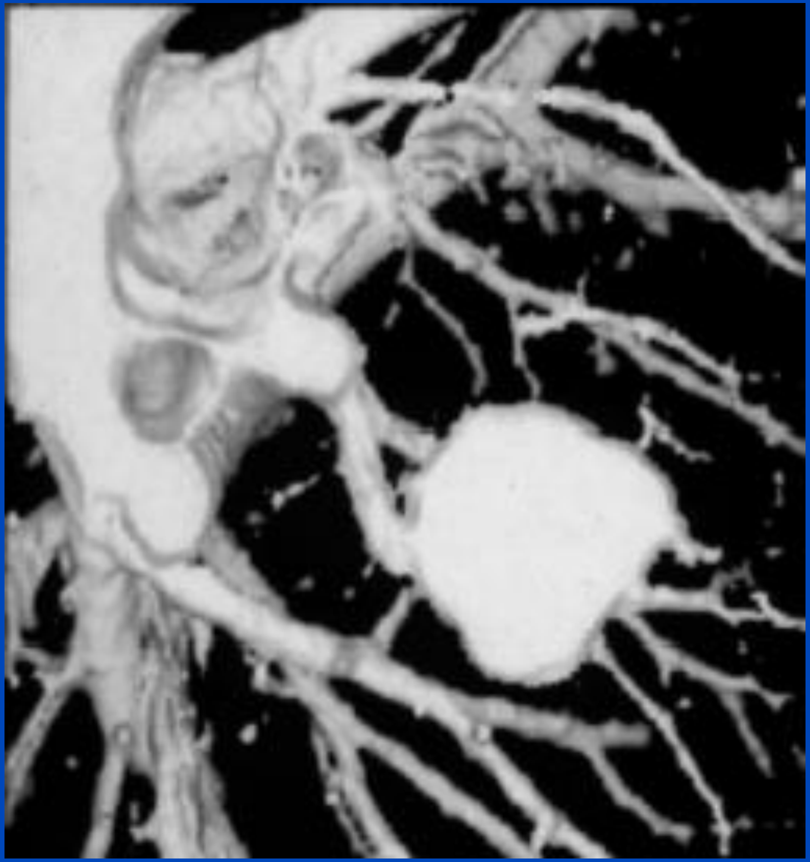

RSNA 2001
MSCT (*M* = 16)

The Pitch Value is the Measure for Scan Overlap

The pitch is defined as the ratio of the table increment per full rotation to the *total* collimation width in the center of rotation:

$$p = \frac{d}{M \cdot S}$$

Recommended by and in:

IEC, International Electrotechnical Commision: Medical electrical equipment – 60601 Part 2-44: Particular requirements for the safety of x-ray equipment for computed tomography. Geneva, Switzerland, 1999.

Examples:

- p=1/3=0.333 means that each z-position is covered by 3 rotations (3-fold overlap)
- p=1 means that the acquisition is not overlapping
- $p=p_{max}$ means that each z-position is covered by half a rotation

The ASSR Algorithm

$$p = \frac{d}{MS} \leq 1.5$$

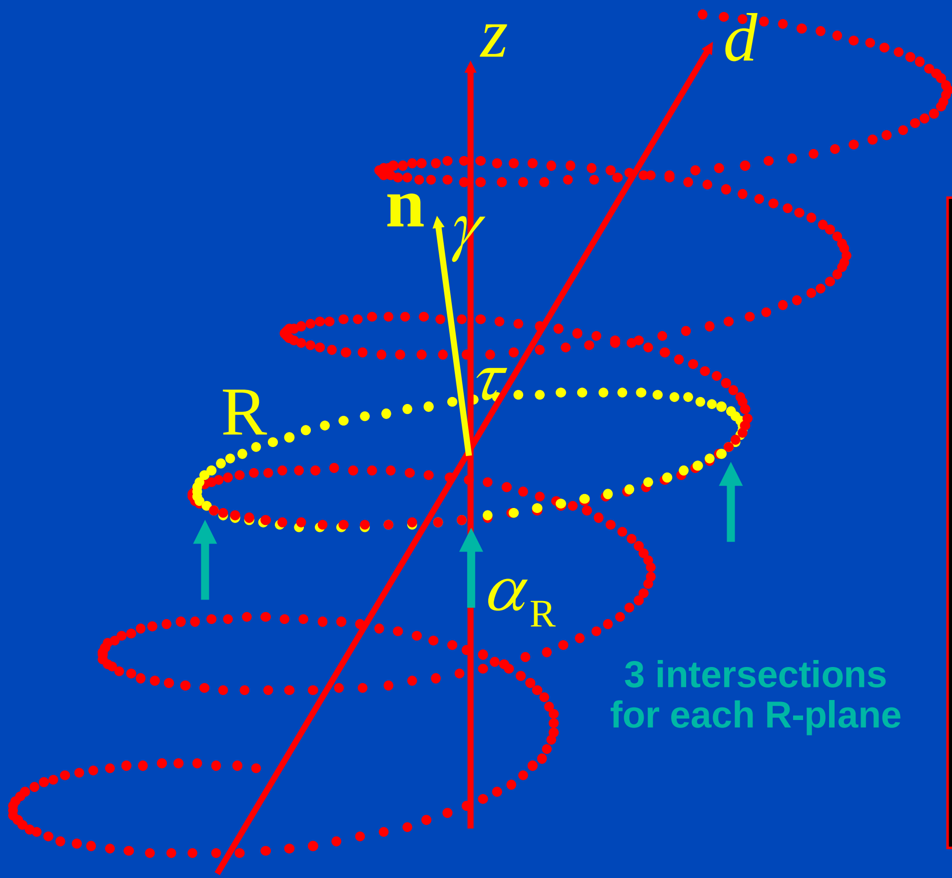

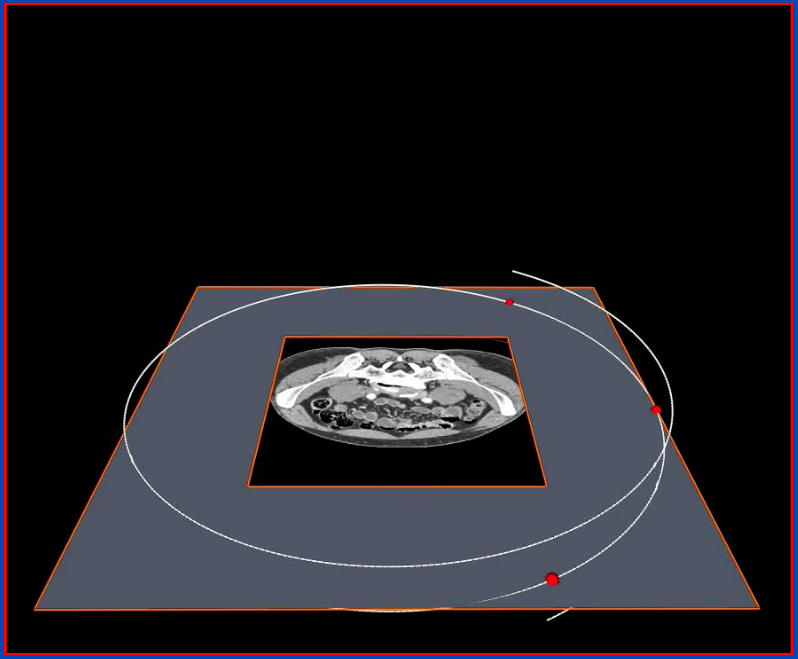

Mean deviation at distance R_M: $\Delta \approx 0.007 \cdot d$

at distance R_F: $\Delta \approx 0.014 \cdot d$

CT-Angiography

Sensation 64 spiral scan with 2·32×0.6 mm and 0.375 s

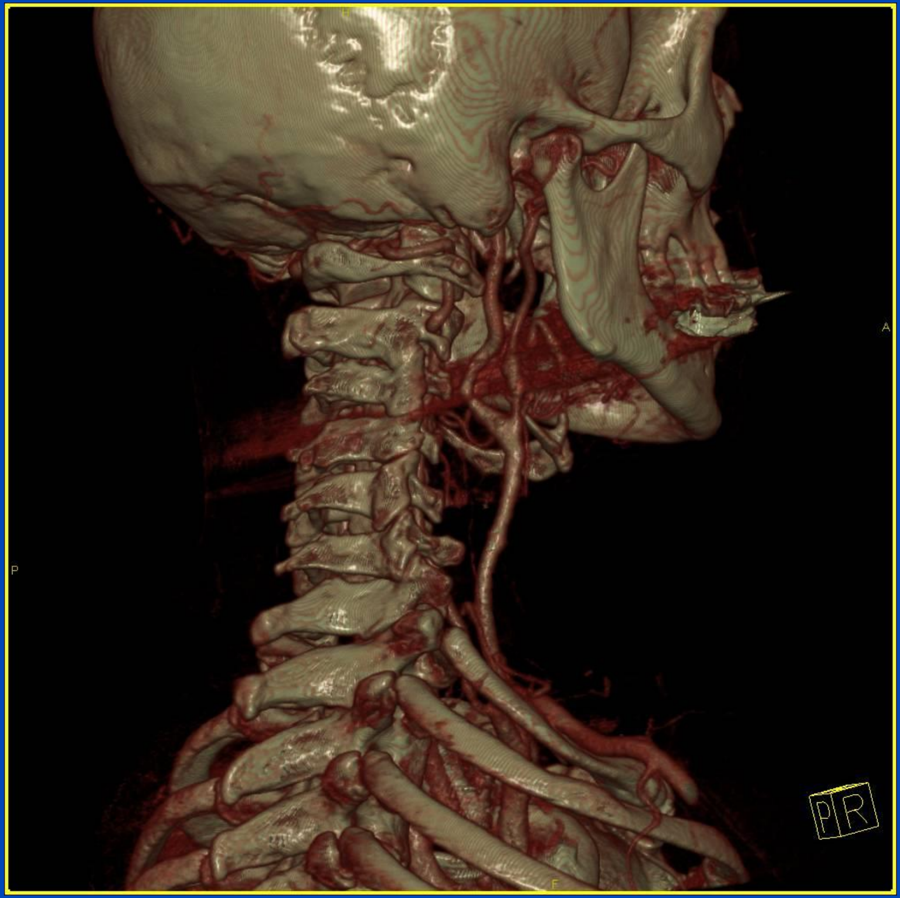

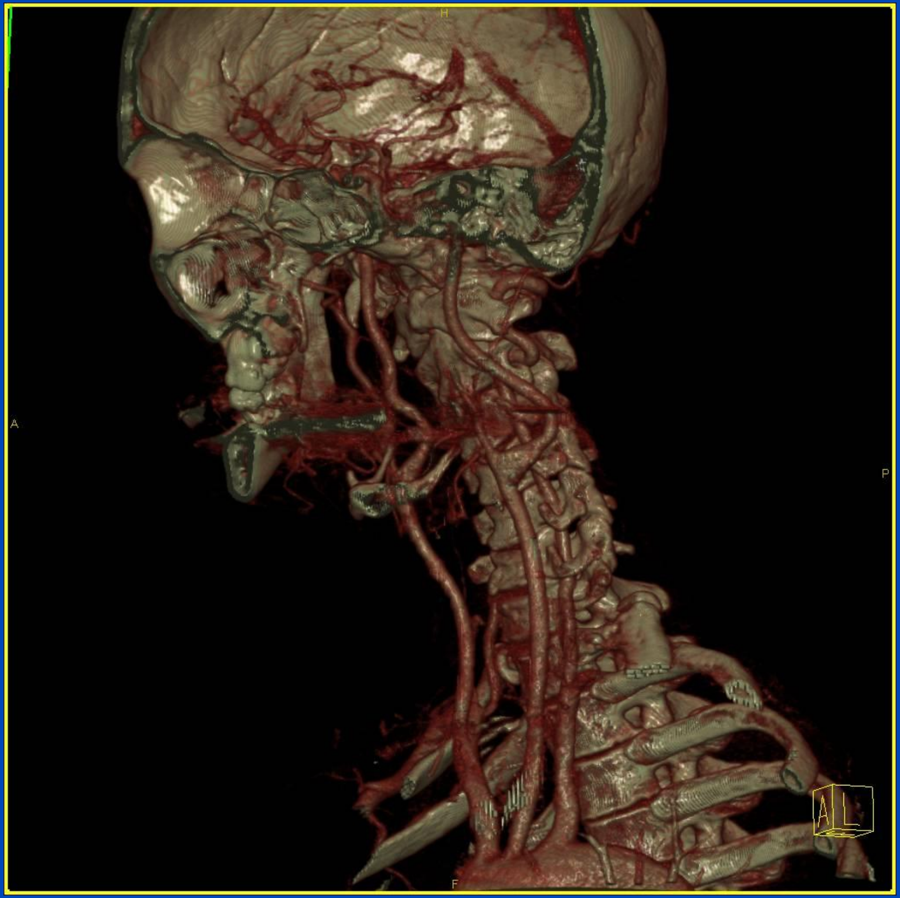

Iterative Image Reconstruction

$$x^2 = y$$

Model

$$\cancel{x = \sqrt{y}}$$

$$(x_n + \Delta x_n)^2 = y$$

$$x_n^2 + 2x_n\Delta x_n + \cancel{\Delta x_n^2} = y$$

$$x_n^2 + 2x_n\Delta x_n \approx y$$

$$\Delta x_n = \tfrac{1}{2}(y - x_n^2)/x_n$$

$$x_{n+1} = x_n + \Delta x_n$$

Update equation

Influence of Update Equation and Model

$0.5\,(3-x_n^2)/x_n$	$0.4\,(3-x_n^2)/x_n$	$0.5\,(3-x_n^{2.1})/x_n$
$x_0 = 1.$	$x_0 = 1.$	$x_0 = 1.$
$x_1 = 2.$	$x_1 = 1.8$	$x_1 = 2.$
$x_2 = 1.75$	$x_2 = 1.74667$	$x_2 = 1.67823$
$x_3 = 1.73214$	$x_3 = 1.73502$	$x_3 = 1.68833$
$x_4 = 1.73205$	$x_4 = 1.73265$	$x_4 = 1.68723$
$x_5 = 1.73205$	$x_5 = 1.73217$	$x_5 = 1.68734$
$x_6 = 1.73205$	$x_6 = 1.73207$	$x_6 = 1.68733$
$x_7 = 1.73205$	$x_7 = 1.73206$	$x_7 = 1.68733$
$x_8 = 1.73205$	$x_8 = 1.73205$	$x_8 = 1.68733$

$$x^2 = 3, \quad x_0 = 1, \quad x_{n+1} = x_n + \Delta x_n$$

Kaczmarz‘s Method = ART

$$\boldsymbol{f}_{\nu+1} = \boldsymbol{f}_{\nu} + \boldsymbol{R}^{\mathrm{T}} \cdot \frac{\boldsymbol{p} - \boldsymbol{R} \cdot \boldsymbol{f}_{\nu}}{\boldsymbol{R}^{2} \cdot \mathbf{1}}$$

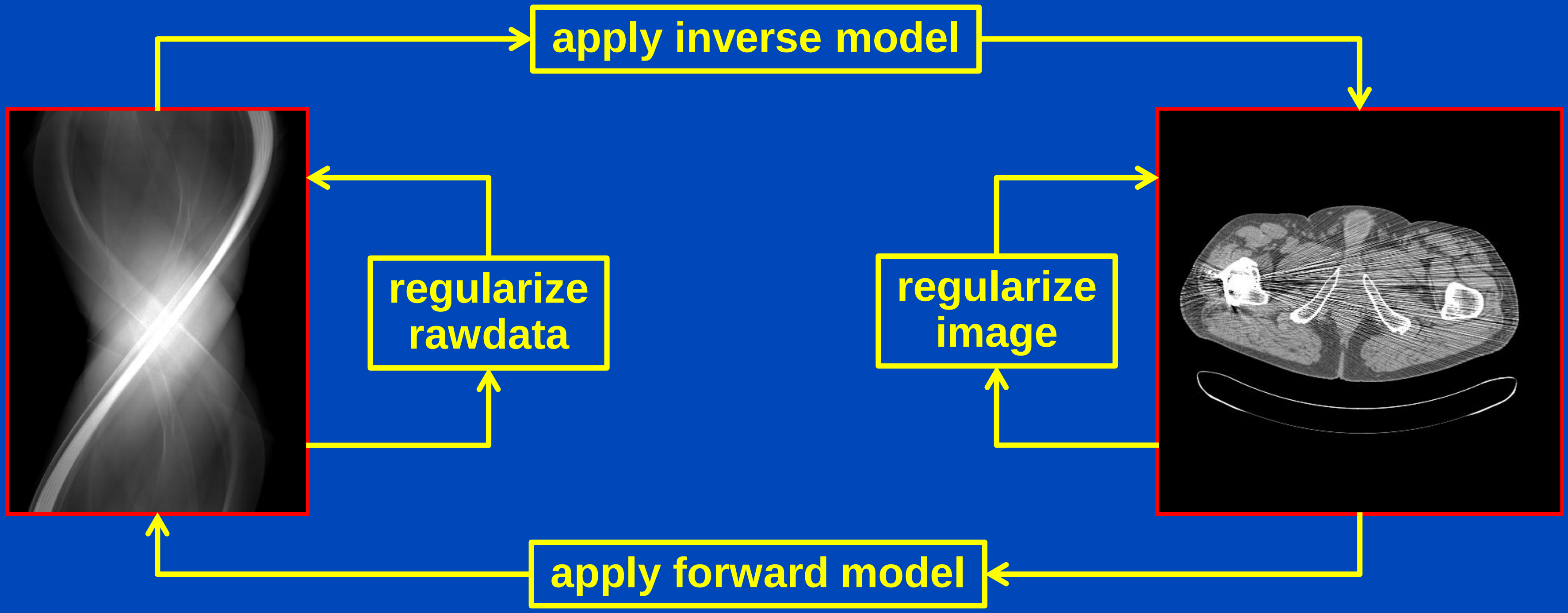

- Rawdata regularization: adaptive filtering[1], precorrections, filtering of update sinograms...
- Inverse model: backprojection (R^T) or filtered backprojection (R^{-1}). In clinical CT, where the data are of high fidelity and nearly complete, one would prefer filtered backprojection to increase convergence speed.
- Image regularization: edge-preserving filtering. It may model physical noise effects (amplitude, direction, correlations, …). It may reduce noise while preserving edges. It may include empirical corrections.
- Forward model (R_{phys}): Models physical effects. It can reduce beam hardening artifacts, scatter artifacts, cone-beam artifacts, noise, …

[1]M. Kachelrieß et al., Generalized Multi-Dimensional Adaptive Filtering, MedPhys 28(4), 2001

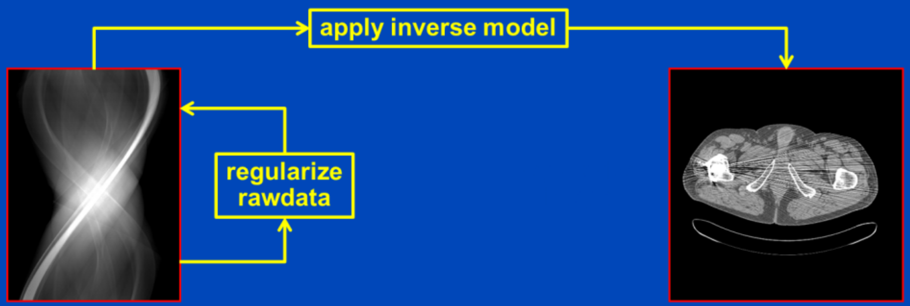

Conventional FBP with rawdata denoising (all vendors)

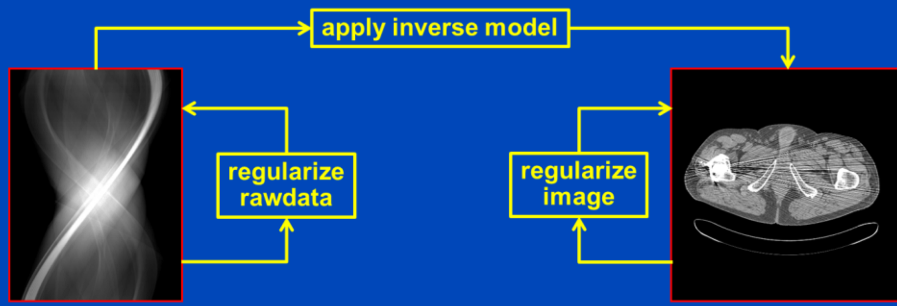

AIDR3D (Canon), ASIR, ASIR-V (Ge), IRIS (Siemens), iDose (Philips), SnapShot Freeze (GE), iTRIM (Siemens)

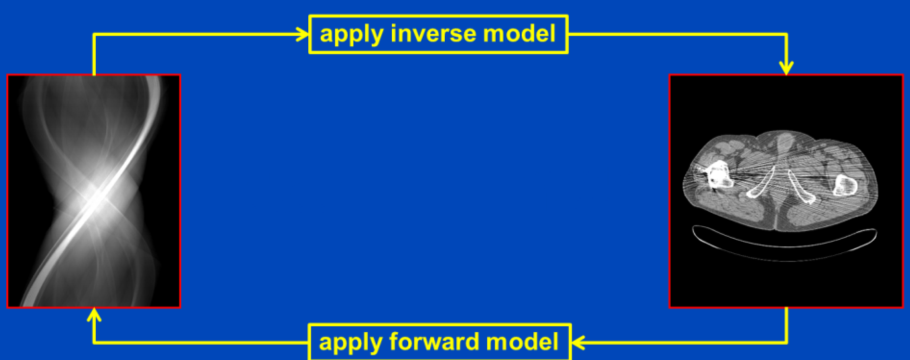

Veo123/MBIR (Ge)

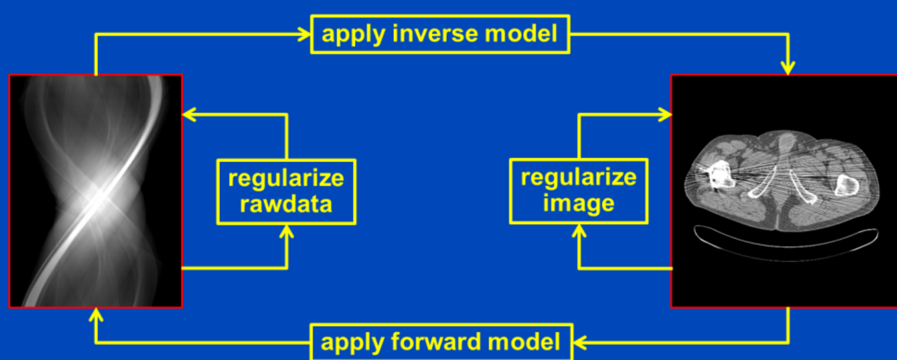

FIRST (Canon), IMR (Philips), SAFIRE, ADMIRE, QIR (Siemens)

Plain FBP

σ = 26.8 HU

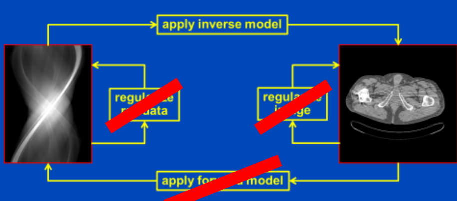

Siemens Standard

σ = 17.6 HU

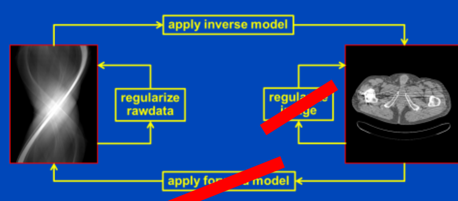

IRIS VA34

σ = 12.3 HU

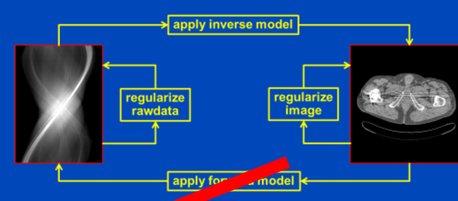

SAFIRE VA40

σ = 7.8 HU

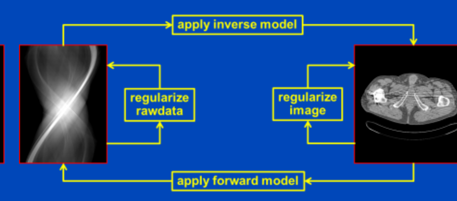

CT images provided by Siemens Healthcare, Forchheim, Germany

DL-Based Image Reconstruction

$$\cancel{x^2 = y} \qquad \cancel{x = \sqrt{y}}$$

$$\cancel{\begin{aligned} \Delta x_n &= \tfrac{1}{2}(y - x_n^2)/x_n \\ x_{n+1} &= x_n + \Delta x_n \end{aligned}}$$

$\{(y^{(d)}, x^{(d)}) \mid d = 1 \ldots D$ with D …

See this Friday's lecture!

Data

$f_{c_1,c_2,\ldots c_P}(y)$ with P being large

Model

$$\boldsymbol{c} = \arg\min_{\boldsymbol{c}} \sum_d \left(f_{\boldsymbol{c}}(y^{(d)}) - x^{(d)}\right)^2$$

Loss

$$x = f_{c_1,c_2,\ldots c_P}(y)$$

Inference

This is a data-driven solution.

Clinical CT vs. FD-CT

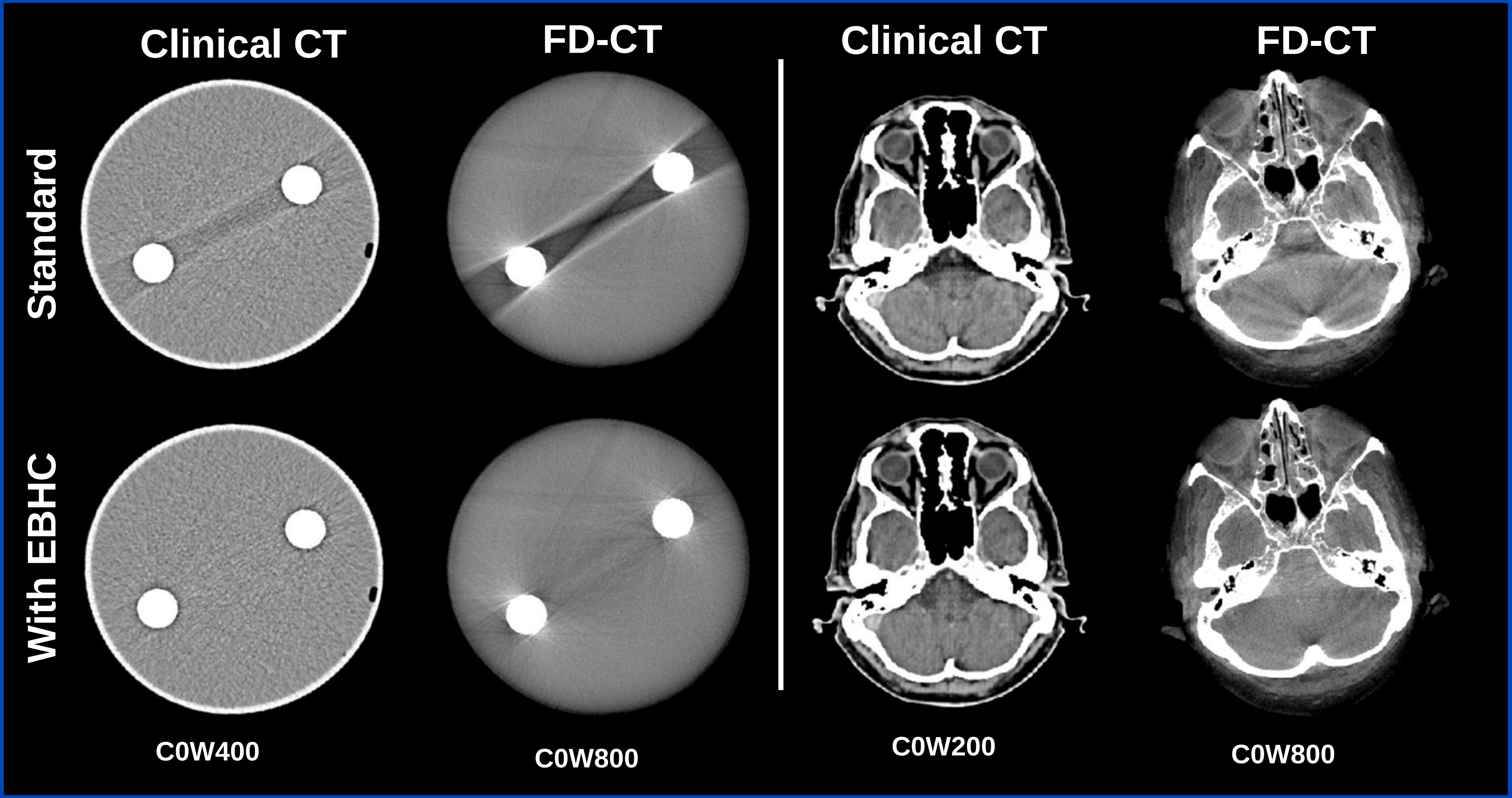

Cone-Beam Artifacts

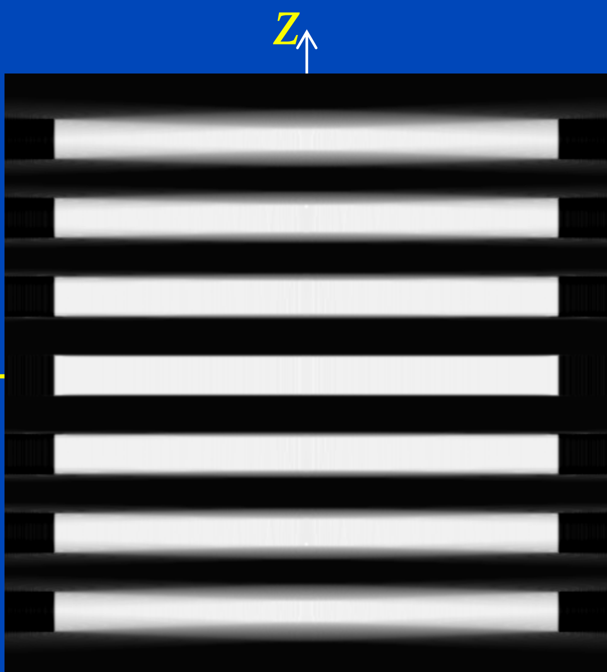

Cone-angle Γ = 6°

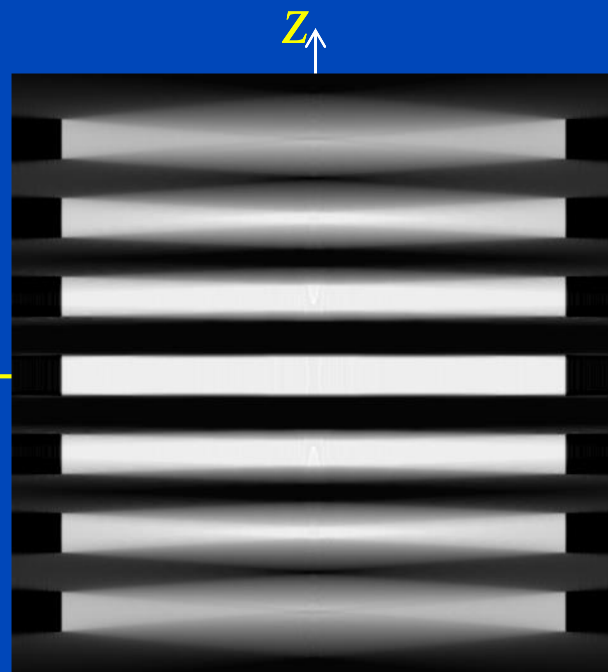

Cone-angle Γ = 14°

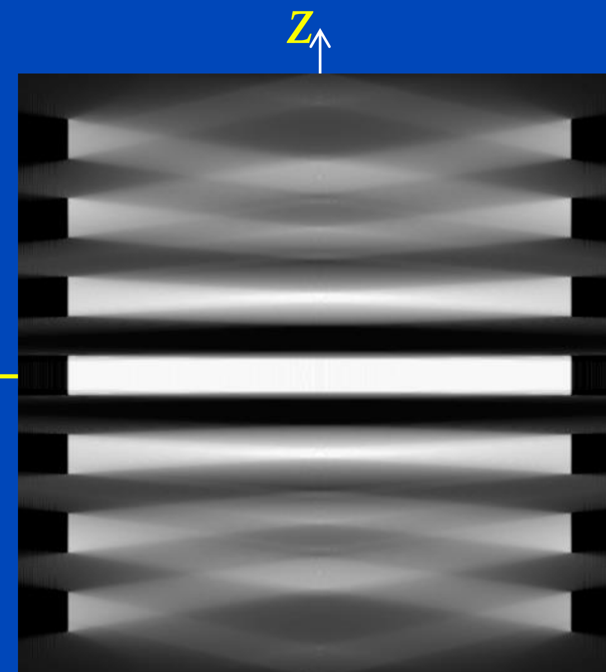

Cone-angle Γ = 28°

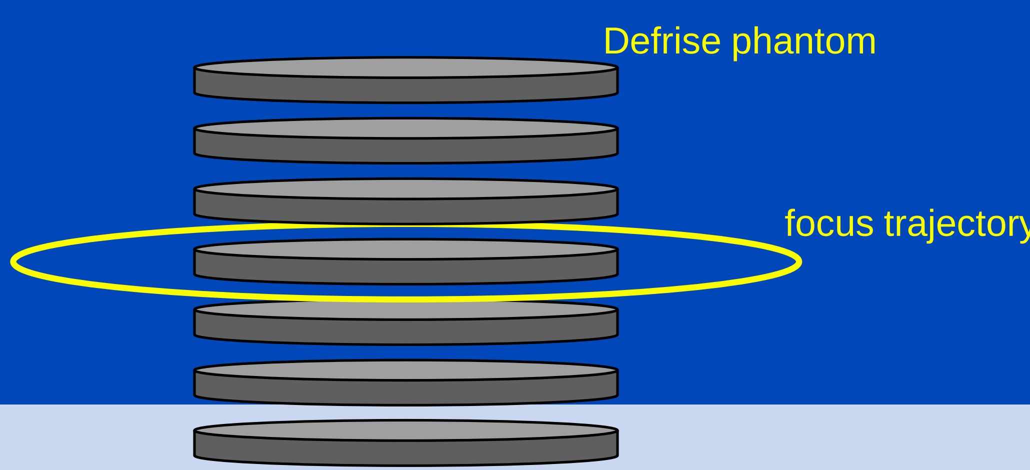

CBCT Uncorrected

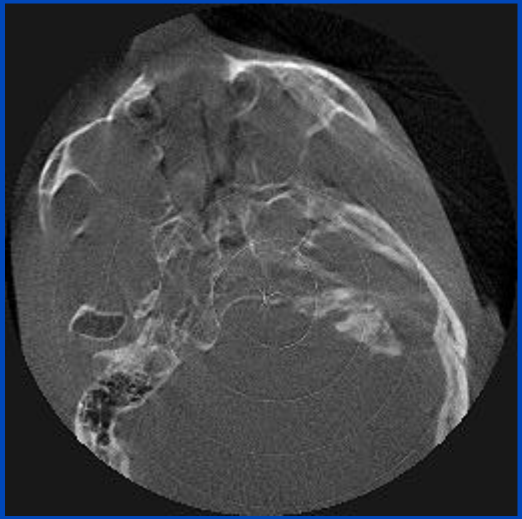

… Plus Geometric Calibration

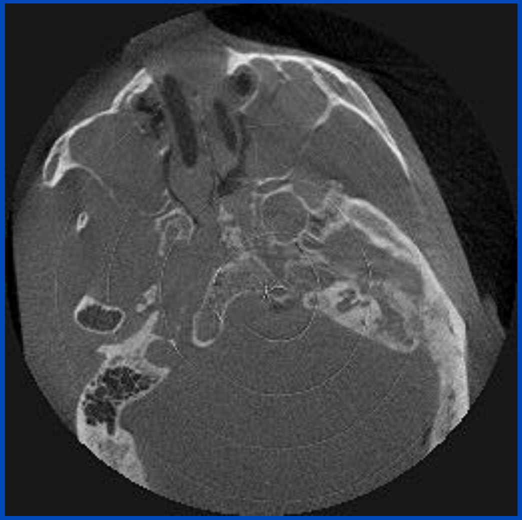

Image courtesy of Dr. Ludwig Ritschl, Ziehm Imaging GmbH, Nürnberg, Germany.

… Plus Detector Calibration

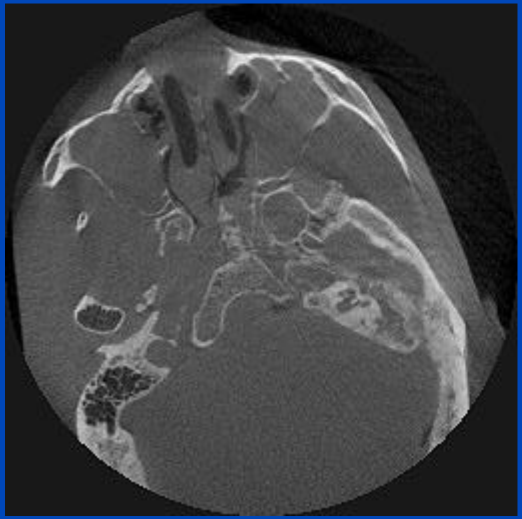

…. Plus Scatter and Beam Hardening Correction

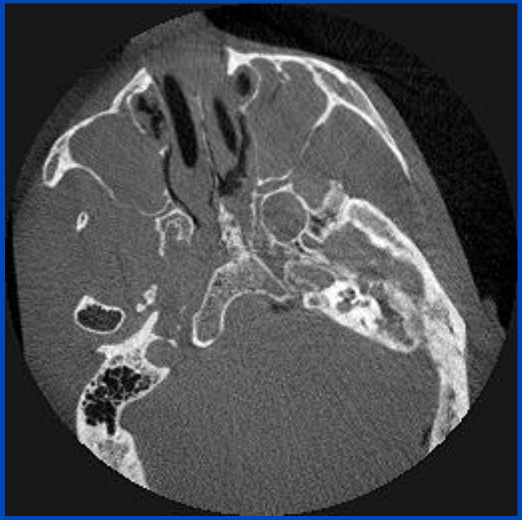

Image courtesy of Dr. Ludwig Ritschl, Ziehm Imaging GmbH, Nürnberg, Germany.

Clinical vs. Flat Detector CT

with some photon
counting CT (PCCT) systems

	Clinical CT	Flat Detector CT
Spatial resolution	0.5 mm → 0.2 mm	0.2 mm
Contrast	3 HU	30 HU
Dynamic range	≈ 20 bit → ∞ bit	≈ 10 bit
Dose efficiency	≈ 90%	≈ 50%
Lowest rotation time	0.25 s	3 s
Temporal resolution	0.06 s	3 s
Frame rate	≈ 5000 fps	≈ 25 fps
X-ray power	100 – 2·120 kW	5 – 25 kW
FOM	50 cm	≈ 20 cm
Scan times	0.1 to 5 s	10 to 60 s
Aspect ratio	≈ 10	≈ 1
Technology	proprietary	buy, plug-and-play

dkfz.

Thank You!

The 8th International Conference on

Image Formation in X-Ray Computed Tomography

Conference Chair

Marc Kachelrieß, German Cancer Research Center (DKFZ), Heidelberg, Germany

This presentation will soon be available at www.dkfz.de/ct.

Job opportunities through DKFZ's international PhD programs or through marc.kachelriess@dkfz.de.

Parts of the reconstruction software were provided by RayConStruct® GmbH, Nürnberg, Germany.